SOY-BASED POLYOL SYNTHESIS FROM EPOXIDISED SOYBEAN OIL WITH SOLID ACID CATALYST

A Thesis Submitted to
the Graduate School of Engineering and Sciences of
İzmir Institute of Technology
in Partial Fulfillment of the Requirements for the Degree of

MASTER OF SCIENCE

in Chemical Engineering

by
Nehir ÇABUK

December 2018
İZMİR

We approve the thesis of **Nehir ÇABUK**

Examining Committee Members:

_____
Prof. Dr. Selahattin YILMAZ
Department of Chemical Engineering, İzmir Institute of Technology

_____
Assist. Prof. Dr. Ali Can KIZILKAYA
Department of Chemical Engineering, İzmir Institute of Technology

_____
Assoc. Prof. Dr. Meral DÜKKANCI
Department of Chemical Engineering, Ege University

24 December 2018

_____
Prof. Dr. Selahattin YILMAZ
Supervisor, Department of Chemical Engineering
İzmir Institute of Technology

_____
Prof. Dr. Erol ŞEKER
Head of Department of Chemical
Engineering

_____
Prof. Dr. Aysun SOFUOĞLU
Dean of Graduate School of
Engineering and Sciences

i

ACKNOWLEDGMENTS

ABSTRACT

SOY-BASED POLYOL SYNTHESIS FROM EPOXIDISED SOYBEAN OIL WITH SOLID ACID CATALYST

In this study, acidic mesoporous catalysts, sulfonated and non-sulfonated Zr-SBA15 (08), Zr-SBA15 (10), Ti-SBA15 (10) and Ti-SBA15 (20), were prepared for oxirane ring opening reaction of epoxidized soybean oil with methanol. Two different amounts of Zr and Ti incorporated into SBA-15. They were prepared by hydrothermal synthesis. Their sulfated forms were prepared by treating Zr-SBA15 based catalyst with H_2SO_4 and Ti-SBA15 based catalysts by $(NH_4)_2SO_4$. The catalytic activities of all catalysts in oxirane ring opening reaction were tested in a 250 ml glass batch reactor at 60 °C.

The catalysts characterisation showed that Zr was succesfully loaded into SBA-15 catalyts. Low Ti content (Ti-SBA-15(20) incorporated into SBA-15 whereas anatase was observed for high Ti content (Ti-SBA15 (20)). All the catalysts had mesopore structure and were acidic. While acidity increased with sulfation significantly, slight acidity change was observed with incoporated metal amount. Zr-SBA15 based catalysts had higher acidity than Ti-SBA15 based catalysts.

The catalysts showed different activities in oxirane ring opening reaction. The activities of the catalysts affected from their acidity. Zr based catalysts showed higher catalytic activity than Ti based catalysts. Higher activities were observed over non sulfated catalysts even they had low acidity. Activity of the catalysts decreased with the acidity. The formation of soy based polyols were determined by FTIR and H-NMR analysis. The highest epoxide conversion was observed over Zr-SBA15 (08) which was 84.08%. This activity was followed by Zr-SBA15 (10) which provided 57.77 %.

ÖZET

EPOKSİDE OLMUŞ SOYA YAĞINDAN ASİDİK KATI KATALİZÖRLER İLE POLYOL SENTEZİ

Bu çalışmada, asidik mezo gözenekli katalizörler, sülfatlanmış ve sülfatlanmamış Zr-SBA15 (08), Zr-SBA15 (10), Ti-SBA15 (10) ve Ti-SBA15 (20), epokside soya yağının metanolle oksiran halka açma tepkimesinde kullanılması için hazırlanmışlardır. Bu katalizörler, SBA15'in iki farklı miktarda Zr ve Ti destelenmesiyle elde edilmiştir. Bu katalizörler hidrotermal sentez yöntemiyle hazırlanmıştır. Zr-SBA15 bazlı katalizörün H_2SO_4 ve Ti-SBA15 bazlı katalizörlerin $(NH_4)_2SO_4$ ile muamele edilmesiyle bu katalizörlerin sülfatlanmış halleri elde edilmiştir. Tüm katalizörlerin oksiran halka açma tepkimesindeki katalitik aktiviteleri 250 mL'lik kesikli bir cam reaktörde 60 °C'de test edilmiştir.

Katalizörlerin karakterizasyon çalışması kapsamında BET, XRD, FT-IR, NH_3-TPD analizleri yapılmıştır. Bu analizler sonucunda, mezo gözenekli SBA15'in, Zr ve Ti ile başarıyla desteklendiği bulunmuştur. Ayrıca, tüm katalizörlerin mezzo gözenekli yapıya sahip olduğu bulunmuştur. Tüm katalizörlerin asidik olduğu bulgulanırken, Zr-SBA15 bazlı katalizörlerin Ti-SBA15 bazlı katalizörlerden daha asidik olduğu görülmüştür.

Katalizörler, oksiran halka açma tepkimesinde farklı etkinlikler göstermişlerdir. Etkinlikleri asitliklerinden etkilenmiştir. Sülfatlanmış katalizörler sülfatlanmamışlara göre daha düşük katalitik etkinlik göstermişlerdir çünkü sülfatlanmamış katalizörlerin asitlikleri sülfatlanmış katalizörlerinkinden yüksektir. Sonuç olarak, sülfatlanmamış katalizörler oksiran halka açma tepkimesinde oldukça etkindirler. Soya bazlı polyollerin oluşumu FT-IR ve H-NMR analizleriyle belirlenmiştir. En yüksek epokside dönüşümü ZrSBA-15 (0.8) varlığında % 84.08 olarak görülmüştür. Bunu, % 57.77 ile Ti-SBA15 takip etmiştir.

TABLE OF CONTENTS

LIST OF FIGURES

LIST OF TABLES

CHAPTER 1

INTRODUCTION

Polyols, polymer resins, which are a group of noncyclic hydrogenated carbohydrates are highly cross-linked and contain multiple hydroxyl groups (Sandler 1999; Anya et al., 2018). They have a great attention on the production of polyurethanes (PUs) and polyesters. Moreover, they are one of the major components in PUs production and they have a comprehensive application area (Rakicka et al., 2017; Sandler 1999; Fan et al., 2012). For instance, they could be used as coatings agents, adhesives, sealants, elastomers, resins, and also used in building and constructions as isolation and coating material (Sandler 1999).

Polyols are traditionally produced from petroleum. However, the production of petroleum-based polyols has some drawbacks such as high energy consumption and high cost. Also, it could have some malign effects on the environment. Furthermore, the diminishing of world crude oil stock and rising prices and more rigid regulations in the matter of the environmental protection cause the sustainable, less costly, environmentally friendly and renewable resources demand (Dworakowska et al., 2012). Cellulose, starch, sugar and vegetable oils, which are extracted from a plant and also known as triacylglycerol, are the alternative renewable sources to petroleum. Vegetable oil-based polyols are one of the most promising alternatives over the petroleum-based polyols (Zhang et al., 2015). The vegetable oils which are most commonly used in PUs production are soybean, palm, rapeseed and sunflower (Dworakowska et al., 2012). Soybean oil is one of the most commonly present in the most part of the world so that it is most abundant and a low-cost vegetable oil (Guo et al., 2007). Besides, refined soybean oil contains more than 99% triglycerides and it has active sites which are three-membered oxirane groups in charge of ring opening reactions (Zhang et al., 2015; Fan et al., 2012). Due to these reasons, it could be concluded that soybean oil is the most promising vegetable oil among the others for the PU production.

Polyols could be synthesized from vegetable oils by several processes which are epoxidation and oxirane ring-opening, thiolene coupling, hydroformylation followed by hydrogenation, microbial conversion, ozonolysis followed by hydrogenation (Fan et al., 2012). Among these methods, epoxidation-hydroxylation is the most commonly used since it is a simple method. It can be controlled easily and different types of polyols could be synthesized by the opening of the epoxide groups using different agents such as methanol, 1,2-Ethanediol, cyclohexanol and phenol (Fang et al., 2016; Dong et al., 2015; Dai et al., 2009). Polyols could be synthesized by this method in two steps which are epoxidation of double bonds of unsaturated fatty acids occur and ring opening of the epoxide group. Consequently, soybean oil has more than four double bonds in each molecule so that it gains great attention to use in the epoxidation process.

The strong Brønsted acids are used to activate epoxide ring in this process. HCl, HBr, p-toluenesulfonic acid could be used to obtain Brønsted acid sides. Besides, the acids should be removed from the reaction media, the reaction needs high reaction temperature and undesirable products like ketones could be formed during the reaction (Ahn et al., 2012). Due to these drawbacks, heterogeneous catalysts, particularly mesoporous catalysts, come into prominence. In the literature, various heterogeneous mesoporous catalysts such as sulfonic acid-functionalized mesostructured silica, sulfamic acid-functionalized APTES coated Fe/Fe_3O_4 nanoparticles (NPs), SAC 13 and Amberlite 15 were used for this process (Ahn et al., 2012). WO_3/Zr-SBA-15 and Zr-SBA-15 catalysts were used for esterification of cetyl alcohol with palmitic acid and 63.1 % yield was observed for Zr-SBA-15 catalyst. In the characterization study of Zr-SBA-15 show that it has a mesoporous structure with acidic properties, so that Zr-SBA-15 catalyst could also be a promising alternative for the production of polyols.

The aim of this study was to investigate the polyol production from epoxide soybean oil over Zr-SBA-15, sulfated Zr-SBA-15, Ti-SBA-15 and sulfated Ti-SBA-15 catalysts. Soybean oil was selected for the polyol production due to its low cost and abundance. Zr-SBA-15 and Ti-SBA-15 catalysts were chosen since they show high reaction activity for esterification reaction. They were prepared for different Zr:Si (0.8 and 1.0) and Si:Ti (10 and 20) molar ratios by hydrothermal synthesis. Then, Zr-SBA15 and Ti-SBA15 catalysts were prepared by using H_2SO_4 and $(NH_4)_2SO_4$, respectively. The catalyst properties were analyzed by XRD, NH_3-TPD, FT-IR and BET analyses. Then,

the prepared catalysts were tested for epoxidized soybean oil alcoholysis by methanol. The activities and selectivities of the catalysts were investigated.

CHAPTER 2

BACKGROUND

2.1. Vegetable Oils and Polyols

Vegetable oils could be derived from various plants such as soybean, sunflower, rapeseed. The structure of vegetable oils consists of triglycerides molecules where the three hydroxyl functions of glycerin are esterified with fatty acids. The fatty acids in vegetable oil could be saturated or unsaturated. The most common saturated fatty acids with non-reactive aliphatic chains are stearic (C 18:0) and palmitic (C 16:0) acids. The most known unsaturated fatty acids with aliphatic chains bearing double bonds are oleic (C 18:1), linoleic (C 18:2), linolenic (C 18:3), and ricinoleic (C 18:1 OH) acid. The composition of vegetable oil varies depending on the fatty acid type and side chains of fatty acid. The chemical structure of vegetable oils and the composition of fatty acids in vegetable oils are illustrated in Figure 2.1., Table 2. 1, and Table 2. 2, respectively (Petrović 2008; Zhang et al., 2015).
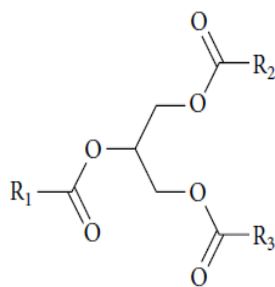
Figure 2. 1. The structure of vegetable oil (R_1, R_2, and R_3-fatty acids).
(Source: Zhang et al., 2015)

Soybean and epoxidized corresponded oils play key role in comparison with other plant oils due to the large amount of worldwide productions, low costs and easier conversion to the polyols by ring opening of three membered oxirane groups. Soybean oil has got high unsaturated fatty acid content.

Table 2. 1. The chemical structure of vegetable oils. (Source: Zhang et al., 2015)
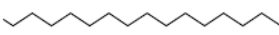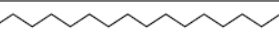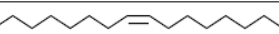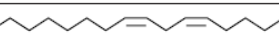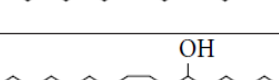
Fatty acids	Structure
Palmitic (C 16:0)	HO_2C
Stearic (C 18:0)	HO_2C
Oleic (C 18:1)	HO_2C
Linoleic (C 18:2)	HO_2C
Linolenic (C 18:3)	HO_2C
Ricinoleic (C 18:1 OH)	HO_2C OH

Table 2. 2. Fatty acid composition of soybean and selected oils. (Source: Petrović 2008)

Carbon atoms: Double bonds	8:0	10:0	12:0	14:0	16:0	16:1	18:0	18:1	18:2	18:3	20:0	20:1	22:0	22:1	24:0	Iodine value range	World production (MMT)[b]
Canola oil				0.1	4.0	0.3	1.8	60.9	21.0	8.8	0.7	1.0	0.3	0.7	0.2	100–115	
Castor oil[c]					2.0		1.0	7.0	3.0							81–91	0.44
Coconut oil	7.1	6.0	47.1	18.5	9.1		2.8	6.8	1.9	0.1	0.1					7–12	3.33
Corn				0.1	10.9	0.2	2.0	25.4	59.6	1.2	0.4		0.1			118–128	2.02
Cottonseed oil			0.1	0.7	21.6	0.6	2.6	18.6	54.4	0.7	0.3		0.2			98–118	3.92
Linseed oil					6.0		4.0	22.0	16.0	52.0	0.5					>177	0.63
Olive oil					9.0	0.6	2.7	80.3	6.3	0.7	0.4					76–88	2.81
Palm oil			0.1	1.0	44.4	0.2	4.1	39.3	10.0	0.4	0.3		0.1			50–55	28.13
Palm kernel oil	3.3	3.4	48.2	16.2	8.4		2.5	15.3	2.3		0.1	0.1				14–19	3.50
Peanut oil				0.1	11.1	0.2	2.4	46.7	32.0		1.3	1.6	2.9		1.5	84–100	4.81
Rapeseed oil				0.1	3.8	0.3	1.2	18.5	14.5	11.0	0.7	6.6	0.5	41.1	1.0	100–115	13.05
Safflower oil				0.1	6.8	0.1	2.3	12.0	77.7	0.4	0.3	0.1	0.2			140–150	
Safflower oil (high oleic)				0.1	3.6	0.1	5.2	81.5	7.3	0.1	0.4	0.2	1.2		0.3	82–92	
Soybean oil				0.1	10.6	0.1	4.0	23.3	53.7	7.6	0.3		0.3			123–139	31.88
Sunflower oil				0.1	7.0	0.1	4.5	18.7	67.5	0.8	0.4	0.1	0.7			125–140	9.49
Sunflower oil (high oleic)					3.7	0.1	5.4	81.3	9.0		0.4		0.1			81–91	

2.1.1. Soybean Oil

The vegetable oils, particularly the unsaturated ones, are of interest since various reactions could be performed by their different groups in order to obtain biobased polyols. The most commonly used vegetable oils to obtain biobased polyols are soybean oil, rapeseed, sunflower seed and palm. Among them, soybean oil is the most widely used

because it contains more than four double bonds per molecule so that it could be converted to polyols easily. Additionally, it is abundant due to the worldwide production and relatively cheaper than the other vegetable oils. The chemical structure of soybean oil is represented in Figure 2.2. and the composition of fatty acids in soybean oil is given in Table 2. 3 (Zhang et al., 2015; Petrović 2008).
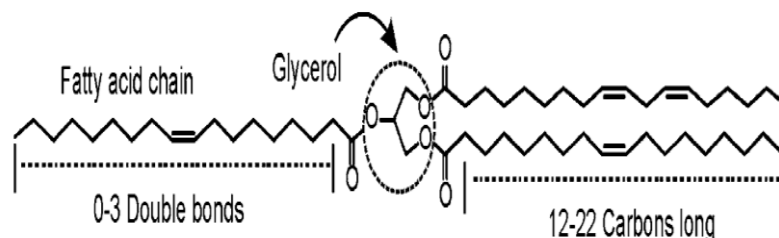
Figure 2. 2. Structure of soybean oil.
(Source: Saremi et al., 2012)

Table 2. 3. The composition of fatty acids in soybean oil. (Source: Saremi et al., 2012)

Soy Fatty Acid	Structure			%
Saturated	Palmitic	CH3(CH2)14COOH	C 16:0	11
	Strearic	CH3(CH2)16COOCH3	C 18:0	4
Unsaturated	Oleic	CH3(CH2)7CH=CH(CH2)7COOCH3	C 18:1	26
	Linoleic	CH3(CH2CH=CH)2(CH2)7COOCH3	C 18:2	52
	Linolenic	CH3(CH2CH=CH)3(CH2)7COOCH3	C 18:3	7

Vegetable oil compositions vary depending on type of fatty acids. Vegetable oils consist of five major fatty acids: palmitic, stearic, oleic, linoleic and linolenic acid. Majority of soybean oil compose of unsaturated fatty acids.

2.1.2. Properties of Vegetable Polyols

A polyol is an alcohol containing multiple hydroxyl groups. A molecule with two hydroxyl groups is a diol, one with three is a triol, one with four is a tetrol and so on. They have wide range of viscosities, hydroxyl numbers and functionalities result in use as raw material for several industry. Polyols thermal and mechanical properties provide important technological advantages and easy process in industry.
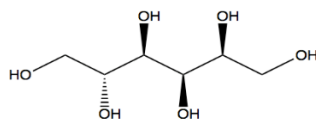
Figure 2. 3. Structure of sorbitol (polyol).

Polyols, also known as polymer resins, could be synthesized using vegetable oils instead of fossil and non-renewable materials since the vegetable oils are renewable, biodegradable and non-toxic raw materials. Additionally, vegetable oils are environmentally friendly. The depletion of fossil and non-renewable materials triggers the replacement of these materials with the renewable materials, particularly vegetable oils. The use of renewable materials protect the environment and reduce the waste disposal (Anya et al., 2018; Sandler 1999; Liu and Biswas 2013).

Vegetable oils could be modified with respect to their hydroxyl, epoxy, amine, polyacid, isocyanate or silane groups in their chemical structure. The functionalized fatty acids are more effective than triglycerides on the structure and properties of polyols (Alagi et al., 2018; Sandler 1999). Yet, the vegetable oil derivatives could include only one type of functionality on the molecule so that the versatility of application areas might be limited (Alagi et al., 2018). Therefore, the functional group determines the usage areas of polyol. For example, the polyols could be in the rigid (structure) foam form or flexible (elastomer) foam form (Członka, et al., 2018). Additionally, increase in the functionality of hyperbranched molecules cause to increase in molecular weight of polyols and the higher molecular weight might be unacceptable for many application areas so that the molecular weight of polyols derived from vegetable oils affects the usage areas of the polyols (Petrović and Cvetković, 2012).

The hydroxyl value could be expressed as milligrams (mg) of potassium hydroxide (KOH) per gram of vegetable oil and it is another important parameter to control the process and quality of polyol (Ping et al., 2011).

The viscosity and glass transition temperature of polyols should be low since these properties play an important role on industrial applications of polyols (Ping et al., 2011; Campanella et al., 2009).

The technical properties of polyols which are produced for polyurethane industry are given in Table 2. 4.

Table 2. 4. Technical requirements for polyols used in polyurethane industry.
(Source: Sakarya and Sennur, 2014)

Classification	Flexible Foam/Elastomer	Rigid/Structural Foam
Molecular Weight	1000 to 6500	400 to 1200
Hydroxyl Value	28 to 160	250 to 1000
Functionality	2 .0 to 3.0	3.0 to 8.0

Consequently, it could be concluded that the produced polyols which have the properties at the given intervals could be used in textile, automotive, building and construction industries.

2.2. Polyols Production Methods

Polyols could be synthesized from vegetable oils by epoxidation and oxirane ring-opening, thiolene coupling, hydroformylation followed by hydrogenation, microbial conversion, ozonolysis followed by hydrogenation (Fan et al., 2012). The process which is used for polyol synthesis from vegetable oils determines the characteristics of the derived polyols.

The epoxidation-hydroxylation is the most widely used process because it is simpler than other processes. This process could be controlled easily and different types of polyols could be synthesized by the opening of the epoxide groups using different agents such as methanol, and 1,2-Ethanediol, (Fang et al., 2016; Dong et al., 2015; Dai et al., 2009). This process consists of two consecutive steps which are epoxidation and hydroxylation reactions. The reaction mechanisms of epoxidation and hydroxylation steps are given in below (Purwanto 2010):

1. Formation of peroxyacid:

$$RCOOH + H_2O_2 \longleftrightarrow RCOOOH + H_2O$$

2. Epoxidation reaction:

$$R_1CH{=}CHR_2 + RCOOOH \longrightarrow R_1CH \overset{}{\underset{O}{\diagdown\diagup}} CHR_2 + RCOOH$$
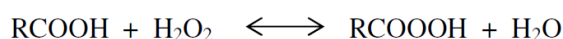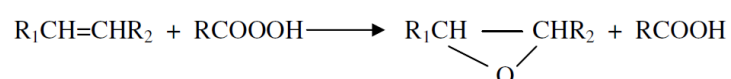
3. Reaction of epoxidized oil with water:

$$R_1CHOCHR_2 + H_2O \longrightarrow R_1\text{-}CH\text{-}CHR_2$$
$$\underset{OH\ OH}{|\ \ \ |}$$

4. Reaction of epoxidized oil with alcohol:

$$R_1CHOCHR_2 + R_3OH \longrightarrow R_1\text{-}CH\text{-}CHR_2$$
$$\underset{R_3O\ \ \ OH}{|\ \ \ \ \ |}$$
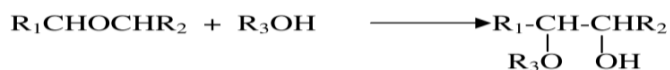
Figure 2. 4. The schematic representation of epoxidized oil reactions. (Source: Purwanto 2010)

Many researches have shown that the hydroxyl value of the final product of polyol could be enhanced by the epoxidation and hydroxylation reactions. In the epoxidation step, unsaturated bonds in vegetable oils are transformed to produce epoxy groups represented by the percentage of oxygen content. The higher percentage of oxygen content in the epoxidized oil indicates that it has more epoxy groups. In the hydroxylation step, the epoxy groups in the epoxidized oil are transformed to the polyol (hydroxyl value). High hydroxyl value show that the polyol has a good quality (Petrović 2008; Purwanto 2010).

2.2.1. Epoxidation and Oxirane Ring Opening

The synthesis of epoxide groups is also known as an epoxidation reaction takes place when an alkene is reacted with an organic peroxy acid (Purwanto 2010). The epoxidation of vegetable oils was carried out in large batch reactors by mixing the oil and the solution obtained by the reaction of peroxyacetic acid in glacial acetic acid and the hydrogen peroxide using a catalyst such as sulfuric acid. However, this process has some drawbacks, for instance, the acetic acid not only causes corrosion but also it is not regenerable. Additionally, the reaction duration can last between 10 and 20 h at a temperature between 30 and 80 °C with respect to the types of feedstock and ratios of reactants, so that the plant investment should be high to achieve the required amount of product. Higher than 90 % conversion could be obtained for this process under the optimized reaction conditions (Piccolo 2016; Li et al., 2015). The epoxidation reaction is given in vegetable oils could be obtained by several ways and they could mainly be classified in four main methods (Saremi et al., 2012; Piccolo 2016):

1. Epoxidation with peroxycarboxilic acids: This method is generally used in the industry and it has some advantages, for example, the acid used in this process is non-toxic and the by-products of this process is simply water. The reaction could be catalyzed by acids or enzymes.

2. Epoxidation with organic and inorganic peroxides: This group includes alkaline and nitrile hydrogen peroxide epoxidation. The reaction is catalyzed by transition metals.

3. Epoxidation with halohydrines: Hypohalous acids (HOX) and their salts are used in this method.

4. Epoxidation with molecular oxygen: The reaction occurs using silver as a catalyst. This method is the simplest and cheapest way. However, only a very low yield could be achieved.

The epoxidized oil term is generally used to refer to an oil which is derived from a vegetable oil by the epoxidation reaction. The epoxidized oil contains epoxide groups or oxirane rings. The term epoxide may be defined as cyclic ethers which consist of three elements in the epoxide ring. The chemical structure of epoxide is illustrated in Figure 2. 5. (Purwanto 2010).

$$\underset{\underset{\displaystyle O}{\diagdown\diagup}}{-\overset{\displaystyle |}{C}-\overset{\displaystyle |}{C}-}$$
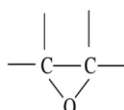
Figure 2. 5. The chemical structure of epoxide.

Polyols could be synthesized from epoxidized vegetable oil by oxirane ring-opening reactions. A wide range of active hydrogen-containing compounds such as alcohols, inorganic and organic acids, amines, water, and hydrogen could be used in the oxirane ring-opening reactions. The epoxidation and oxirane ring-opening reactions are carried out in two separate steps, although a one-step process which is the combination of epoxidation and ring-opening reactions has been reported (Li et al., 2015).

The types of ring-opening agents and feedstock characteristics affect the properties of polyols synthesized via epoxidation and followed by oxirane ring-opening. For instance, polyols with higher hydroxyl functionalities could be produced using

vegetable oils with a higher degree of unsaturation. Oxirane ring-opening agents can be divided into three major categories which are alcohols, acids, and hydrogen (Li et al., 2015).

If monoalcohols are utilized for the ring-opening reaction, then each epoxy moiety has only one secondary hydroxyl group. It is known that the primary hydroxyl groups are more reactive than the secondary ones. The most commonly used monoalcohol in ring opening reaction is methanol since it has low molecular weight, low boiling point, and low cost. Diols, particularly 1,2-propanediol and ethylene glycol, could be used in ring-opening reactions to obtain primary hydroxyl groups so that the functionalities and hydroxyl numbers of polyols can be enhanced yet it causes an increase in viscosity of polyols (Li et al., 2015).

Carboxylic acids, especially formic and acetic acids, could be utilized for ring-opening of epoxidized vegetable oils in order to produce polyester polyols, which have displayed a great potential for anti-wear applications. HCl, HBr, and H_3PO_4 which are inorganic acids could also be used as ring-opening agents yet polar organic solvents such as acetone and t-butyl alcohol should be added since there is an incompatibility between the inorganic acids and epoxidized vegetable oils. The usage of inorganic acids has some disadvantages. For example, if HCl and HBr are used as a ring-opening agent, the obtained polyols are in the form of wax at room temperature and if H_3PO_4 is used, an oligomerization occurs between the oxirane groups so that the produced polyols contain considerable fractions of oligomers (Li et al., 2015).

Hydrogen could be used as a ring-opening agent for polyol production from the epoxidized vegetable oils in the presence of Raney nickel catalyst and the obtained polyol is in the form of grease at room temperature (Li et al., 2015).

Soy-based polyol synthesis process consists of two main steps which are the epoxidation of soybean oil and functionalization of hydroxyl groups to enhance isocyanate reactivity and the typical reaction for this process is shown in Figure 2. 6. (Lubguban 2009).

Epoxidation reaction takes places by preformed or in situ prepared peracids. The reaction can take place in bulk or solution under either homogeneous or heterogeneouscatalysis (Li et al., 2015). The properties of polyols synthesized from

epoxidized soybean oil using different oxirane ring-opening agents are listed in Table 2. 5.

Table 2. 5. The list of the properties of polyols produced from epoxidized soybean oil using different oxirane ring-opening agents. (Source: Li et al., 2015)

Ring-opening agents	Polyol Properties					
	Hydroxyl Number (mgKOH/g)	Hydroxyl Group Type	Acid Number (mg KOH/g)	f_n^c	Viscosity (Pa.s)	Moleculer Weight (g/mol)
Methanol	199	Secondary	-[b]	3.7	12 (25 °C)[d]	1053
	180	Secondary	-	-	0.6 (45 °C)	-
	148-174	Secondary	-	2.6-3.2	-	1001-1025[a]
1,2-Ethanediol	253	Primary, secondary	-	-	1 (45 °C)	-
	187-226	Primary, secondary	-	3.4-4.2	-	1005-1038[a]
1,2-Propanediol	289	Primary, secondary	-	-	1 (45 °C)	-
	211-237	Primary, secondary	-	3.8-4.6	-	1010-1084[a]
Lactic acid	210[a]	Secondary	-	4.2	-	1120
	171[a]	Secondary	3.6	5.3	47[c]	1738[a]
Glycolic acid	203[a]	Primary, secondary	2.6	4.9	221[c]	1352[a]
Acetic acid	188[a]	Secondary	1.8	4.3	55[c]	1281[a]
Formic acid	104-162	Secondary	1.8-2.5	1.9-3.2	3-10 (30 °C)	1027--1086
Linoleic acid	76-112	Secondary	4-25	-	1.4-2.8 (22 °C)	-
Ricinoleic acid	152-163	Secondary	5-16	-	7.7-9.4 (22 °C)	-
Hydrochloric acid	197	Secondary	-	3.8	Grease[f]	1071
Hydrobromic acid	182	Secondary	-	4.1	Grease[f]	1274
Phosporic acid	153	Secondary	1.4-48	12.8-17.5[a]	3.2-5.3	3870-4700
Hydrogen	212-225	Secondary	-	3.5-3.8	Grease[f]	938-947

a- Calculated values, b- Not reported, c- Functionality, d- Testing temperature, e- Testing temperature not reported, f- At room temperature
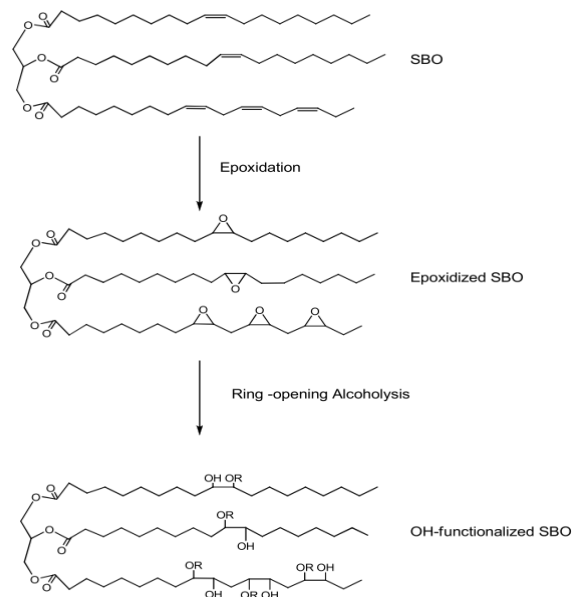
Figure 2. 6. Reaction mechanism of soy-based polyol synthesis.
(Source: Lubguban 2009)

In order to open an oxirane ring to allow hydroxylation reaction of acid or base catalyst can be applied. The oxirane ring opening reaction mechanism using an acid catalyst and a base catalyst are shown in Figure 2. 7. and Figure 2. 8., respectively (Purwanto 2010):
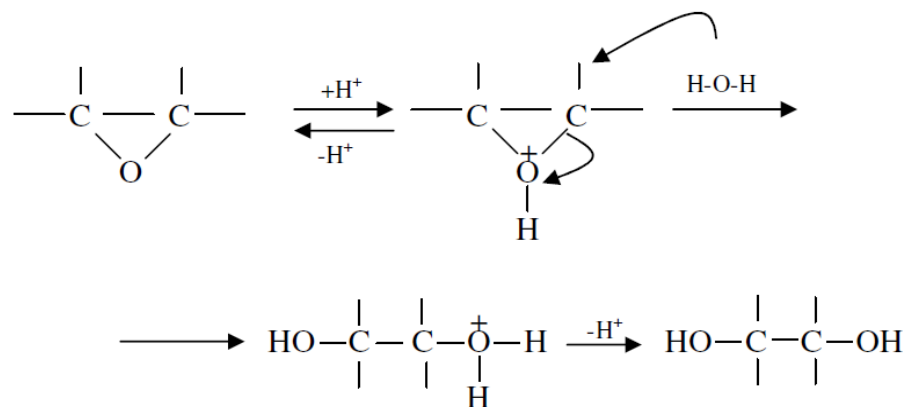
Figure 2. 7. Oxirane ring opening reaction mechanism using an acid catalyst.
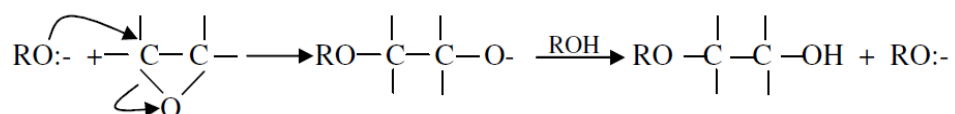
Figure 2. 8. Oxirane ring opening reaction mechanism using a base catalyst.

During the reaction, the ring-opening of epoxide takes place through the cleavage of one of the carbon-oxygen bonds. Firstly, the epoxide is activated by a proton supplied by a Bronsted acid catalyst present in the reaction mixture. Then, the activated epoxide undergoes nucleophilic attack by the hydroxyl group. This mechanism named as nucleophilic substitution (SN2).

CHAPTER 3

LITERATURE SURVEY

In literature, there are many studies about the polyol production from epoxidized soybean oil. Various alcohols in the presence of homogeneous and heterogeneous catalysts have been applied. The most related studies with this thesis were selected and are summarized briefly in main two sections in spite of the type of used catalyst. Finally, the outcomes from the literature is explained.

3.1. Polyol Production by Homogeneous Catalysts

Guo et al. (2007) performed a study over the ring opening reaction of epoxidized soybean oil (ESO) with water in the presence of phosphoric acid. The effect of the solvent type, namely, acetone, tetrahydrofuran, 2-propanol, *tert*-butyl acetate, and *tert*-butyl alcohol and the influence of their amount were studied. The experiments were carried out at a temperature range between 60 °C and 120 °C with respect to the used solvent for 6 h. The properties of obtained polyols using different solvents are given in Table 3. 1. (Guo et al., 2007).

Table 3. 1. The properties of polyols from ESO synthesized using different solvents. (Source: Guo et al., 2007)

Parameters	Solvents				
	Acetone	THF	2-Propanol	t-butyl acetate	t-butyl alcohol
ESO/Solvent (w/w)	1.0/0.5	1.0/0.5	1.0/0.5	1.0/0.5	1.0/0.5
Phosporic Acid	2%	2%	2%	2%	2%
Water	10%	10%	10%	10%	10%
%Oxirane Content	3.41	2.64	1.16	0.03	0.5
Acid Value	1.35	1.96	2.24	48	4.16
Hydroxyl Value	-	-	153	235	253
Viscosity (cps)	3,010	3,780	5,310	4,760	3,160
Molecular (g/mol)	-	-	4,700	4,018	3,870

The experimental results implied that *tert*-butyl alcohol was the best solvent for this process and the optimum ESO/solvent (tert-butyl alcohol) was determined as 1:0.5. Additionally, the influence of phosphoric acid concentration on reaction time and derived products characterization was investigated. As the acid concentration increased, the reaction time decreased. Whereas the molecular weight and viscosity of the products increased at 2, 3 and 4 % of acid content, lower molecular weight and viscosity was observed at 10 % of the acid content. The effect of water content was studied and the results indicated that the water content did not have a significant effect. Besides, the characterization study of derived products conducted. Due to the loss of oxirane groups, the hydroxyl and phosphate ester groups appeared. They analyzed via FT-IR spectrum and the theoretical hydroxyl value was determined as 495 mg KOH/g. The experimental hydroxyl value determined by the chemical and spectroscopic method as 5.27 ppm and 2.68 ppm, respectively. The difference (~50%) between the experimental and theoretical hydroxyl value indicated that the loss amount used for the formation of oligomeric ethers. Additionally, the theoretical and average molecular weight of the products compared and it was concluded that the products had the oligomeric nature. The reactions of phosphate esters formation are given in Figure 3. 1.
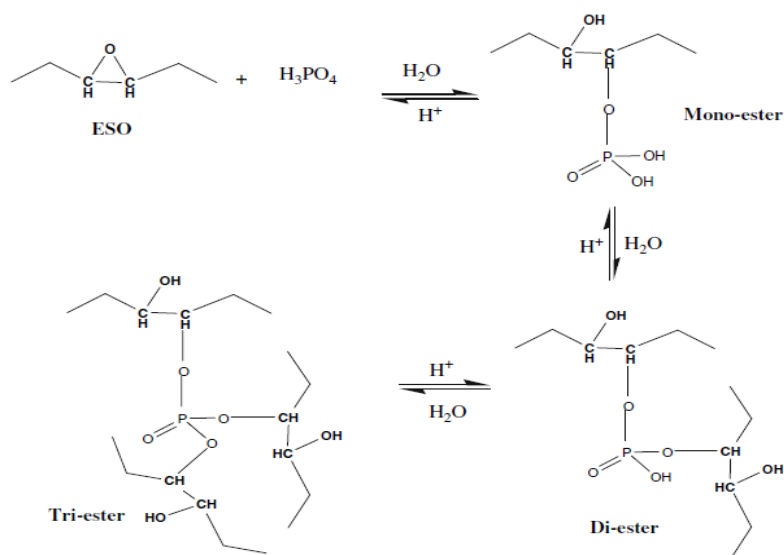
Figure 3. 1. The reactions of phosphate esters formation.
(Source: Guo et al., 2007)

Dai et al. (2009) performed a study over the production of the different soy-based polyols and the spectroscopic, chemical and physical methods were applied to characterize the synthesized polyols. In this study, the ring opening of the epoxidized

soybean oil was carried out using methanol (b), 1,2-Ethanediol (c), and 1,2-Propanediol (d)in the presence of tetrafluoroboric acid. The molar ratio of epoxy groups to alcohol was 1:11 and the used catalyst amount was chosen as 1% of total weight of ESO (a) and used alcohol. The reaction temperature was 95 °C. ESO was added into reaction mixture in the first one hour and then, the reaction allowed for 2 hours. According to the experimental results, the polyol synthesized using methanol show the lowest viscosity, viscous flow energy, molecular weight and melting point. The viscosities and activation energies of ESO and derived polyols are given in Table 3. 2. (Dai et al., 2009).

Table 3. 2. The viscosities and activation energies of ESO and derived polyols.
(Source: Dai et al. 2009)

Samples	Viscosity at 45 °C (mPa s)	E (kj/mol)
ESO	144.6 ($\pm$ 1.5)	29.56 ($\pm$ 0.35)
Polyol (1)	567.0 ($\pm$ 1.6)	39.99 ($\pm$ 0.22)
Polyol (2)	935.5 ($\pm$ 2.3)	38.80 ($\pm$ 1.12)
Polyol (3)	1003 ($\pm$ 3.5)	49.88($\pm$ 1.36)

Polyol (1), polyol (2), polyol (3) were synthesized from ESO by oxirane ring opening with methanol, 1,2-ethanediol and 1,2-propanediol, respectively.

The polyol synthesized using1,2-Ethanediol and 1,2-Propanediol follow the polyol synthesized using methanol. All synthesized polyols were in the crystalline solid form below their melting point. Among the synthesized polyols, the polyol synthesized using methanol had a large number of hydroxyl groups and molecular weight and they lead improvements on the properties of polyurethanes. GPC results of ESO and derived polyols are given in Figure 3. 2.
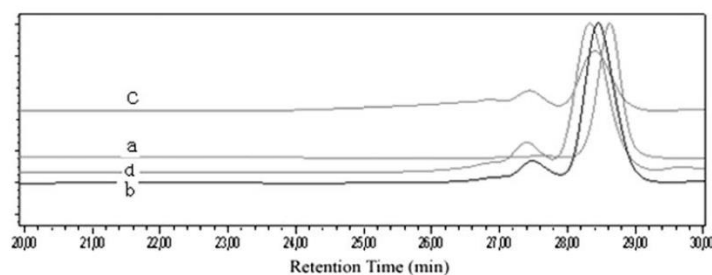
Figure 3. 2. GPC results of ESO and derived polyols.
(source: Dai et al. 2009)

Liu and Biswas (2013) carried out a study in order to investigate the catalytic performance of fluoroantimonic acid hexahydrate for ring-opening polymerization of epoxidized soybean oil (30 g) in ethyl acetate solution (30 ml) at milder reaction conditions for 3 h. The produced polymer was a typical cross-linked polymer and its glass transition temperature values were varied between -13 to -21 °C due to the long fatty acid chains. Additionally, the produced polymers were thermally stable up to 200 °C according to the TGA results (Liu and Biswas 2013).

Sakarya and Sennur (2014) studied the preparation of soy based polyol by oxirane ring opening with polyethylene glycol (PEG400) in the presence of a tetrafluoroboric acid catalyst. Three different PEG400-ESO were prepared in this study. The first one, PEG400-ESO-1, was prepared at 100 °C and consisted of PEG400 and ESO at a stoichiometric molar ratio of 1:1. The second one, PEG400-ESO-2, was prepared at 110 °C. The third one, PEG400-ESO-3, was prepared at 100°C in the presence of a double amount of tetrafluoroboric acid. The preparation duration for all of them was 24 h. The properties of polyols such as OH numbers, viscosities, water contents, and acids were investigated. According to the results, as the temperature increased, lower OH numbers were obtained. They investigated the effects of reaction temperature and catalyst amount on the PEG400-ESO soy-based polyols by different methods such as spectroscopic, chemical and physical methods. The reaction parameters and the properties of polyols are shown in Table 3. 3.

Table 3. 3. The reaction parameters and the properties of polyols from ESO.
(Source: Sakarya and Sennur 2014)

	PEG400-ESO-1	PEG400-ESO-1	PEG400-ESO-1
Reaction time (h)	24	24	24
Reaction temperature (°C)	100	110	100
OH number (mg KOH/g)	167	146	169
Viscosity (cPa)	3850	3500	5500
Water content (ppm)	2.12	4.01	3.10
Acid (mg KOH/g)	6.15	6.06	6.54

Dong et al. (2015) studied the production of polyurethane rigid foams (PU-C, PU-M, and PU-P) from three different soy-based polyols by the ring opening of epoxidized soybean oil (ESO) with cyclohexanol, phenol, and methanol. The molar ratio

of ESO:alcohol was chosen as 1:11 and the fluoroboric acid catalyst concentration was 0.2% of the total weight of reaction mixture. The experiments were carried out at 65 °C for 2 h. The experimental results showed that the PU-P had the smallest cell size, the highest density and thermal conductivity for the same soy-based polyol content (25 %). Whereas phenol leads to provide the thermal and mechanical properties of the bio-foam, the usage of cyclohexanol did not provide an improvement on the bio-foam properties. The properties of ESO and polyols synthesized by three different alcohols are given in Table 3. 4. Polyol-M, Polyol-C, Polyol-P were synthesized from ESO by oxirane ring opening with methanol, cyclohexanol and phenol, respectively.

Table 3. 4. General properties of ESO and polyols. (Source: Dong et al., 2015)

Polyol	Hydroxyl Number (mg KOH/g)	Acid Number (mg KOH/g)	Epoxy Content (wt.%)	M_n(Da)	M_w/M_n	F_n (Relative)	Viscosity (mPas)
ESO	-	-	6.2	989	1.045	-	390
Polyol-M	175	1.5	<0.1	1120	1.302	3.49	550
Polyol-C	150	1.1	<0.1	1438	2.420	3.84	890
Polyol-P	164	2.0	<0.1	1293	1.858	3.78	950

Li and Sun (2015) investigated the polyols production from epoxidized soybean oil using glycolic acid and lactic acid in the absence of solvent and catalyst. The epoxide and the lactic acid or glycolic acid were used at molar ratio of 1:11. The reaction temperature and reaction duration were 90 °C and 6 h, respectively. The epoxy conversion rate was obtained over the 93% for both polyols. Whereas polyol (ESOGA), which is synthesized using epoxidized soybean oil and glycolic acid, had a weight-/number-average molecular weight (M_w/M_n) of 27,700/3900 g/mol and average hydroxyl functionality (f_{OH}) of 12.9, polyol (ESOLA), which was synthesized using epoxidized soybean oil and lactic acid had M_w/M_n of 8800/3000 g/mol and f_{OH} of 11.7. The results imply that the glycolic acid could provide to higher molecular weight polyols since it is more reactive than lactic acid due to its stronger acidity and primary hydroxyl function to react with epoxidized soybean oil. The structure of the synthesized polyols was characterized via FT-IR and their rheology and thermal properties were investigated and the results are given in Table 3. 5. (Li and Sun 2015).

Table 3. 5. Thermal properties of ESO and derived polyols. (Source: Li and Sun 2015)

Sample	T_g (°C)	ΔC_p (J/g °C)	T_c (°C)	ΔH_c (J/g)	T_m (°C)	ΔH_m (J/g)
ESO	-63.9	0.51	-3.21	14.4	-14.5	35.54
ESOGA	-21.3	0.48	-2.0	0.78	4.8	1.37
ESOLA	-22.2	0.52	-2.0	0.97	4.3	1.17

T_g, glass transition temperature, T_c, crystallization temperature, T_m, melting temperature, ΔH_c, heat capacity of crystallization, ΔH_m, heat capacity of melting, ΔC_p, heat capacity.

3.2. Polyol Production over Heterogeneous Catalysts

Barluenga et al. (2002) used the hydrated copper (II) tetrafluoroborate as a catalyst (10% mol percentage of ESO) for the ring opening reaction of epoxides. The experiments carried out with the methanol at room temperature for 1 h. This study shows that the ring opening reaction could occur at an optimum ratio of 1:4 molar ratio of cyclohexene oxide:methanol (Barluenga et al., 2002).

Rios et al. (2005) carried out a study over the effect of alcohol molecular configurations (α- and β-branched alcohols) and resin structures on the acid-resin catalyzed alcoholysis of epoxidized fatty esters. The molar ratio of ESO and alcohol (methanol, buthanol, pentanol, iso-buthanol, neopentanol, tert-buthanol) was 1:10 for each alcohol. The catalyst amount was 10 % wt. of ESO. The reactions were carried out at 60 °C and the reaction duration were varied from 1 h to 48 h. The epoxide conversion is given in Figure 3. 3. The study shows that acid resins are convenient for alcoholysis of epoxidized fatty esters since acid centers are attainable to activate the epoxide (Rios et al., 2005).

The selectivity decreased while the branched alcohols were used for the ring opening reaction. Whereas the epoxide ring opening reaction rate increased with respect to the acid strength, it decreased due to the increase in a number of branches and size of alcohols. For example, SAC13 showed better catalytic activity than the other catalyst because of the stronger acid sites. These stronger acid sites lead to decrease the activation

energy. If the catalysts have more acidic sites, then polyether and polyester can form as by-product. Therefore, the acidic sites should be optimized. In Figure 3. 4, the reaction of epoxidized methyl oleate (EMO) with alcohols are given as an example to show the by-product formation. Besides, higher steric hindrance was observed for α-branched alcohols.
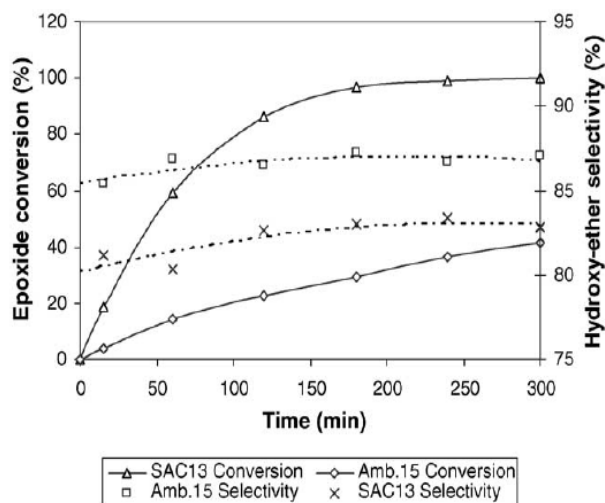
Figure 3. 3. The epoxide conversion and TOF for the addition of methanol to epoxidized methyl oleate. (Source: Rios et al., 2005)
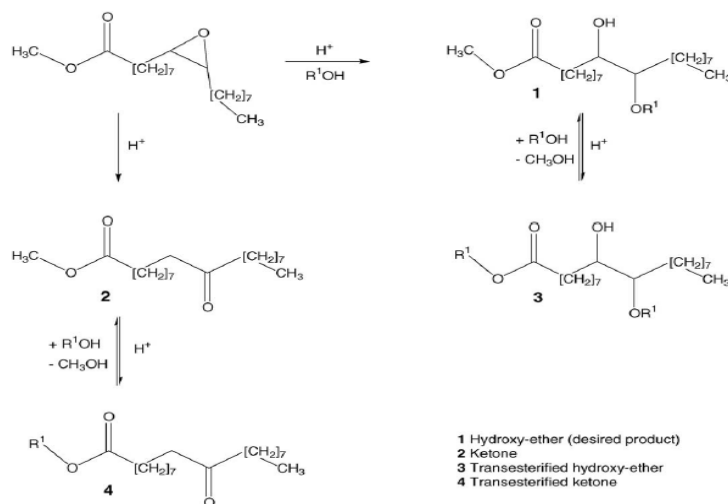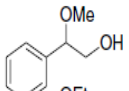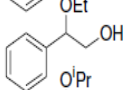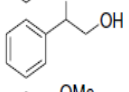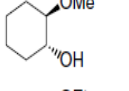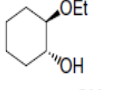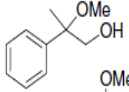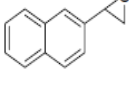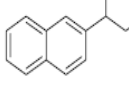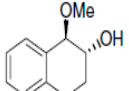
Figure 3. 4. The reaction of alcohols with EMO. (Source: Rios et al., 2005)

Robinson et al. (2007) performed a study over synthesize of mesoporous aluminosilicate catalyst and its catalytic performance on the ring opening reaction of epoxides was tested in the presence of different alcohols (methanol, ethanol and propanol) and different epoxides. Reaction temperature and reaction time changed due to the type

of alcohol and epoxide. Epoxide (120 mg), alcohol (10 ml) and catalyst amount was selected as 50 mg. The reaction time varied between 1 h and 4.5 h depending on the type of alcohol and epoxide. The production of β-alkoxyalcohols from epoxides by the addition of alcohols in the presence of mesoporous aluminosilicate catalyst was observed in short reaction duration and high yield. Aluminosilicate catalyst with Si/Al ratio=14 show higher efficiency for the nucleophilic ring-opening of styrene oxide with methanol because the polyol production dependent on the Lewis acid sites. Obtained products and yields are given in Table 3.6.

Table 3. 6. The products and yields obtained for different epoxides.
(Source: Robinson et al., 2007)

Entry	Epoxide[a]	Time (h)	Product[b,c]	Yield[d] (%)
1		1.5		95
2		2.5		86
3		3.5		52
4		1		69
5		1		96
6		3		97
7		4.5		90[e,f]
8		1		99

Lathi and Mattiasson (2007) studied the synthesis of biodegradable lubricant base stock derived from epoxidized soybean oil in the presence of the cationic ion exchange resins as a catalyst. The process consisted of two steps which were ring opening reaction of epoxidized soybean oil with different alcohols such as *iso*-amyl alcohol, *n*-butanol, and 2-ethylhexanol using Amberlyst 15 which is a solid acid catalyst and followed by esterification of the resultant hydroxy group. These organic catalysts have microporous gel type structure so that they show low cleavage efficiencies in comporasion with homogeneous catalysts. Thus, they have good catalytic activity. Additionally, their solute

ions have to diffuse through the particle to interact with the exchange site which may enhance the overall efficiency. The reaction conditions are given in Table 3. 7.

Table 3. 7. ESO ring opening reaction conditions.
(Source: Lathi and Mattiasson 2007)

Alcohol	Temperature (°C)	Mole Ratio	Catalysts loading (%)	Reaction Time (h)
n- Butyl alcohol	100	1:2	2	15
n- Butyl alcohol	100	1:3	2	15
iso- Amyl alcohol	110	1:2	2	17
2- Ethyl hexanol	120	1:2	2	24

The higher amount of hydroxyl group of ring opening product was obtained using *n*-butanol. The usage of branching epoxidized soybean oil in the ring opening reaction cause the low pour point and 2-ethylhexanol provided low pour point. The long chain or branched alcohols let to longer reaction duration and higher reaction temperature. According to the experimental study, the catalyst was stable and reusable. The obtained lubricants are biodegradable and non-toxic.

Lozada et al. (2009) performed a study for the soy-based polyols production in the presence of six different acidic catalysts, namely, formic acid, phosphoric acid, POLYCATV® 5, *p*-toluenesulfonic acid monohydrate, POLYCATV® SA-1, and DABCOV® BL17 by alcoholysis reaction. The acid number, oxirane oxygen content and color analyses were carried out to comprehend their catalytic performance. In the experiments, 200 g of ESO and 12.41 g of ethylene glycol (EG) and 4.80 g of methanol (ME) were used. The reactions were carried out using 0.5 % wt. catalyst at 150 °C for 2 h to determine the oxirane oxygen content and acid number. *P*-toluenesulfonic acid monohydrate provided the highest oxirane oxygen content reduction and low acid number. Furthermore, no side reaction was observed in the presence of this catalyst so that it was appropriate to use in alcoholysis reaction. In order to optimize the reaction parameters such as reaction duration (between 2 and 9 hours) and reaction temperature (130, 150 and 170 °C), several experiments were performed. They were optimized as 150 °C between 4 and 11 h for each catalyst. The properties of ESO and derived polyols with

p-toluenesulfonic acid monohydrate are given in Table 3. 8. The emergence of the hydroxyl group was confirmed via FT-IR analysis (Lozada et al., 2009).

Table 3. 8. Properties of the Alkoxyl Hydroxyl ESO polyols.
(Source: Lozada et al., 2009).

Sample	Temp/Time (°C/h)	Acid Value (mg KOH/g)	% Oxirane Oxygen	Saponification (mg KOH/g)	OH Exp. (mg KOH/g)	Color Index[a]
ESBO	25/0	0.5	7.0	183.3	11.5	0.0
Control	25/0	0.7	7.0	177.7	166.0	1.0
A	130/2	0.7	6.0	168.7	157.4	1.0
B	130/4	0.7	5.7	168.3	159.0	1.0
C	130/6	0.7	4.9	170.0	162.6	1.0
D	130/9	0.7	4.5	172.4	157.6	1.0
E	150/2	0.7	5.2	177.5	156.2	2.0
F	150/4	0.7	3.5	171.7	158.4	2.0
G	150/6	0.7	2.2	170.2	154.0	3.0
H	150/9	0.7	2.1	176.0	150.0	3.0
I	150/11	0.7	0.4	174.6	129.6	3.0
J	170/0.75	0.8	4.8	167.7	159.4	1.0
K	170/2	1.0	3.0	167.4	153.8	3.0
L	170/4	16.5	0.2	162.4	109.6	5.0
M	170/6	17.7	0.0	164.4	101.4	6.0

Das and Asefa (2011) examined epoxide (styrene oxide, chlorophylene oxide, and 2-methyl-1,2-epoxypropane) ring opening reactions with different alcohols which were methanol, ethanol, isopropyl alcohol, propyl alcohol, butyl alcohol, isobutyl alcohol in the presence of mesoporous silica supported Fe(III) catalyst which was prepared by hydrothermal synthesis. Immobilizing the metal complexes onto the surface of acidic mesoporous catalysts could increase their heterogeneous and mesoporous form. In order to achieve this goal, iron metals grafted onto the surface of mesoporous silica (SBA-15). Hence, its catalytic activity and efficiency of alcholoysis reaction increased. Firstly, styrene oxide and alcohols tested at the conditions given in Table 3.9.
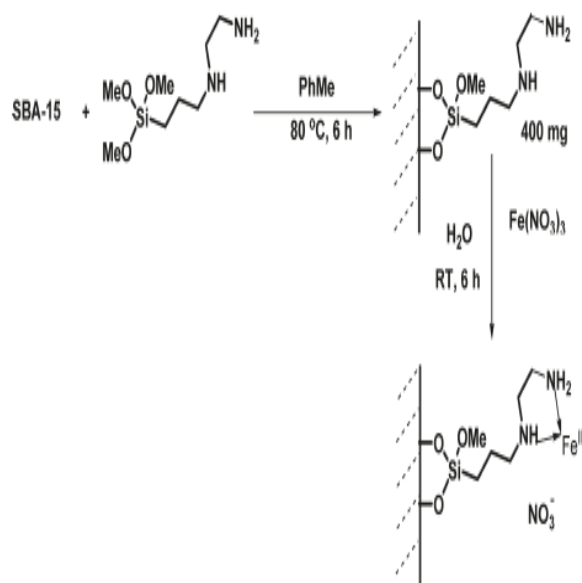
Figure 3. 5. The mesoporous silica supported Fe(III) catalyst preparation steps.
(Source: Das and Asefa 2011)

Table 3. 9. The reaction conditions of ring opening reaction of styrene oxide and
alcohols. (Source: Das and Asefa 2011).
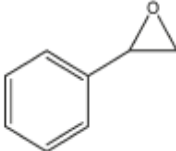
Entry	Alcohol	Temp (°C)	Time (h)	% Yield[b]	TOF (h^{-1})[c]
1	H$_2$O	RT	2	~100	157 343
2	MeOH	RT	6	~100	52 448
3	EtOH	RT	9	~100	34 965
4	n-PrOH	80	45	93	6503
5	i-PrOH	80	72	50	2185
6	n-BuOH	80	56	96	5395
7	i-BuOH	80	144 (6 days)	62	1355
8	t-BuOH	80	144 (6 days)	9	197

b, yield of polyol is calculated by GC. c, calculated using the 0.143 mmol/g Fe(III) that was obtained by ICP_AES for the Ext-SBA-15- en-Fe(III) sample.

Attempted reaction between styrene oxide and MeOH without the Ext-SBA-15-en-Fe(III) catalyst gave no product in 5 and 48 h and only 11% after 96 h. Then, different epoxides were tested with methanol at a molar ratio of 1:10 (ESO:methanol). The catalyst

amount was 2 % wt. of the solution. The reaction conditions and the results are given in Table 3. 10.

Table 3. 10. The reaction conditions and the results of ring opening reaction of different epoxides with methanol. (Source: Das and Asefa 2011)

Entry	Epoxide	Alcohol	Temperature (°C)	Time (h)	% Yield
1.		MeOH	50	5	~100 [b]
2.		MeOH	50	6	30 [c]
3.		MeOH	50	6	85 [d]

a, reaction between 0.9 mmol of epoxide and 5 ml of anhydrous MeOH in the presence of 20 mg of Ext-SBA15enFe(III) catalyst. b, the more substituted alcohol regioisomer 2-methoxy-2-phenylethannol was obtained. c, the less substituted alcohol regioisomer 1-chloro-3-methoxy-2-propanol was obtained. d, the more substituted alcohol regioisomer 2-methoxy-2-methyl-1-propanol was obtained.

The catalyst reacted with styrene oxide faster than the other epoxides using methanol. Among the alcohols, methanol gave the highest yield and conversion. According to the experimental results, it could be deduced that if the alkyl groups of linear alcohols were longer, then the reaction rates were slower.

Dhakshinamoorthy et al. (2012) synthesized graphene oxide by Hummers method and tested its catalytic performance on the ring opening reaction of epoxides at the milder reaction conditions. $NaNO_3$ and $KMnO_4$ were used as oxide source and they were dissolved in concentrated H_2SO_4. Then, the solution was used to oxidize graphite into graphite oxide. The ring opening reaction 1 ml of styrene oxide and 10 ml of methanol in the presence of 5 mg of graphene oxide was performed at the room temperature and almost >99% conversion and 93% selectivity was achieved in 1 h. Graphene and similar materials have fast charge mobility and high mechanical resistance so that they have

attracted much interest in chemistry to use as adsorbent, biosensor and heteregonous catalyst. They exhibited high surface area, solubility so there are no barries to mass transfer for molecule reaching the catalyst surface. For this reason, these material comparatively suitable as catalyst. The sulfate groups present in the GO were sufficient to as recoverable and recyclable Bronsted acid sites. The experimental results are given in Table 3. 11.

Table 3. 11. The experimental results. (Source: Dhakshinamoorthy et al., 2012)

Run	Catalyst	Time/min	Conversion[b] (%)	Selectivity[b] (%)	
				2a	3a
1	GO	10	91	99	1
2	GO	20	96	96	4
3	GO	60	99	93	7
4	GO	60	2[c]	100	-
5	GO	60	99[d]	97	3
6	GO	60	69[e]	91	9
7	GO	240	97[e]	90	10
8	GO	360	98[e]	90	10
9	Norit A	60	5	99	-
10	H_2SO_4	5	99	99	-
11	p-CH_3-C_6H_4-SO_3H	5	99	99	-
12	CH_3COOH	60	-	-	-

a, reaction conditions:1a (1 ml), methanol (10 ml), catalyst (5 mg), room temperature, b, determine by GC, c, with 0.1 ml of pyridine. d, after third reuse. e, reaction conditions: 1a (3 ml), methanol (15 ml), catalyst (2 mg), room temperature.

Ahn et al. (2012) carried out a study over the production of soy oil-based polyols using a heterogeneous catalyst, which was sulfamic acid-functionalized iron (iron/iron oxide core-shell) nanoparticles (NPs). In this study, firstly, superparamagnetic core/shell Fe/Fe_3O_4 nanoparticles synthesized and then, they were coated with 3-aminopropyl triethoxysilane (APTES). Finally, they were functionalized using sulfamic acid. The

synthesis steps of catalyst are given Figure 3. 6. Fe/Fe$_3$O$_4$ nanoparticles exhibited higher catalytic activity. They were synthesized environmentally friendly and used in alcoholysis reaction. New sulfamic acid functionalized APTES coated catalyst gave high conversion.
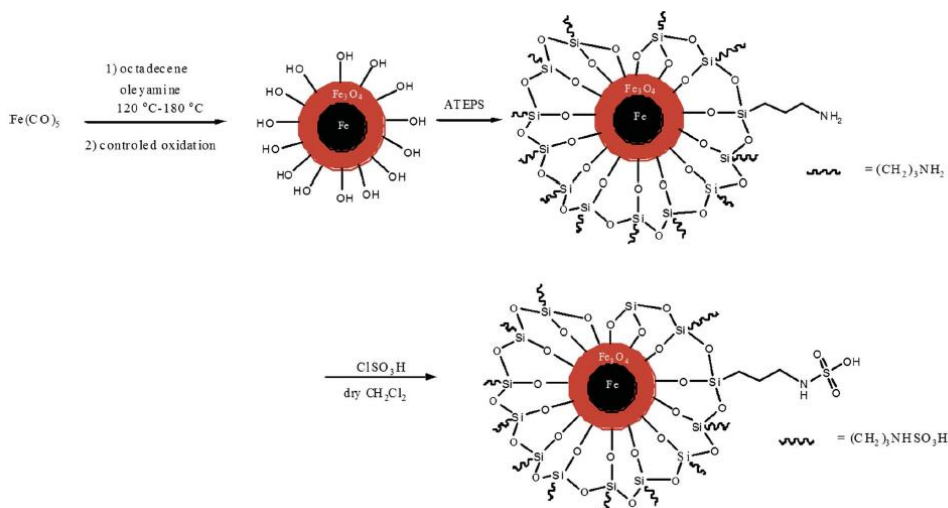
Figure 3. 6. The synthesis steps of sulfamic acid-functionalized iron (iron/iron oxide core-shell) nanoparticles (NPs). (Source: Ahn et al., 2012)

The synthesized catalyst used for the ring opening of epoxidized methyl oleate (EMO). The experiments were carried out using 0.2 g of EMO and 0.2 g of methanol at room temperature for 30 min. The comparison of the efficiency of the SAC 13 and Amberlite 15 with the synthesized catalyst implied that this catalyst showed higher yield, lower reaction duration, and temperature. Also, if the synthesized catalyst and sulfuric acid are compared, it could be concluded that the synthesized catalyst cause to produce clean products rather than the sulfuric acid. The synthesized catalyst tested for reuse performance and found that 100% epoxy ring-opening conversion and 100% selectivity of a-methoxy-hydroxylation in five subsequent uses. In order to investigate the environmental effect of this chemical process, a life cycle assessment study was carried out and it was found that the synthesized catalyst is equal or superior to SAC 13 and Amberlite 15 (Ahn et al., 2012).

Kahandal (2012) et al. carried out a study over the epoxide ring opening reaction with ethanol in the presence of sulphated yttria-zirconia catalyst. The molar ratio of alcohol:ESO was selected as 1:1 and the catalyst loading was 10 % wt. with respect to the amount of ESO. The characterization study of the synthesized catalyst was performed

via XRD, TGA, SEM/EDAX, and total acidity. The results show that the synthesized catalyst was an environmentally benign, regioselective, efficient, economical and reusable catalyst. This catalyst was used as a Lewis acid and regioselective epoxidation reaction took place in the presence of this catalyst. The efficiency and reusability of catalyst is given in Table 3. 12 and Table 3. 13, respectively.

Table 3. 12. The efficiency of sulphated yttria-zirconia catalyst.
(Source: Kahandal et al., 2012)

Entry	Catalyst/wt %	Yield[b] (%)
1	5	55
2	10	96
3	15	96
4	20	97

Table 3. 13. The reusability of sulphated yttria-zirconia catalyst.
(Source: Kahandal et al., 2012)

Run	Isolated Yield
1	96
2	96
3	95
4	94

Additionally, it could be used for plenty of aliphatic, aromatic alcohols and aromatic amines. This process did not need to use any solvent so that it could be concluded that this process is efficient and environmentally friendly.

3.3. Outcomes from Literature Survey

Many studies about the polyol synthesis from epoxidized vegetable oils are carried out by several methods. Among these methods, the epoxidation-hydroxylation is the most commonly used process since it is simple and could be controlled easily. Also, different types of polyols could be formed by the opening of the epoxide groups using various agents such as methanol, and propanol.

Polyol production by the epoxidation-hydroxylation was carried out using different type of vegetable oils. Soybean oil is one of the most commonly used vegetable oil to produce vegetable oil based polyols since it is abundant, relatively cheaper than the others. Furthermore, it has more than four double bonds per molecule so it is a good

alternative to produce vegetable oil based polyol production. Therefore, it was decided to use soybean oil to produce polyol by epoxidation-hydroxylation method.

In the literature survey part, particularly, soybean oil based polyols which were produced by epoxidation-hydroxylation in the presence of homogeneous and heterogeneous catalysts were summarized. The studies show that the heterogeneous catalysts can give higher yield and lower reaction duration than the homogeneous ones. The ring opening reaction is performed over heterogeneous catalysts, especially, mesoporous and acidic because they show higher catalytic activity and efficient in the ring opening reaction. Therefore, in the light of the literature survey, it was aimed to prepare Zr and Ti incorporated SBA-15 catalysts to test their performance on production of soy based polyol.

According to the literature survey, various type of alcohol was used in the ring opening reaction step and it could be concluded that, if the branched alcohols were used in the ring opening reaction, the selectivity decreases. Methanol was the most commonly used ring opening agent, and hence, it was decided to use methanol in this thesis.

CHAPTER 4

EXPERIMENTAL STUDY

In this study, Zr and Ti incorporated SBA-15 catalysts were synthesized and tested for polyol production from epoxidized soybean oil. Zr–SBA15 and Ti-SBA15 catalysts were prepared through hydrothermal synthesis. Their sulfated forms were also prepared as catalysts.

4.1. Materials

The list of chemicals used and the properties of ESO in this study are given in Table 4. 1. and Table 4. 2., respectively.

Table 4. 1. The list of chemicals used in this study.

Chemicals	Brand / Purity
Pluronic P123	Aldrich average $M_w \sim 5{,}800$
Zirconium (IV) oxychloride octahydrate	Sigma Aldrich ≥ 99.5
Tetraethyl orthosilicate (TEOS)	Aldrich 98%
Titanium isopropoxide (TISOP)	Sigma Aldrich $\geq 97\%$
Hydrochloric acid (HCl)	Sigma Aldrich 37%
Ammonium Sulfate $(NH_4)_2SO_4$	Sigma Aldrich $\geq 99\%$
Sulfuci Acid (H_2SO_4)	Sigma Aldrich $\geq 95\text{-}98\%$
ESO	Plastifay Kimya Endüstrisi A.Ş.

Table 4. 2. The properties of ESO used in this study.

Oxirane Oxygen	7.2%
Acidity	1 (mg.KOH/g)
Density	0.993 g/cm^3
Viscosity	4.2 cP
Molecular Weight	1000 g/mole

4.2. Catalyst Preparation

4.2.1. Preparation of Zr-SBA15 and Sulfated Zr-SBA15 Catalysts

Zr-SBA15 was synthesized for two different Zr contents where the molar ratio of Zr:Si were 0.08:1 and 0.1:1. They were labelled as Zr-SBA15 (08) and Zr-SBA15 (10), respectively. The catalyst preparation procedure was based on the study by Değirmenci et al. (Değirmenci et al., 2009).

The Zr-SBA15 (08) catalyst was prepared for the molar ratio of P123:Si:Zr:H$_2$O as 0.017:1.0:0.08:220. The amphiphilic copolymer P123 was used as the surfactant and 5 g of P123 was dissolved in 150 ml of deionized water with continuous stirring at 37 °C until the transparent solution was obtained. Besides, 1.31 g zirconium (IV) oxychloride octahydrate was dissolved in 50 ml of deionized water with continuous stirring at room temperature until the clear solution was obtained. Then, 11.53 ml of TEOS and the aqueous zirconium (IV) oxychloride octahydrate solution was added to the P123 solution. The mixture was vigorously stirred at 37 °C for 24 h. After stirring the gel formed was transferred into a Teflon-lined stainless steel autoclave and kept at 100 °C for 24 h. The obtained gel was centrifuged with an excess amount of deionized water for four times to remove the impurities. After that, the gel was dried overnight at room temperature. Finally, the dried gel was calcined at 550 °C for 4 h. During the calcination step, the heating rate to 550 °C was 5 °C/min and the cooling rate to 35 °C was 3 °C/min. In order

to prepare Zr-SBA15 (10) catalyst, the same procedure was repeated using 1.63 g zirconium (IV) oxychloride octahydrate.

To prepare SO$_4$/Zr-SBA15 (08) and SO$_4$/Zr-SBA15 (10) catalysts, previously obtained Zr-SBA15 (08), Zr-SBA15 (10) were sulfated with 1 M H$_2$SO$_4$. Firstly, 1 g of Zr-SBA15 (08) was mixed with 5 mL of 1 M H$_2$SO$_4$ at 37 °C for 3 h. Then, the obtained gel was calcined at 550 °C for 4 h. During the calcination step, the heating rate to 550 °C was 5 °C/min and the cooling rate to 35 °C was 3 °C/min. This procedure was also applied for the preparation of SO$_4$/Zr-SBA15 (10) catalyst using Zr-SBA15 (10) catalyst.

4.2.2. Preparation of Ti-SBA15 and Sulfated Ti-SBA15 Catalysts

Ti-SBA15 was synthesized for the two different Ti contents, Si:Ti molar ratio 1:10 and 1:20 which were labeled as Ti-SBA15 (10) and Ti-SBA15 (20), respectively. They were prepared based on the method given by Sharma et al. (Sharma et al., 2012).

Ti-SBA15 (10) catalyst was prepared for the molar ratio of TEOS:TISOP:P123: HCl:H$_2$O as 0.095:0.0095:0.0016:0.046:12.2. The amphiphilic copolymer P123 was used as the surfactant. Firstly, 9 g of P123 was dissolved in 220 ml of deionized water at 40 °C. Secondly, 3.78 mL of HCl (37%) was added drop by drop into the solution and the final solution was stirred for 2 h. Thirdly, the mixture of TEOS and TISOP was prepared by mixing 21.4 mL of TEOS and 2.9 mL of TISOP. Fourthly, the mixture of TEOS and TISOP was added drop by drop into the solution at 40 °C and stirred for 24 h. The final mixture was put into the autoclave and kept at 40 °C for 24 h. After that, it was dried at 100 °C for 12 h and calcined at 550 °C for 6 h. During the calcination step, the heating rate to 550 °C was 5 °C/min and the cooling rate to 35 °C was 3 °C/min. Finally, Ti-SBA15 (10) catalyst was obtained. In order to prepare Ti-SBA15 (20) catalyst, the same procedure was repeated using 2.9 mL of TISOP.

In order to synthesize SO$_4$/Ti-SBA15 (10) and SO$_4$/Ti-SBA15 (20) catalysts, the prepared Ti-SBA15 (10), Ti-SBA15 (20) and 1 M (NH$_4$)$_2$SO$_4$ were used. Firstly, 1 g of Ti-SBA15 (10) was mixed with 5 mL of 1 M (NH$_4$)$_2$SO$_4$ at 40 °C for 3 h. Then, the obtained gel was calcined at 550 °C for 6 h. During the calcination step, the heating rate

to 550 °C was 5 °C/min and the cooling rate to 35 °C was 3 °C/min. The same procedure was repeated for the preparation of SO$_4$/Ti-SBA15 (20) catalyst using Ti-SBA15 (20) catalyst.

4.3. Characterization of Catalysts

The characterization study was carried out in order to investigate the characteristic properties of the prepared catalysts which are Zr-SBA15 (08), Zr-SBA15 (10), SO$_4$/Zr-SBA15 (08), SO$_4$/Zr-SBA15 (10), Ti-SBA15 (10), Ti-SBA15 (20), SO$_4$/Ti-SBA15 (10) and SO$_4$/Ti-SBA15 (20). In this context, N$_2$ adsorption, skeletal FT-IR Spectroscopy, X-Ray Diffraction (XRD), Pyridine Adsorbed FT-IR, and Temperature Programmed Desorption of Ammonia (NH$_3$-TPD) analyses were performed. The analysis details are given under the following subheadings.

4.3.1. N$_2$ Adsorption (BET)

Nitrogen physisorption studies were performed using Micromeritics ASAP2010 model static volumetric adsorption instrument. All catalysts were degassed at 200 °C for 2 hours prior to adsorption experiments. N$_2$ adsorption was performed at 77 K.

4.3.2. Skeletal FT-IR Spectroscopy

The framework vibration of synthesized all catalysts was examined by FT-IR spectroscopy. KBr pellet technique was employed to obtain infrared spectra of the samples at room temperature. The pellets were prepared with a sample amount of 3 wt%. The spectra were retrieved in the wavenumber range of 400 – 4000 cm^{-1} with a resolution of 4 cm^{-1} by an infrared spectrometer type Shimadzu FTIR 8400S.

4.3.3. X-Ray Diffraction (XRD)

The crystalline structures of the samples were determined by X-Ray diffraction type Philips X'Pert diffractometer with CuK radiation. The scattering angle 2Θ was changed from 5° to 80° with a step length of 0.002.

4.3.4. Pyridine Adsorbed FT-IR

Bronsted and Lewis acidity characteristics of the catalysts were determined by IR spectroscopy using pyridine adsorption/desorption method. For the analysis, the samples were activated at 300 °C under vacuum (2×10^{-2} mmHg) for 2 hours. Adsorption of pyridine was carried out at 150 °C for 30 min. Before FT-IR analysis the samples were kept at 120 °C under an N_2 flow of 30 ml/min for 2 h in order to desorb the physisorbed pyridine. IR analyses were carried out between 400 and 4000 cm^{-1} with Shimadzu FT-IR 8400s model FT-IR Spectrometer using KBr pellet technique. KBr pellets were prepared by pressing a mixture of 2 mg of pyridine adsorbed catalyst sample and 150 mg KBr.

4.3.5. Temperature Programmed Desorption of Ammonia

The acidity of the synthesized catalysts was determined by Temperature-Programmed Desorption of Ammonia (NH_3-TPD) method using Micromeritics AutoChem II Chemisorption Analyzer instrument.

The catalysts samples were heated up to 400 °C by increasing the temperature at a rate of 5 °C/min and kept at this temperature for 30 min under He gas flow of 70 ml/min. Then, the sample was cooled under He flow of 30 ml/min to 60 °C at a rate of 5 °C/min. After this step, it was followed by switching the flow to NH_3-He gas mixture at the rate of 30 ml/min for 30 min. Physically adsorbed NH_3 was removed by degassing the sample at 60 °C under He flow of 70 ml/min for 120 min. NH_3 desorption of the sample was

analyzed by heating the sample at the rate of 10 °C/min from 60 °C to 700 °C. TCD signal was recorded during the NH$_3$-TPD.

4.4. Catalyst Testing

Soy based polyol synthesis reactions by Zr-SBA15 (08), Zr-SBA15 (10), SO$_4$/Zr-SBA15 (08), SO$_4$/Zr-SBA15 (10), Ti-SBA15 (10), Ti-SBA15 (20), SO$_4$/Ti-SBA15 (10) and SO$_4$/Ti-SBA15 (20) catalysts were carried out in a three neck round bottom flask (250 mL) equipped with a Teflon coated magnetic stirring bar and a Dean Stark apparatus surmounted with a reflux condenser. The experimental set-up is shown in Figure 4. 1. Catalyst testing reaction carried out using ESBO with 7.2% oxirane content and methyl alcohol. Feed composition was selected as molar ratio of methyl alcohol and epoxide 11:1 and catalyst amount was 2 wt% of reaction solution. Reaction temperature and time were 60 °C and 6 h, respectively.

Figure 4. 1. Experimental Set-Up.

4.4.1. Polyol Production by Homogeneous Catalyst (H_2SO_4)

The homogeneous catalyst experiments were carried out solvent free, taking a molar ratio of methanol:ESO as 11:1 and 10 wt% H_2SO_4 catalyst (0.003) with respect to total weight. The reaction temperature and reaction duration were 60 °C, and 4 h, respectively.

Firstly, methanol (39.6 g) and H_2SO_4 (50 mL) were added into a 250 ml three neck flask and they were mixed until reaching the desired temperature for 15 min. Then, epoxidized soy bean oil (25 g) was added dropwise over a period of 1 h. After that, the mixture was allowed to react at 60 °C for 4 h and the samples were taken in every hour during the reaction. After cooling to room temperature, ammonia (%30) was added to the mixture in order to neutralize the solution. Finally, the solvent was removed by a rotary evaporator under a low vacuum at 60 °C for 0.5 h, followed by 95 °C for 1 h. Finally, the obtained products were analyzed by FT-IR, H-NMR and analytic method to determine oxirane content.

4.4.2. Polyol Production over Heterogeneous Catalysts

The heterogeneous catalyst experiments were also carried out solvent free system, taking a molar ratio of methanol:ESO as 11:1 and 2 wt% catalysts (Zr-SBA15 (08), Zr-SBA15 (10), SO_4/Zr-SBA15 (08), SO_4/Zr-SBA15 (10), Ti-SBA15 (10), Ti-SBA15 (20), SO_4/Ti-SBA15 (10) and SO_4/Ti-SBA15 (20)) with respect to total weight. The reaction temperature and reaction duration were 60 °C and 6 h, respectively.

Firstly, methanol (39.6 g) and Zr-SBA15 (08) (0.5 g) were added into a 250 ml three neck flask and they were mixed until reaching the desired temperature of 60 °C for 15 min. Then, epoxidized soy bean oil (25 g) was added into the mixture. After that, the mixture was allowed to react at 60 °C for 6 h and the samples were taken every two hours during the reaction. They were centrifuged to separate the catalyst, polyol and methanol. Firstly, methanol was removed by a pipette. Secondly, polyol and catalyst were separated

by filtration. Finally, the obtained products were analyzed by FT-IR, H-NMR and analytic method to determine oxirane content.

4.5. Product Analysis

4.5.1. Proton Nuclear Magnetic Resonance Spectroscopy (H-NMR)

In order to determine the H-NMR spectra, firstly, 3 µL of products were dissolved in 5 mL of chloroform. The prepared solutions were analyzed via 300 MHz NMR spectrometer, Bruker Biospin.

4.5.2. FT-IR Spectroscopy

The framework vibration of the products was examined by FT-IR spectroscopy. KBr pellet technique was employed to obtain infrared spectra of the samples at room temperature. The pellets were prepared with a sample amount of 3 wt%. The spectra were retrieved in the wavenumber range of $400 - 4000$ cm^{-1} with a resolution of 4 cm^{-1} by an infrared spectrometer type Shimadzu FTIR 8400S.

4.5.3. Viscosity

The viscosities of products were determined by a Haake Mars II model rheometer device in Psa unit at room temperature.

4.5.4. Gel Permeation Chromatography (GPC)

The molecular weight of products was determined via gel permeation chromatography using polystyrene standard in THF (elution rate: 1 mL/min) at 35 °C. These analyses were conducted via Waters 600E GPC unit equipped with a refractive index detector model Waters 2410. The flow of injection was 0.4 mL/min.

4.5.5. Oxirane Number

ESO with %6-7 oxirane index was supplied from Plastifay Kimya Endüstrisi A.Ş. Molecular weights of ESO was also determined by GPC analysis. Oxirane oxygen number was determined using the given formula by hydrohalogenation procedure (Gerhard Maerker, 1965). In this procedure, hydrogen ion in HBr (37 %, 1 N) was used to open oxirane ring in products at a stoichiometric ratio and the reaction mechanism is shown in Figure 4. 2.
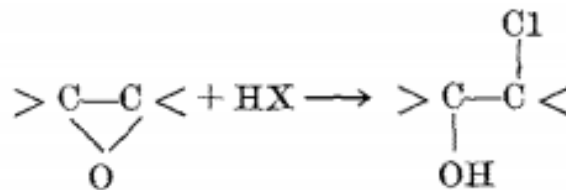
Figure 4. 2. Oxirane ring opening reaction
(source: Gerhard Maerker, 1965)

$$\% \text{ oxirane} = \frac{\text{Consumed HBr} * N_{HBr} * MW_{oxygen}}{\text{Sample mass}} \qquad Eqn(\,4.1.\,)$$

Consumed HBr, mL

N_{HBr}: normality of HBr, g/L

MW_{oxgyen}: Molecular weight of oxygen, g/mol

Sample mass: g

CHAPTER 5

RESULTS AND DISCUSSION

5.1. Characterization of the Catalysts

5.1.1. SBA-15

Small angle X-ray diffraction (SXRD) patterns of SBA-15 given in Figure 5. 1. It showed a typical pattern of a hexagonal phase with the occurrence of three well resolved diffraction peaks correspond to the planes indexed to (100), (110) and (200). This is associated with highly ordered mesoporous SBA-15 with two dimensional hexagonal symmetry (Mutlu and Yılmaz., 2016).
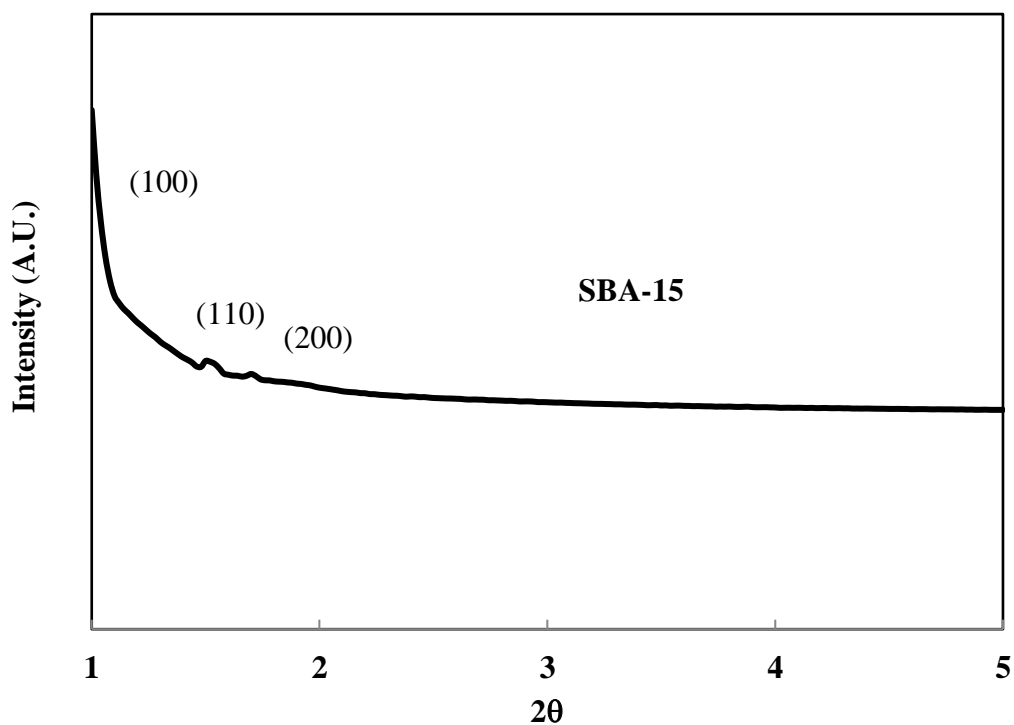

Figure 5. 1. XRD patterns of SBA-15.

The NH$_3$-TPD profile of SBA-15 is given in Figure 5. 2. Temperature – programmed sdesorption of NH$_3$-TPDwas employed to compare with NH3-TPD patterns of prepared caalysts. SBA-15 did not show any acid sites (Mutlu and Yılmaz., 2016).
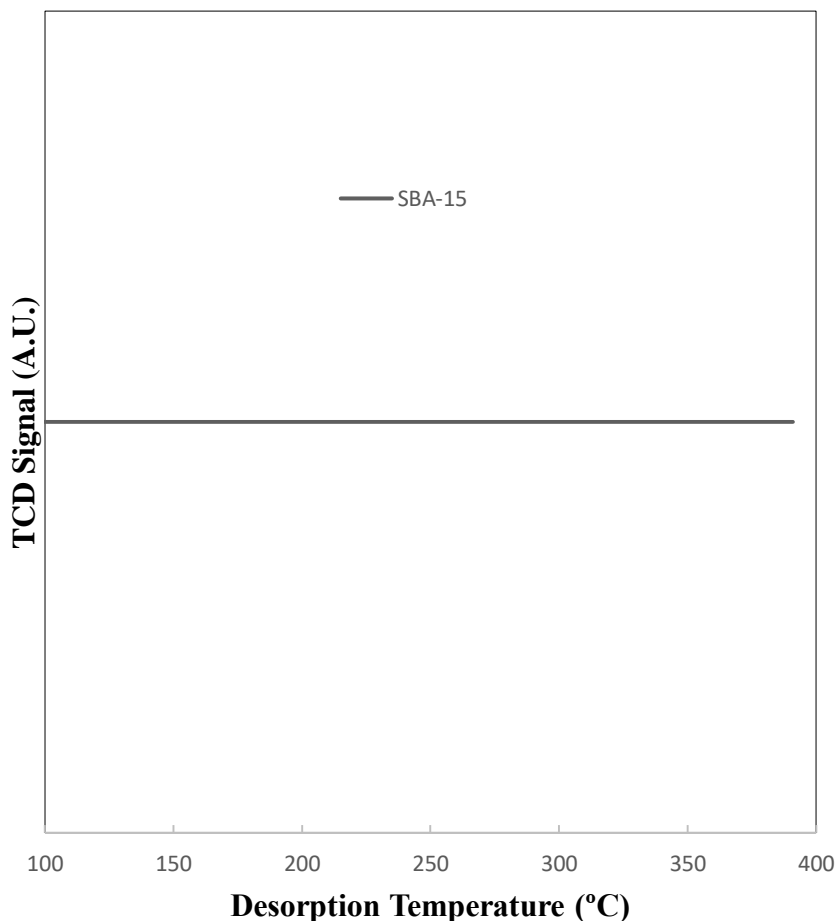
Figure 5. 2. NH$_3$- TPD profile of SBA-15

5.1.2. Zr-SBA15 (08) and Zr-SBA15 (10) Catalysts

N$_2$ adsorption isotherms of Zr-SBA15 (08) and Zr-SBA15 (10) are given in Figure 5. 3. Adsorption on mesoporous solids proceeds via multilayer adsorption followed by capillary condensation. According to the characteristic features of isotherm, its hysteresis loop proves that the capillary condensation takes place in mesoporous. The adsorption isotherms of type IV, which indicated that Zr-SBA15 (08) and Zr-SBA15 (10) catalysts have mesoporous structure.
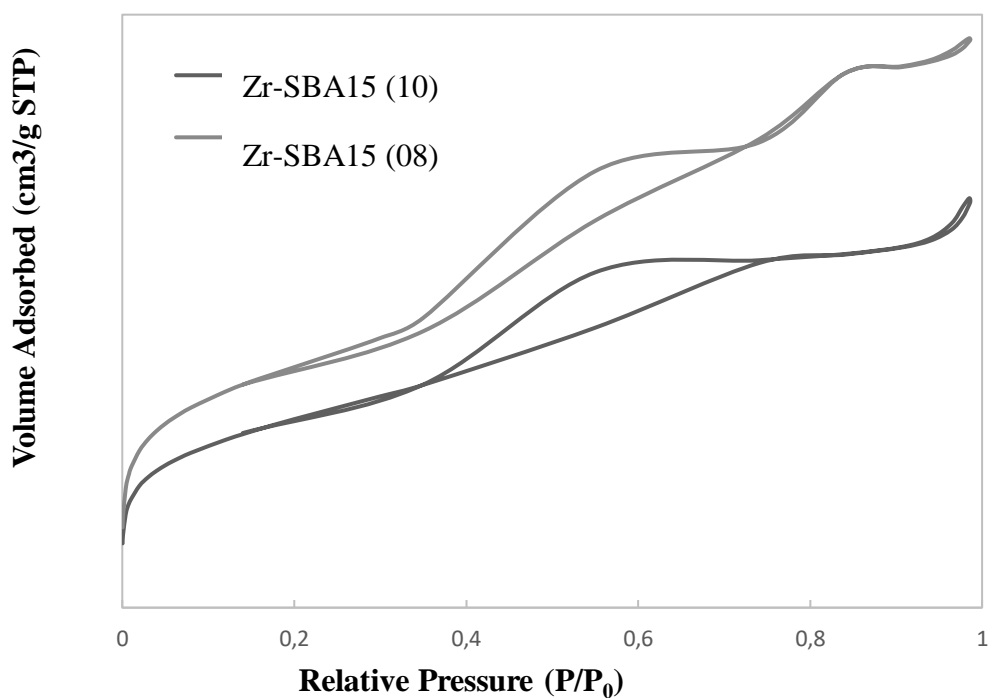
Figure 5. 3. N$_2$ adsorption/desorption isotherm of Zr-SBA15 (08) and Zr-SBA15 (10) catalysts.

The specific surface area, pore volume and pore diameter of Zr-SBA15 (08) and Zr-SBA15 (10) were determined by BET method and the results are given in Table 5. 1. The Zr-SBA15 (08) had higher BET surface area, pore volume and pore diameter than the Zr-SBA15 (10). Zr amount was higher for Zr-SBA15 (10) than Zr-SBA15 (08), so that it might cause the clogging of the SBA15 pores and a decrease in BET surface area, pore volume and pore diameter.

Table 5. 1. Textural properties analysis of Zr-SBA15 (08) and Zr-SBA15 (10) catalysts.

Catalyst	BET Surface Area, m²/g	Pore Volume, cm³/g	Pore Diameter, Å	Total Acidity (mmol NH$_3$/g cat.)
Zr-SBA15 (08)	696.77	0.74	42.63	1.2
Zr-SBA15 (10)	554.68	0.53	38.50	1.8

The crystal structure of Zr-SBA15 (08) and Zr-SBA15 (10) was investigated with X-Ray Diffraction where the 2θ angles changed from 5 ° to 80 ° and the results are given in Figure 5. 4. The higher peaks close to 25° refer that Zr which was successfully incorporated in SBA15. No peaks of Zr was observed. This indicated that Zr was successfully incorporated (Dong et. al., 2010).
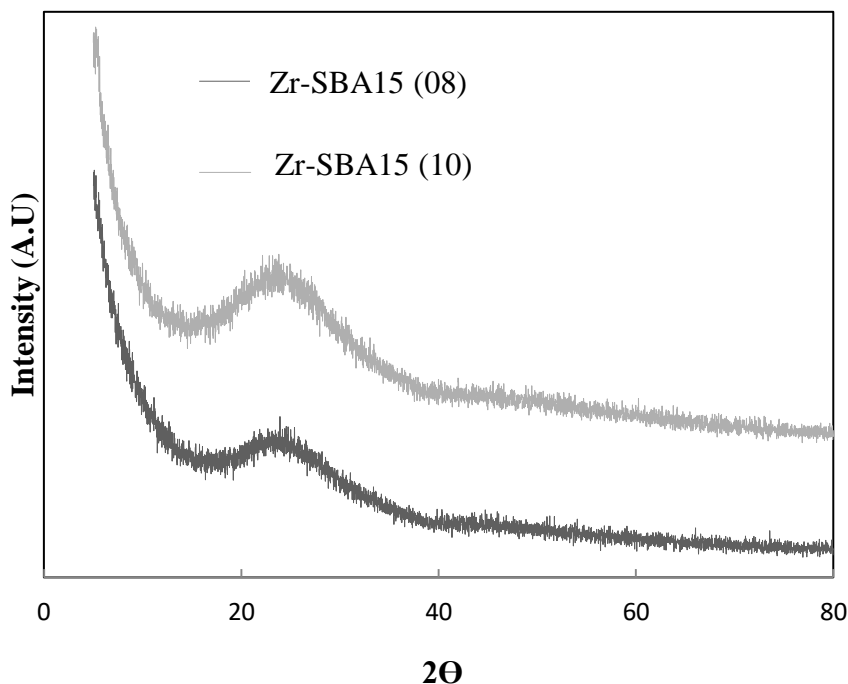

Figure 5. 4. XRD patterns of Zr-SBA15 (08) and Zr-SBA15 (10) catalysts.

The acidity of Zr-SBA15 (08) and Zr-SBA15 (10) catalysts were determined by NH_3-TPD analysis. The results are shown in Figure 5. 5. The peak of Zr-SBA15 (08) and Zr-SBA15 (10) catalysts were widely spread. Zr-SBA15 (10) had higher acidity than Zr-SBA15 (08). The desorption peaks were centered around 300 °C and 560 °C. The peak at low temperature (around 300 °C) and the peak at high temperature (around 560 °C) refer to as weak and strong acid sites. Zr-SBA15 (08) had higher amount strong acid sites (Mutlu and Yılmaz, 2016). Total acidity of the Zr based catalysts increased with Zr amount. While Zr-SBA15 (08) had 1.2 mmol NH_3/g catalyst, Zr-SBA15 (10) had 1.8 mmol NH_3/g catalyst.
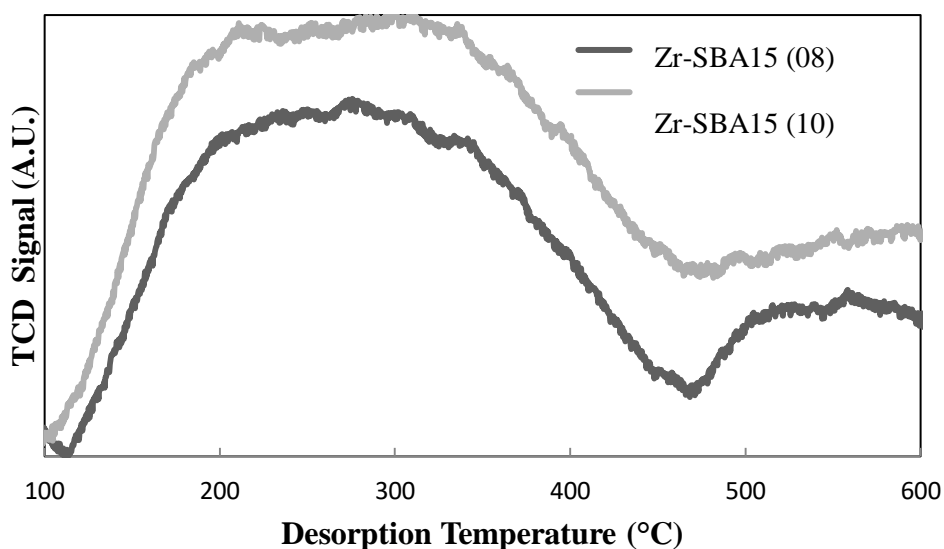
Figure 5. 5. NH$_3$-TPD profiles of Zr-SBA15 (08) and Zr-SBA15 (10) catalysts.

The skeletal FT-IR spectra of Zr-SBA15 (08) and Zr-SBA15 (10) catalysts is given in Figure 5. 6. The symmetric stretching of Si-O-Si bonds cause the peaks observed at the range of 1053 cm^{-1} and 1220 cm^{-1}. Additionally, a peak was observed at 418 cm^{-1} due to the vibration of Si-O-Si bond. The Si-O-Zr bond, which is formed by the incorporation of Zr on the SBA15, was observed at 966 cm^{-1}. The existence of this band proves that the incorporation of Zr in SBA15 for Zr-SBA15 (08) and Zr-SBA15 (10) catalysts was successfully achieved (Dong et.al., 2010).
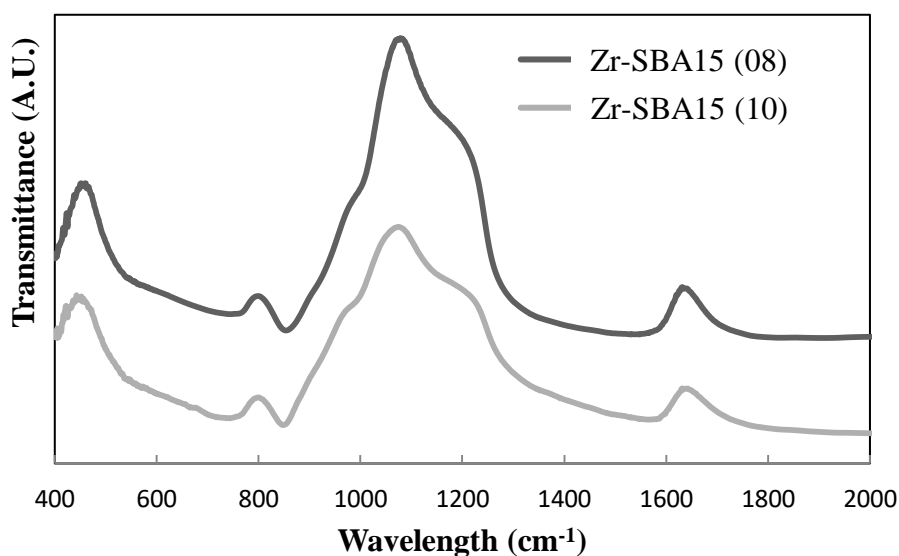
Figure 5. 6. Skeletal FT-IR spectra of Zr-SBA15 (08) and Zr-SBA15 (10) catalysts.

The FT-IR spectra of pyridine adsorbed Zr-SBA15 (08) is given Figure 5. 7. The peak 1445 cm^{-1} indicates that Lewis acid sites. 1495 cm^{-1} indicates that both Lewis and Bronsted acid sites. 1540 cm^{-1} indicates Bronsted acid sites.
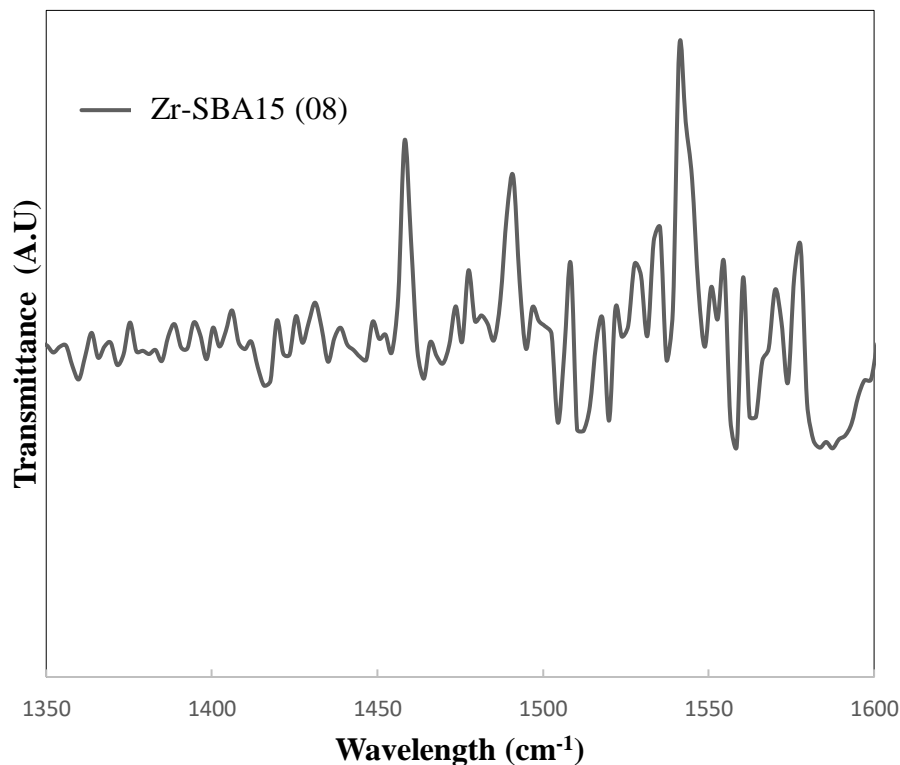

Figure 5. 7. FT-IR spectra of pyridine absorbed Zr-SBA15 (08) catalysts.

5.1.3. SO$_4$/Zr-SBA15 (08) and SO$_4$/Zr-SBA15 (10) Catalysts

N$_2$ adsorption/desorption isotherms of SO$_4$/Zr-SBA15 (08) and SO$_4$/Zr-SBA15 (10) are given in Figure 5. 8. and Figure 5. 9. The specific surface area, pore volume and pore diameter of SO$_4$/Zr-SBA15 (08) and SO$_4$/Zr-SBA15 (10) were determined by BET method and the results are given in Table 5. 2. SO$_4$/Zr-SBA15 (08) and SO$_4$/Zr-SBA15 (10) had mesoporous structure. This indicated that the structure was preserved after sulfonation.
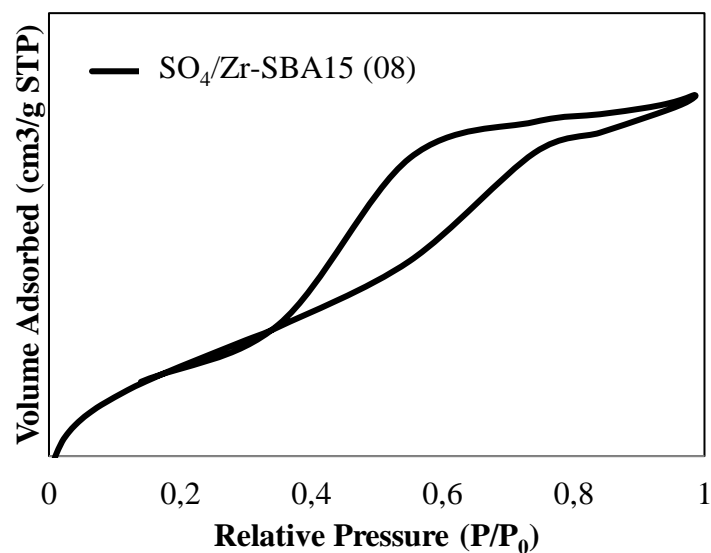
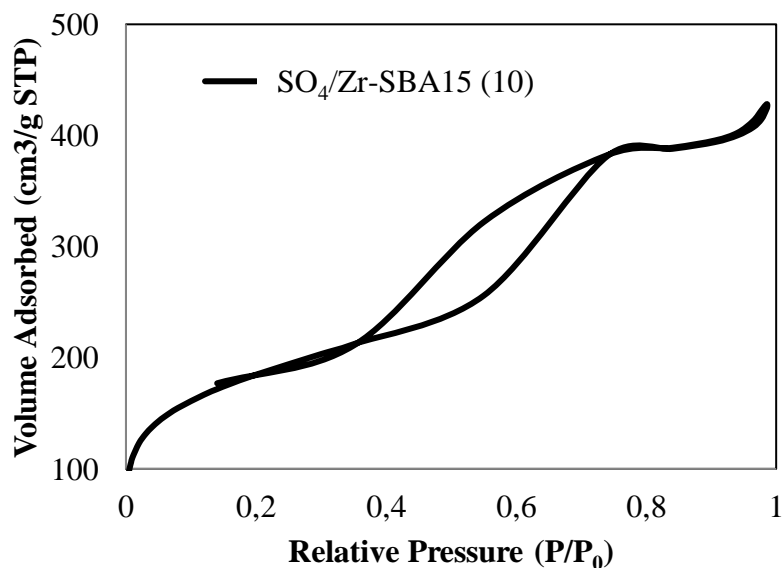Figure 5. 8. N_2 adsorption/desorption isotherms of SO_4/Zr-SBA15 (08) catalyst.

Figure 5. 9. N_2 adsorption/desorption isotherms of SO_4/Zr-SBA15 (10) catalyst.

Table 5. 2. Textural properties of SO_4/Zr-SBA15 (08) and SO_4/Zr-SBA15 (10) catalysts.

Catalyst	BET Surface Area, m^2/g	Pore Volume, cm^3/g	Pore Diameter, Å	Total Acidity (mmol NH_3/g cat.)
SO_4/Zr-SBA15 (08)	639.51	0.66	41.22	3.9
SO_4/Zr-SBA15 (10)	630.77	0.66	41.10	3.2

According to BET results, the SO_4/Zr-SBA15 (08) and SO_4/Zr-SBA15 (10) had close BET surface areas and the similar pore volume and pore diameter. Whereas SO_4/Zr-SBA15 (08) had lower BET surface area, pore volume and pore diameter than Zr-SBA15 (08), SO_4/Zr-SBA15 (10) had higher BET surface area, pore volume and pore diameter than Zr-SBA15 (10). Therefore, sulfonation affected surface areas of the catalysts differently.

The crystal structure of SO_4/Zr-SBA15 (08) and SO_4/Zr-SBA15 (10) was investigated with X-Ray Diffraction where the 2θ angles changed from 5 ° to 80 ° and the results are given in Figure 5. 10. XRD patterns of the sulfated catalysts were similar to their parent forms. Therefore, it could be said that the structure was preserved after sulfonation.
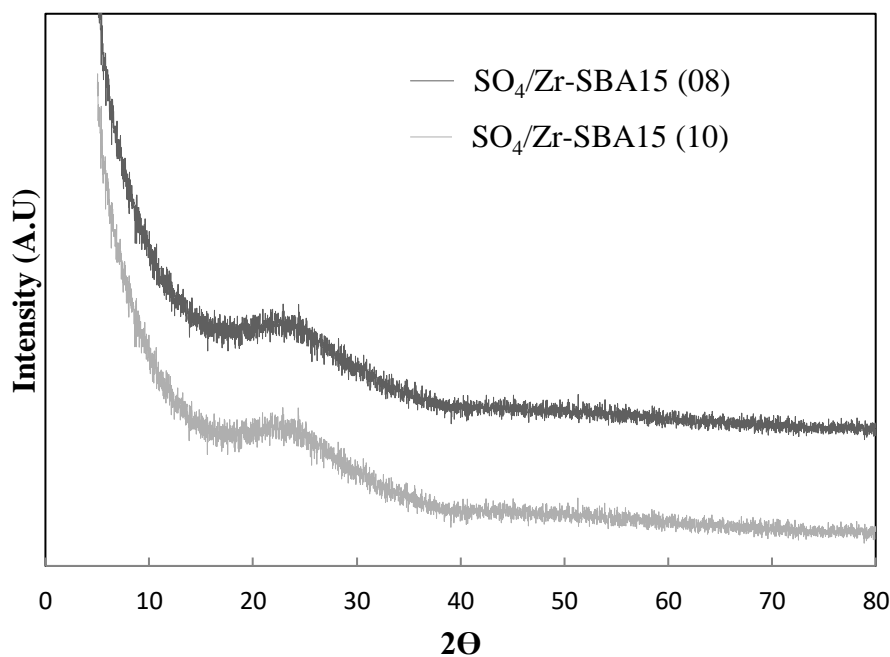

Figure 5. 10. XRD patterns of SO_4/Zr-SBA15 (08) and SO_4/Zr-SBA15 (10) catalysts.

The acidity of SO_4/Zr-SBA15 (08) and SO_4/Zr-SBA15 (10) catalysts were determined by NH_3-TPD analysis. The results are shown in Figure 5. 11. The catalyst showed one desorption peak mainly. The desorption temperature ranged from about 100 °C to 550 °C for SO_4/Zr-SBA15 (08) catalyst and from 140 °C to 480 °C for SO_4/Zr-SBA15 (10) catalyst. This indicated that SO_4/Zr-SBA15 (08) had higher acidity (3.9 mmol NH_3/g catalyst) than SO_4/Zr-SBA15 (10) (3.2 mmol NH_3/g catalyst). Similar results were obtained in the study of Yi et al. (Yi et al., 2015).
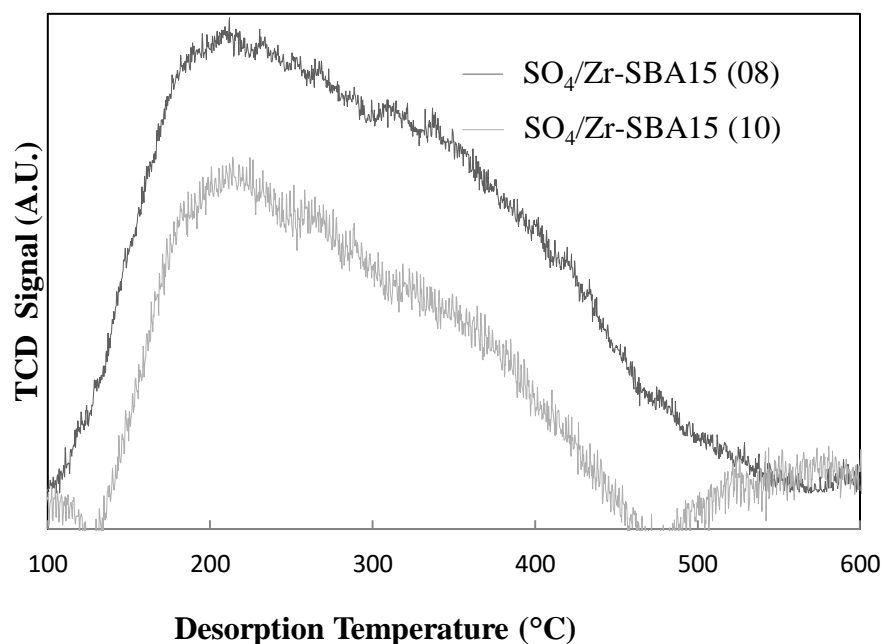
Figure 5. 11. NH$_3$-TPD profiles of SO$_4$/Zr-SBA15 (08) and SO$_4$/Zr-SBA15 (10) catalysts.

The skeletal FT-IR spectra of SO$_4$/Zr-SBA15 (08) and SO$_4$/Zr-SBA15 (10) catalysts is given in Figure 5. 12. The pyridine adsorbed FT-IR spectra of SO$_4$/Zr-SBA15 (08) catalysts is given in Figure 5. 13. Sulfated catalysts had similar FT-IR spectra with their parent forms. This indicated that sulfonation did not change the structure of the catalysts. The catalysts had Bronsted and Lewis acid sites.
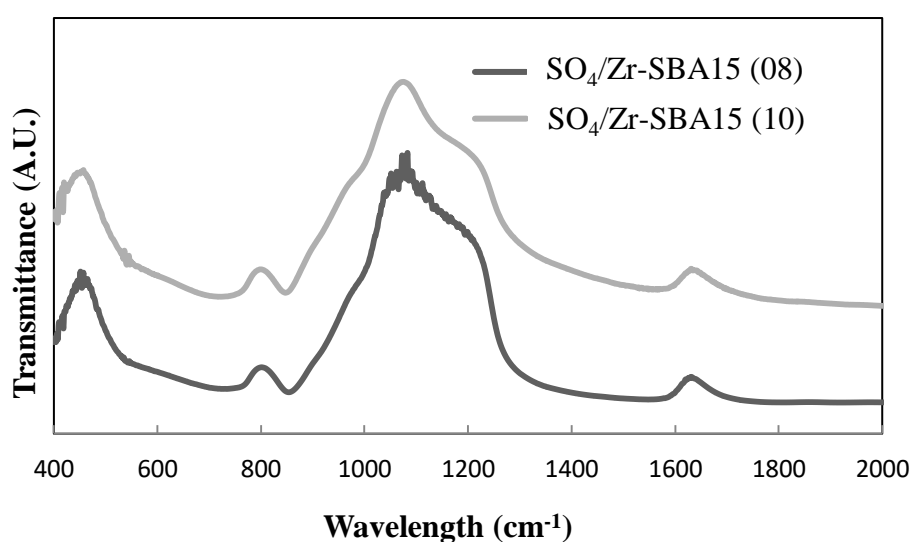

Figure 5. 12. The skeletal FT-IR spectra of SO$_4$/Zr-SBA15 (08) and SO$_4$/Zr-SBA15 (10) catalysts.
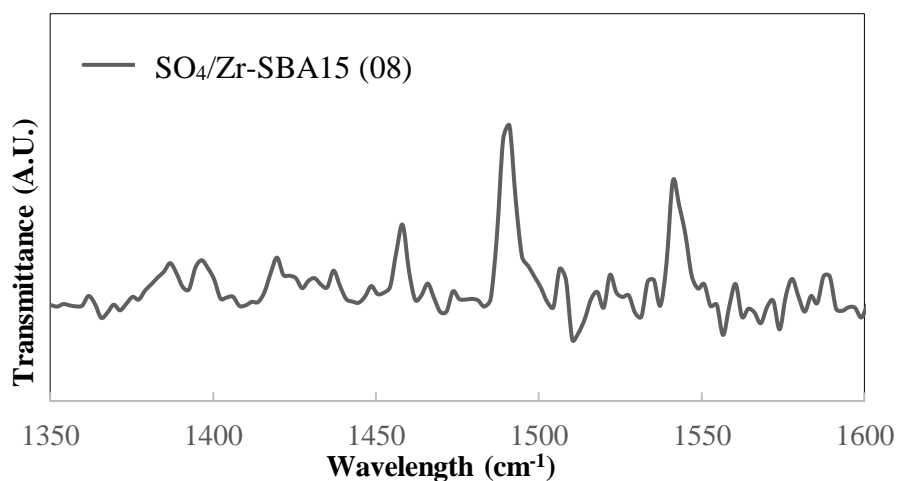
Figure 5. 13. FT-IR spectra of pyridine absorbed SO_4/Zr-SBA15 (08) catalyst.

5.1.4. Ti-SBA15 (10) and Ti-SBA15 (20) Catalysts

N_2 adsorption isotherms of Ti-SBA15 (10) and Ti-SBA15 (20) catalysts are given in Figure 5. 14. and Figure 5. 15. According to results, Ti-SBA15 (10) and Ti-SBA15 (20) catalysts represent type IV isotherm this indicated that mesoporous structure presence in Ti based catalysts.
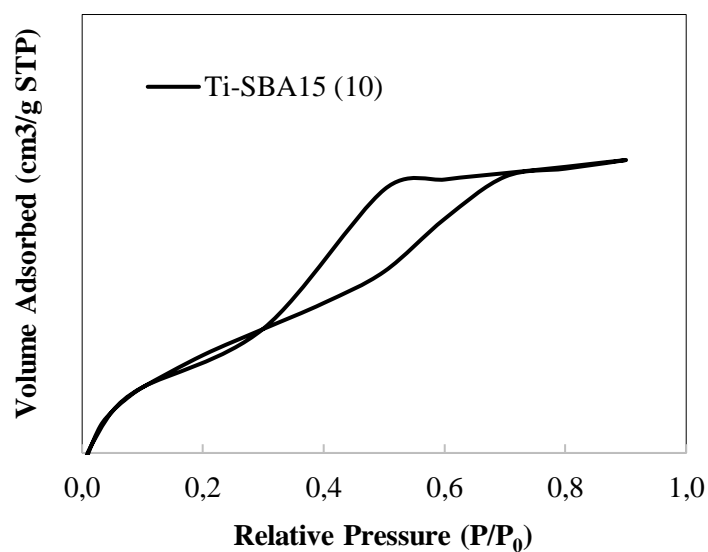

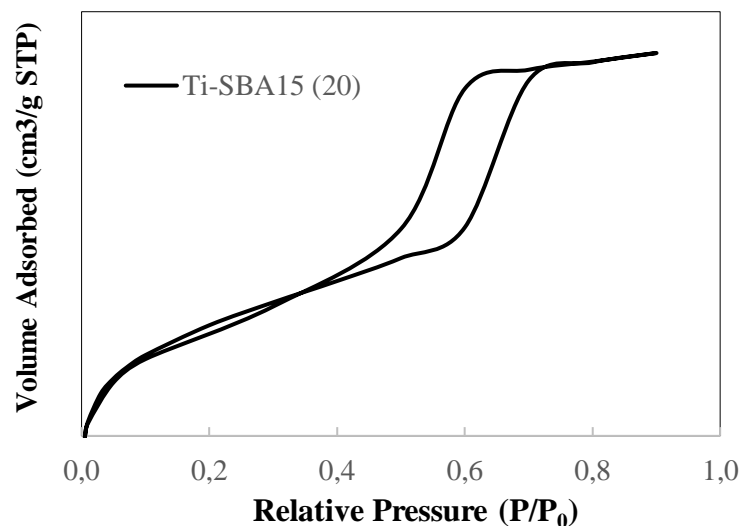Figure 5. 14. N_2 adsorption isotherms of the Ti-SBA15 (10) catalyst.

Figure 5. 15. N_2 adsorption isotherms of the Ti-SBA15 (20) catalyst.

The specific surface area, pore volume and pore diameter of Ti-SBA15 (10) and Ti-SBA15 (20) were determined by BET method and the results are given in Table 5. 3. Ti-SBA15 (10) and Ti-SBA15 (20) catalysts had higher BET surface area than Zr-SBA15 (08) and Zr-SBA15 (10) catalysts. They also had higher pore volume and pore diameter than Zr-SBA15 (08) and Zr-SBA15 (10) catalysts. The surface area of catalysts increased with Ti content.

Table 5. 3. Textural properties analysis of Ti-SBA15 (10) and Ti-SBA15 (20) catalysts

Catalyst	BET Surface Area, m^2/g	Pore Volume, cm^3/g	Pore Diameter, Å	Total Acidity (mmol NH_3/g cat.)
Ti-SBA15 (10)	856.11	0.85	39.48	1.0
Ti-SBA15 (20)	913.60	0.92	40.70	0.9

The crystal structure of Ti-SBA15 (10) and Ti-SBA15 (20) were investigated with X-Ray Diffraction where the 2θ angles changed from 5 ° to 80 ° and the results are given in Figure 5. 16. No peaks of Ti was observed which showed successfully incorporation of Ti (Sharma et al., 2012).
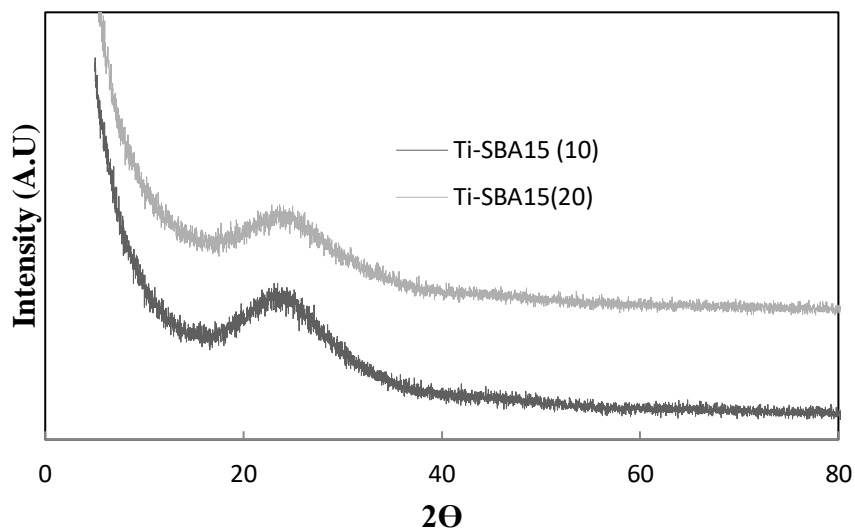
Figure 5. 16. XRD Patterns of Ti-SBA15 (10) and Ti-SBA15 (20) catalysts.

The acidity of Ti-SBA15 (10) and Ti-SBA15 (20) catalysts determined by NH_3-TPD analysis. The results are shown in Figure 5. 17. The desorption peaks are centered at low and high temperature which are 200 °C and 400 °C, respectively. The peak at low temperature and the peak at high temperature refer to the weak and strong acid sites. Besides, the acid strength of Ti-SBA15 (10) and Ti-SBA15 (20) catalysts were widely spread (Sharma et al., 2012). Total acidity of Ti based catalysts gave similar results. This indicated that Ti content did not affect the acidity of the catalysts. Ti-SBA15 (10) had 1.0 mmol NH_3/ g catalyst, Ti-SBA15 (20) had 0.9 mmol NH_3/ g catalyst.
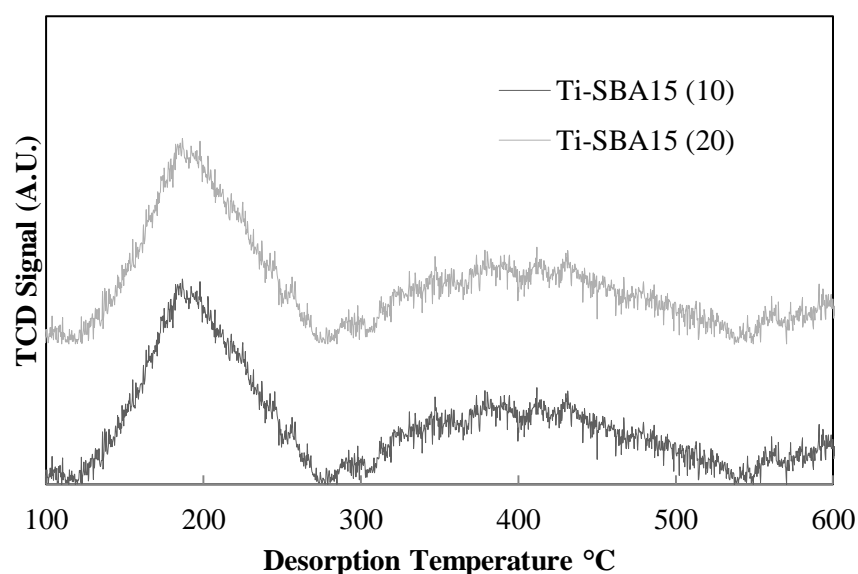

Figure 5. 17. NH_3-TPD profiles of Ti-SBA15 (10) and Ti-SBA15 (20) catalysts.

The skeletal FT-IR spectra of Ti-SBA15 (10) and Ti-SBA15 (20) catalysts are given in Figure 5. 18. and. The symmetric stretching of Si-O-Si bonds cause the peaks observed at the range of 1070 cm^{-1} and 1220 cm^{-1}. Additionally, a peak was observed at 465 cm^{-1} due to the vibration of Si-O-Si bond. The Si-O-Ti bond, which is formed by the incorporation of Ti on the SBA15, was observed around 1600 cm^{-1}. The existence of this band proves that the incorporation of Ti on SBA15 for Ti-SBA15 (10) and Ti-SBA15 (20) catalyst synthesis was successfully achieved (Sharma et al., 2012).
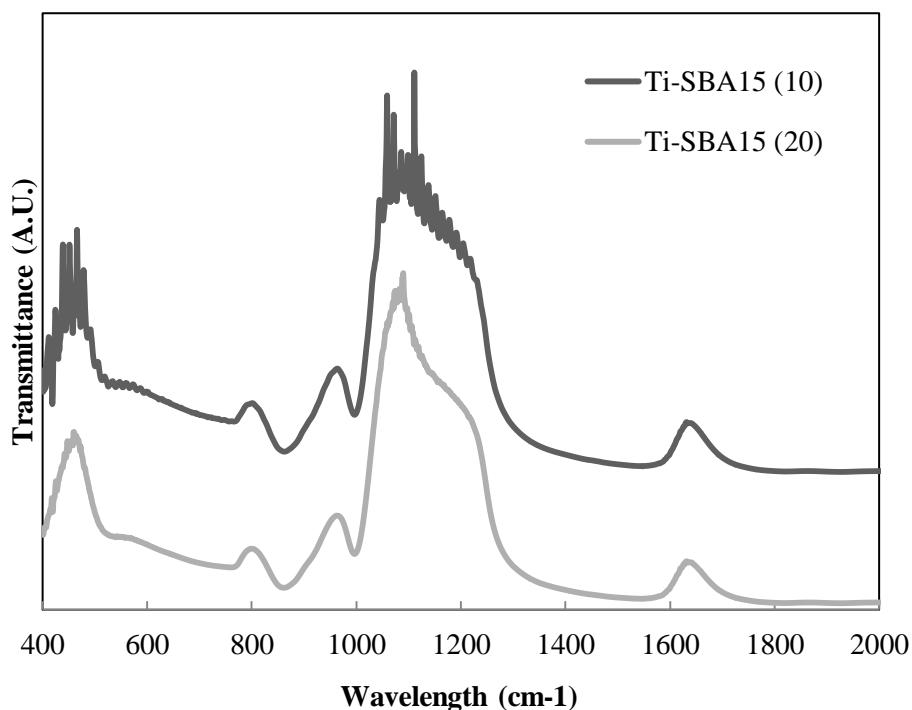

Figure 5. 18. The skeletal FT-IR spectra of Ti-SBA15 (10) and Ti-SBA15 (20) catalysts.

5.1.5. SO$_4$/Ti-SBA15 (10) and SO$_4$/Ti-SBA15 (20) Catalysts

N$_2$ adsorption isotherms of SO$_4$/Ti-SBA15 (10) and SO$_4$/Ti-SBA15 (20) catalysts are given in Figure 5. 19. and Figure 5. 20. According to the results, N$_2$ adsorption of these catalysts could be described by IV isotherm. The presence of hysteresis loop and multilayer adsorption at low P/P$_0$ indicated that these catalysts have mesoporous structure (Sharma et al., 2012).
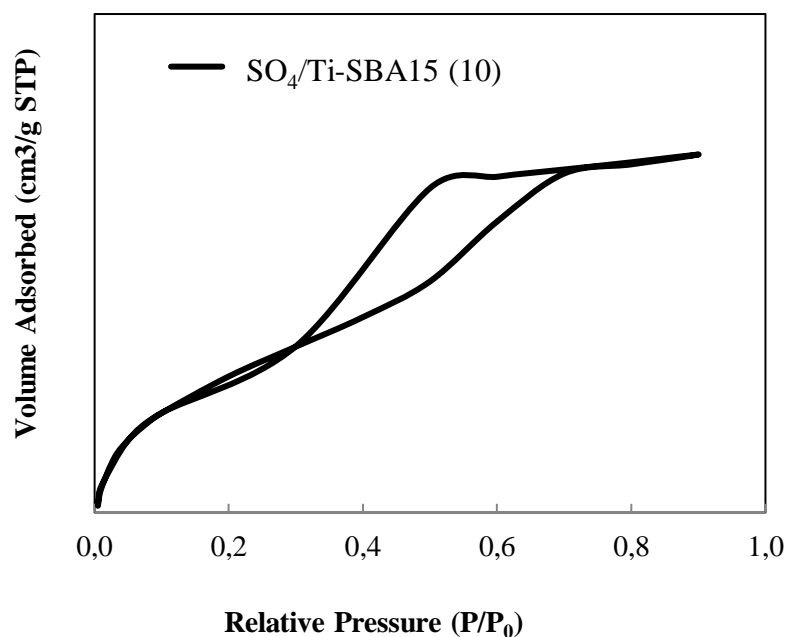
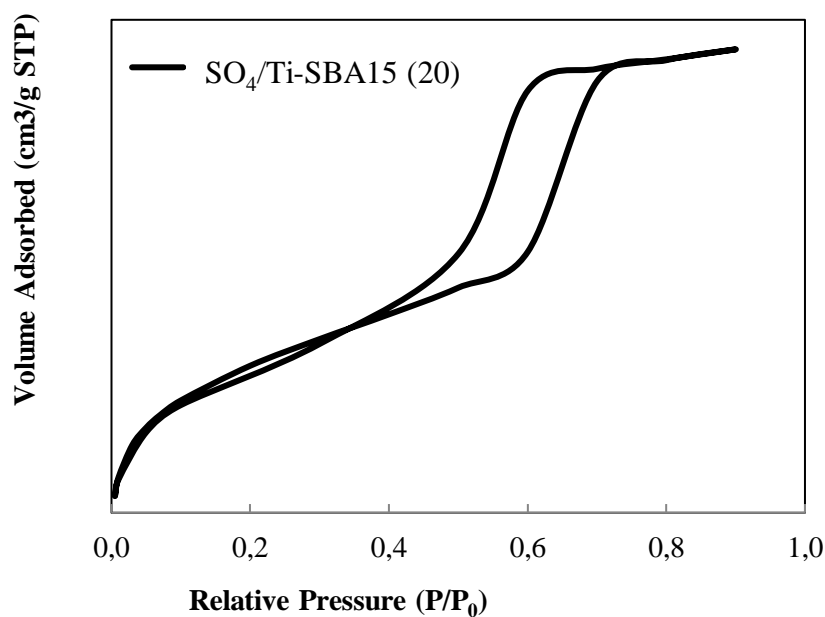Figure 5. 19. N_2 adsorption/desorption isotherms of SO_4/Ti-SBA15 (10) catalyst.

Figure 5. 20. N_2 adsorption/desorption isotherms of SO_4/Ti-SBA15 (20) catalyst.

The specific surface area, pore volume and pore diameter of SO_4/Ti-SBA15 (10) and SO_4/Ti-SBA15 (20) were determined by BET method and the results are given in Table 5. 4. According to BET results, the SO_4/Ti-SBA15 (10) and SO_4/Tİ-SBA15 (20) had lower BET surface areas and lower pore volume and pore diameter than Ti-SBA15 (10) and Ti-SBA15 (20) catalysts. Therefore, sulfonation affected Ti based catalysts negatively (Sharma et al., 2012).

Table 5. 4. Textural properties of SO_4/Ti-SBA15 (10) and SO_4/Ti-SBA15 (20) catalysts.

Catalyst	BET Surface Area, m^2/g	Pore Volume, cm^3/g	Pore Diameter, $A°$	Total Acidity (mmol NH_3/g cat.)
SO_4/Ti-SBA15 (10)	723.41	0.45	29.57	2.8
SO_4/Ti-SBA15 (20)	744.37	0.60	38.53	4.9

The crystal structure of SO4/Ti-SBA15 (10) and SO_4/Ti-SBA15 (20) were investigated with X-Ray Diffraction where the 2θ angles changed from 5 ° to 80 ° and the results are given in Figure 5. 21. Diffraction peaks at 2Ө of 25°, 37° and 53° of SO_4/Ti-SBA15 (10) showed b is responsible for anatase titanium. This is also a characteristic value for SO_4/Ti-SBA15 (10) and SO_4/Ti-SBA15 (20) catalysts. These results indicated that after sulfonation the structure was preserved. Sulfated catalysts similar XRD patterns to Ti-SBA15 (10) and Ti-SBA15 (20).
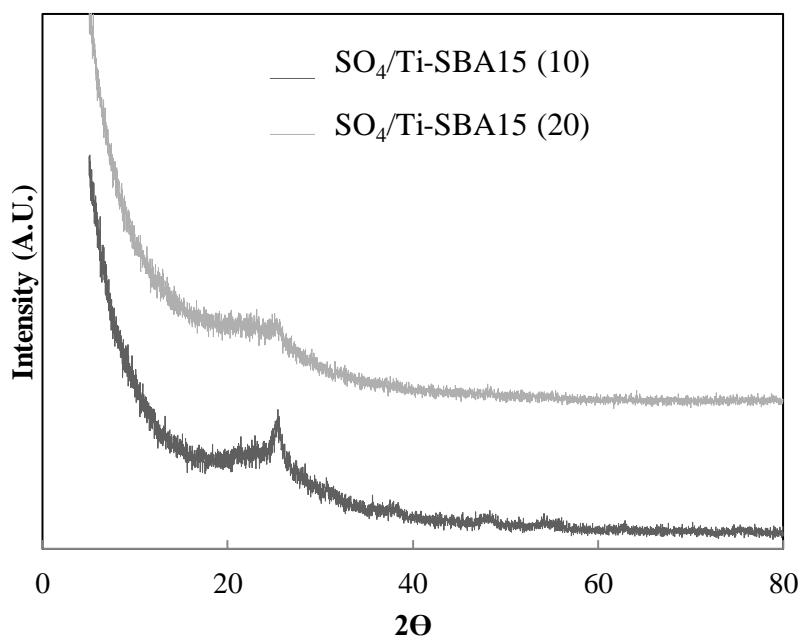

Figure 5. 21. XRD Patterns of SO_4/Ti-SBA15 (10) and SO_4/Ti-SBA15 (20) catalysts.

The acidity of Ti-SBA15 (10) and Ti-SBA15 (20) catalysts determined by NH_3-TPD analysis. The results are shown in Figure 5. 22. Two desorption peaks were appeared, one broad in the weak range (180 ºC – 320 ºC) and another broad peak in the weak range (around 400 ºC-500 ºC). These peaks indicated that SO4/Ti-SBA15 (10) and SO_4/Ti-SBA15 (20) catalysts have medium and strong acid sites (Sharma et al., 2012).

While total acidity of SO$_4$/Ti-SBA15 (10) catalyst was 2.8 mmol NH$_3$/ g catalyst, SO$_4$/Ti-SBA15 (20) was 4.9 mmol NH$_3$/g catalyst. This indicated that after sulfonation acidity of Ti based catalyst increased. Higher acidity was obtained with lower Ti content.
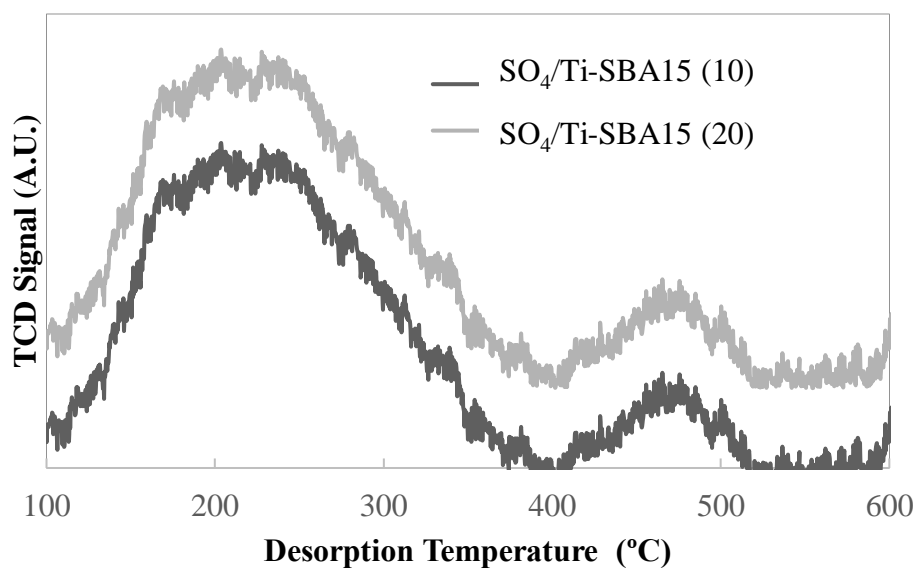

Figure 5. 22. NH$_3$-TPD profiles of SO$_4$/Ti-SBA15 (10) and SO$_4$/Ti-SBA15 (20) catalysts.

The skeletal FT-IR spectra SO$_4$/Ti-SBA15 (10) and SO$_4$/Ti-SBA15 (20) catalysts are given in Figure 5. 23. The characteristic peaks of Ti-SBA15 (10) and Ti-SBA15 (20) catalysts were observed at the same wavelengths after the sulfonation.
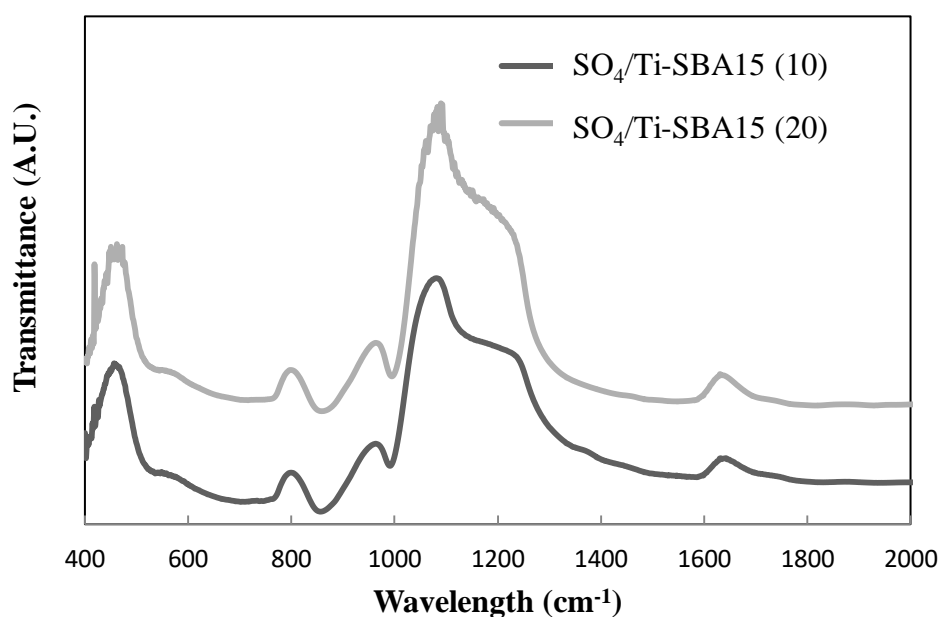

Figure 5. 23. The skeletal FT-IR spectra of SO$_4$/Ti-SBA15 (10) and SO$_4$/Ti-SBA15 (20) catalysts.

5.1.6. Summary of Catalyst Properties

The textural properties and acidities of Zr-SBA15 (08), Zr-SBA15 (10), SO$_4$/Zr-SBA15 (08), SO$_4$/Zr-SBA15 (10), Ti-SBA15 (10), Ti-SBA15 (20), SO$_4$/Ti-SBA15 (10) and SO$_4$/Ti-SBA15 (20) catalysts are tabulated in Table 5. 5 and Table 5. 6. Whereas the sulfonation affected on total acidity of catalysts positively, BET surface areas, pore volumes and pore diameters affected negatively except Zr-SBA15 (10). Total acidities of all catalysts increased after sulfonation. BET surface areas, pore volumes and pore diameters were affected by metal content and sulfonation. Increasing Zr and Ti content decreased surface area,pore volume and pore diameter. Acidity increased to some extent. Upon sulfonation surface areas, pore diameter and pore volume decreased except Zr-SBA15 (10). Acidity increased with sulfonation. While the lowest BET surface area was obtained as 554.68 m^2/g for Zr-SBA15 (10), the highest BET surface area was obtained as 913.60 m^2/g for Ti-SBA15 (20). Acidity values of catalysts were varied between 0.9 and 4.9 mmol NH$_3$/g cat. Whereas the lowest acidity was observed for Ti-SBA15 (20) and the highest acidity was observed for SO$_4$/Ti-SBA15 (20).

Table 5. 5. The textural properties and acidities of Zr based catalysts.

Catalyst	BET Surface Area, m²/g	Pore Volume, cm³/g	Pore Diameter, Å	Total Acidity (mmol NH$_3$/g cat.)
Zr-SBA15 (08)	696.77	0.74	42.63	1.2
Zr-SBA15 (10)	554.68	0.53	38.50	1.8
SO$_4$/Zr-SBA15 (08)	639.51	0.66	41.22	3.9
SO$_4$/Zr-SBA15 (10)	630.77	0.66	41.10	3.2

Table 5. 6. The textural properties and acidities of Ti based catalysts.

Catalyst	BET Surface Area, m²/g	Pore Volume, cm³/g	Pore Diameter, Å	Total Acidity (mmol NH₃/g cat.)
Ti-SBA15 (10)	856.11	0.85	39.48	1.0
Ti-SBA15 (20)	913.60	0.92	40.70	0.9
SO4/Ti-SBA15 (10)	723.41	0.45	29.57	2.8
SO4/Ti-SBA15 (20)	744.37	0.60	38.53	4.9

5.2. Catalysts Testing

5.2.1. Activity of Homogeneous Catalyst (H_2SO_4) in Polyol Production

Homogeneous catalysis reactions were performed with 0.003 M H_2SO_4. ESO:alcohol mol ratio was chosen as 1:11 based on a study which was carried out by Dai et al. (Dai et al. 2009). In this study, no solvent was used, so the alcohol was used as excess because it was not only used as a reactant but also as a solvent. The amount of alcohol used was calculated based on the oxirane content in epoxidized soybean oil according to the formula (Eqn 4.1.). FT-IR and H-NMR of reaction products are given in Figure 5. 24. and Figure 5. 26., respectively.
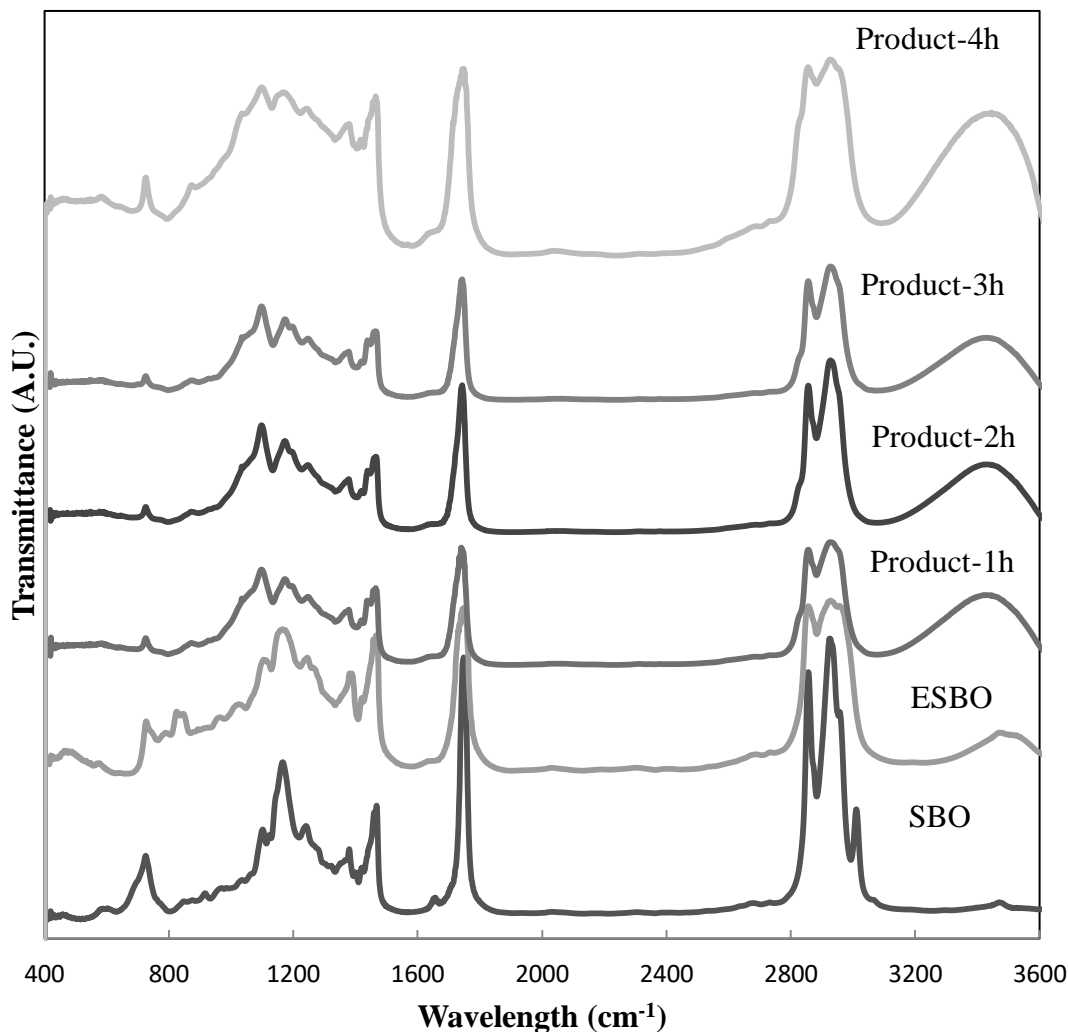
Figure 5. 24 FT-IR spectra of the products formed by 0.003 M H_2SO_4.

The bands of C=O, C-O stretching vibrations of aliphatic ester groups and secondary hydroxyl group were observed at 1743, 1240 and 1080 cm^{-1}, respectively. The peaks around at 2900 cm^{-1} was assigned to CH2 asymmetric stretching vibrations. Besides, while the epoxy groups which were observed at 843cm^{-1} decreased during the reaction duration, the products were formed and they give a characteristic peak around 3400 cm^{-1} (Ji et al., 2015).

The H-NMR analysis of products formed by 0.003 M H_2SO_4 are given in Figure 5. 26. and Figure 5. 26. The new peaks were observed between 3.2 and 4.0 ppm referred to methylinic proton (H-C-OH) in the H-NMR spectra of products and the proton is associated with the OH groups (Dai et. al. 2009). Therefore, the results of H-NMR prove the attachment of hydroxyl groups. Polyol structure was obtained with reaction time.
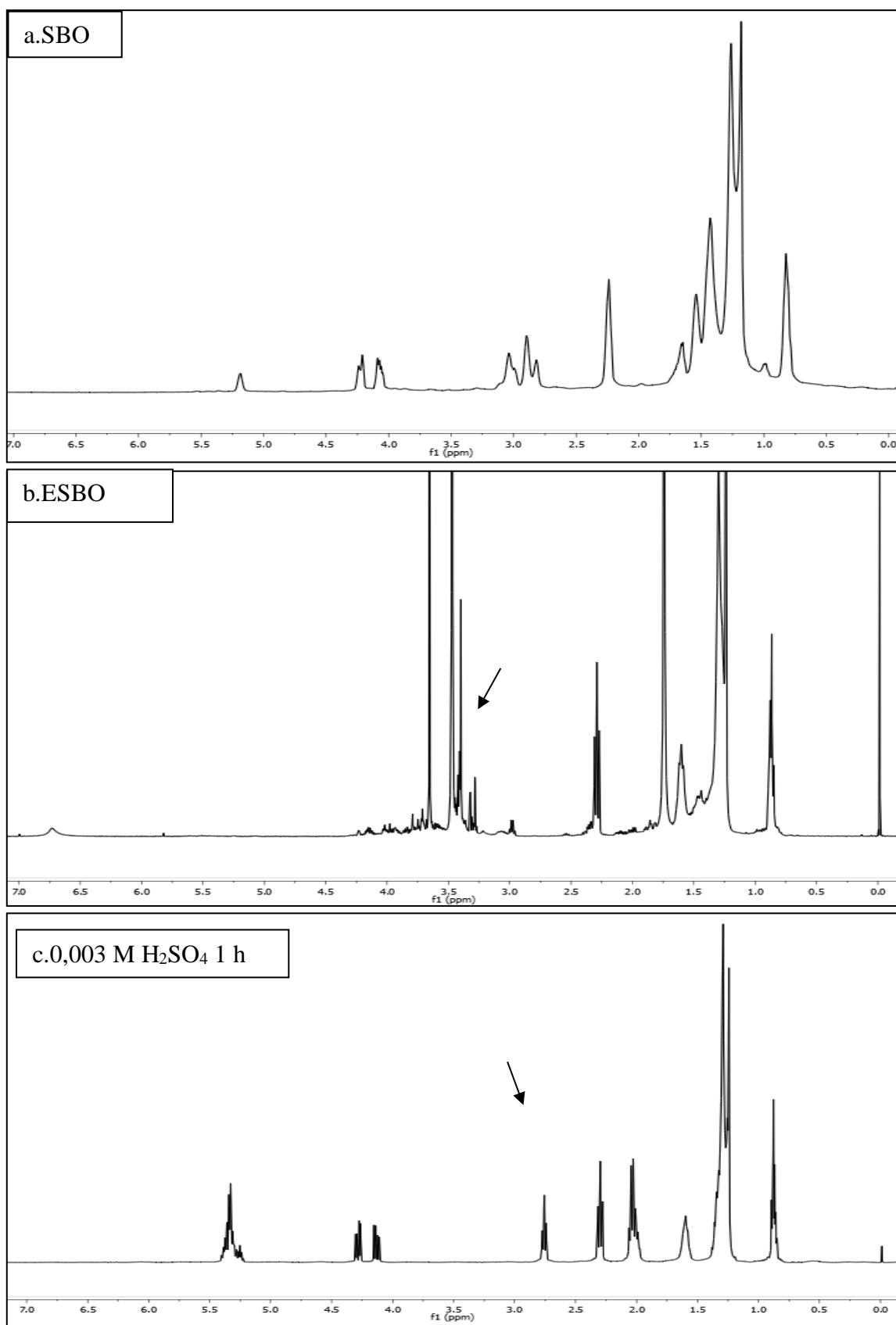
Figure 5. 25. H-NMR analysis of products by 0.003 M H_2SO_4 at different reaction times.
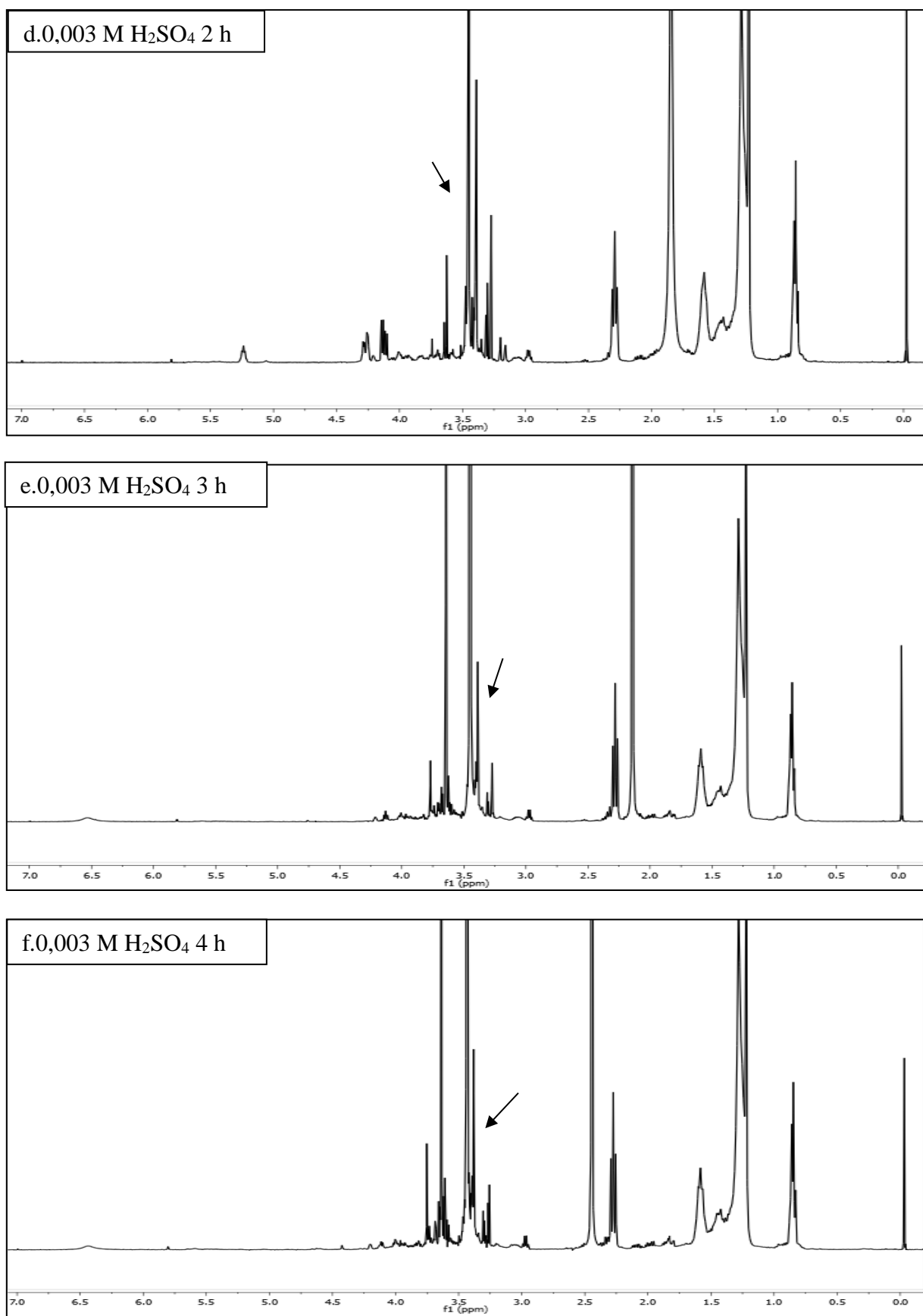
Figure 5. 26. H-NMR analysis of products by 0.003 M H_2SO_4 at different reaction times.

The oxirane content in the epoxidized soybean oil for the 0.003 M H_2SO_4 reaction is given in Figure 5. 27. Oxirane content decreased with reaction time. Oxirane conversion was determined as almost 99.98 % by Eqn 4.1.
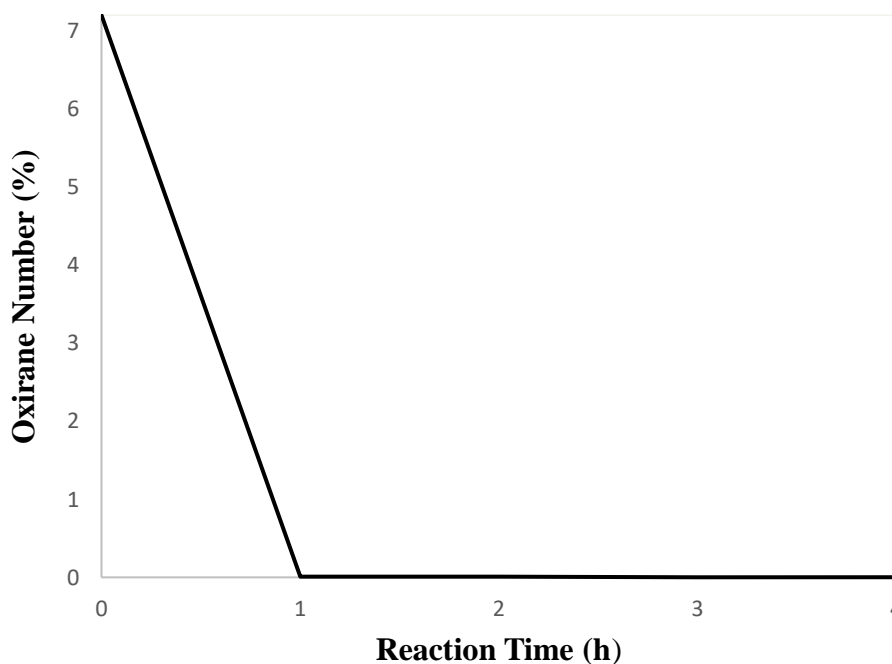

Figure 5. 27. The change in oxirane concentration with time over 0.03 M H_2SO_4 catalyst.

5.2.2. Activity of   Zr-SBA15 and Ti-SBA15 Based in Polyol Formation

Firstly, the Zr-SBA15 (08) and Zr-SBA15 (10) catalysts were tested for their catalytic activity for polyol production. The obtained products were analyzed to determine product formation. The FT-IR analysis of the products formed over Zr-SBA15 (08) are given in Figure 5. 28. The bands of at 1743 cm^{-1} and 1240 cm^{-1} corresponded, respectively to the C=O and C-O stretching vibrations of aliphatic ester groups, while the peak appearing at 1080 cm^{-1} was assigned to the secondary hydroxyl group. The ESBO characteristic peak at 843 cm^{-1}, attributed to the epoxy group, disappeared after the epoxy group opening reaction. The results indicated that the soy based polyols were synthesized during the ring opening reaction. For polyol, the peak at around 3400 cm^{-1} (Ji et al., 2015 and Fang et al.).
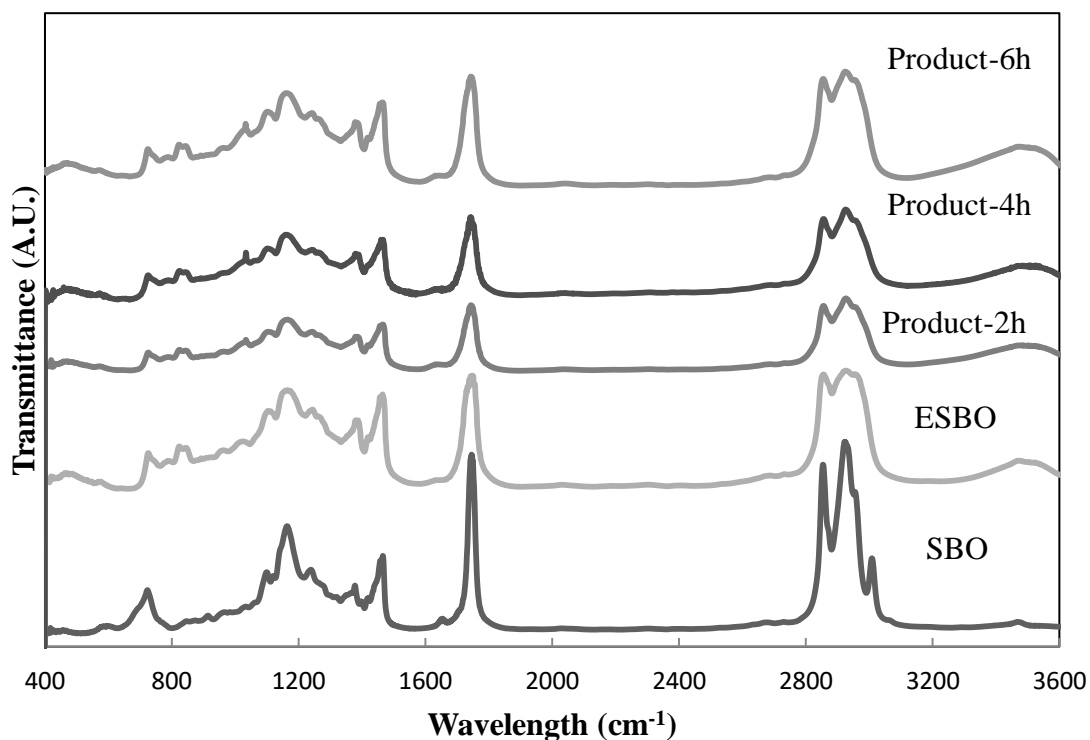
Figure 5. 28. The FT-IR analysis of products formed over Zr-SBA15 (08).

The oxirane contents of the products formed over Zr-SBA15 (08) are given in Figure 5. 29. Oxirane content decreased with reaction time and oxirane conversion of 84.03 % was achieved by using Eqn 4.1.
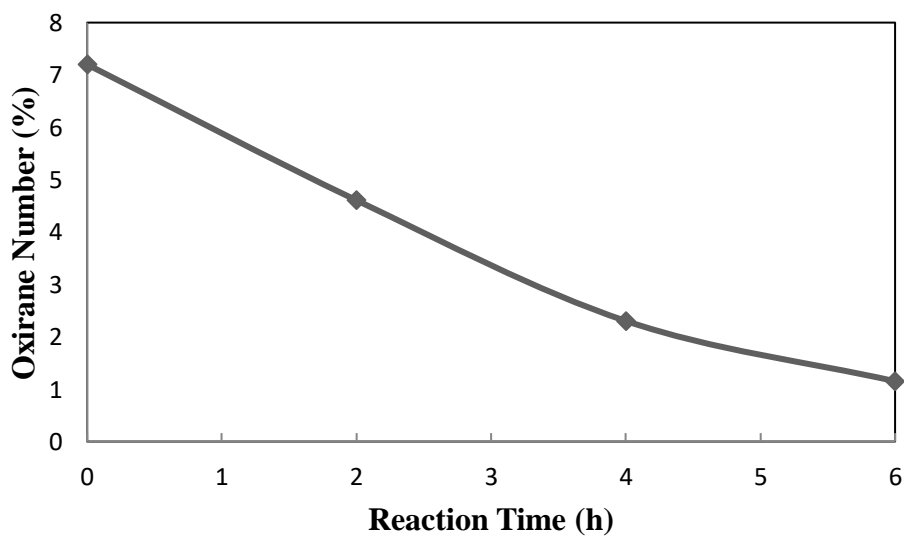

Figure 5. 29. The change in oxirane concentration with time over Zr-SBA15 (08).
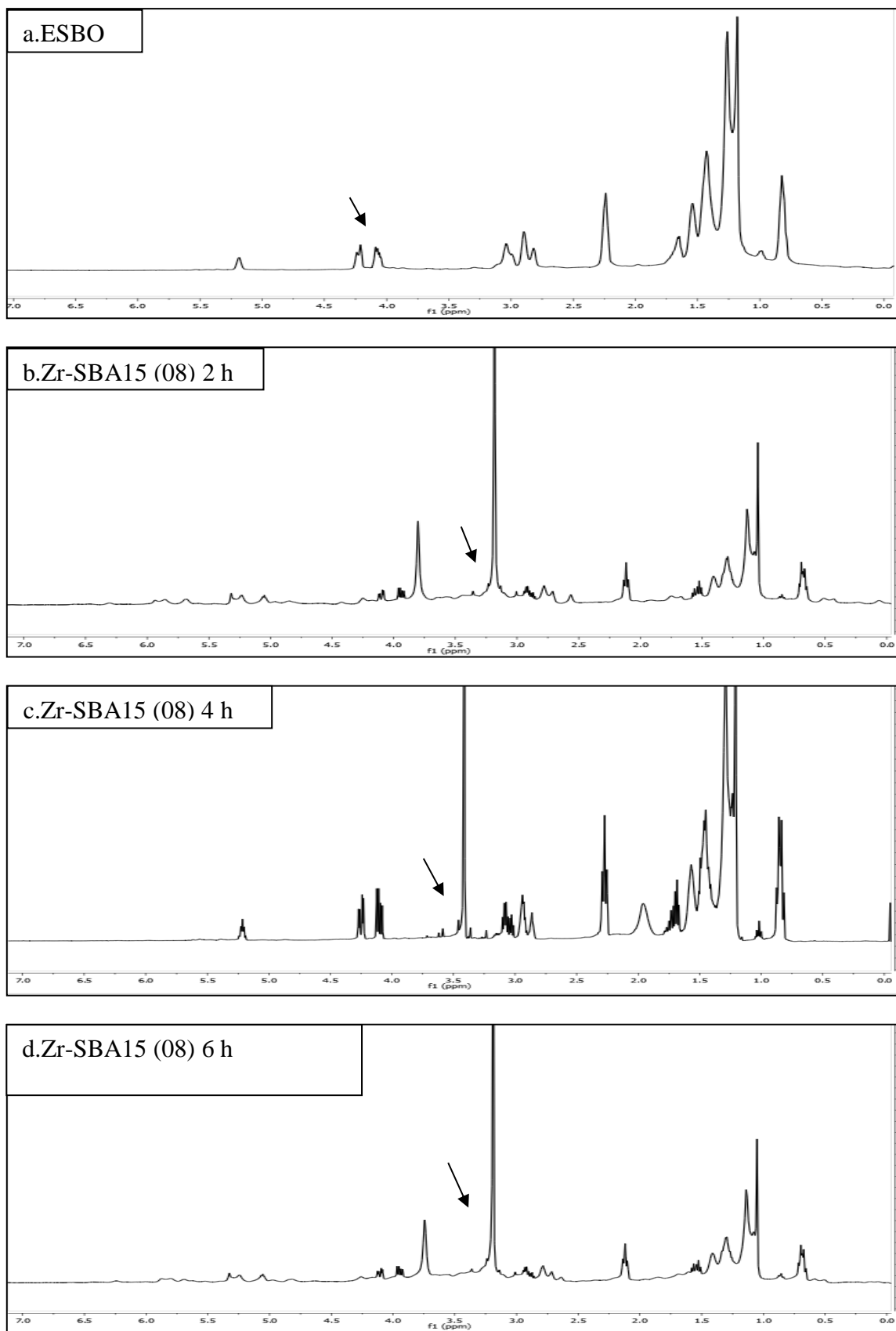
Figure 5. 30. H-NMR analysis of products formed over Zr-SBA15 (08).

The H-NMR analysis products of obtained over Zr-SBA15 (08) are given in Figure 5. 30. The soy based polyol structure was obtained from the H-NMR spectra in Fig. 5.30.b-d. The epoxy protons were observed between 2.8 and 3.0 ppm (Fig. 5.30. a.). The new peaks were observed between 3.2 and 4.0 ppm were the protons of –CH-OH. Therefore the results of H-NMR prove the attachment of hydroxyl groups with the reaction time (Dai et. al. 2009).

The FT-IR analysis of the products formed over Zr-SBA15 (10) is given in Figure 5. 31. The C=O, C-O stretching vibrations of aliphatic ester groups and secondary hydroxyl group were observed at 1743, 1240 and 1080 cm^{-1}, respectively. Whereas the epoxy groups decreased during the reaction duration, the formed products increased. They give a characteristic peak around 3400 cm^{-1} (Ji et al., 2015). The peaks were observed at the same wavelength for Zr-SBA15 (08) and Zr-SBA15 (10). They were also similar with that of H_2SO_4.
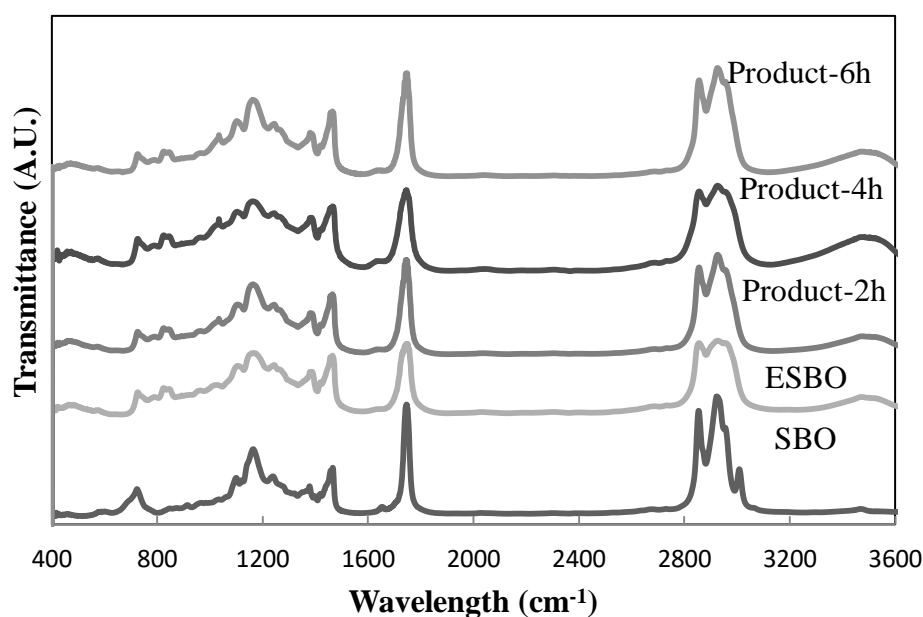

Figure 5. 31. The FT-IR analysis of products formed over Zr-SBA15 (10).

The H-NMR analysis of products formed over Zr-SBA15 (10) are given in Figure 5. 32. The soy based polyol structure was obtained from the H-NMR spectra in Fig. 5.32. b-d. The epoxy protons were observed between 2.8 and 3.0 ppm (Fig. 5.32. a.). The new peaks were observed between 3.2 and 4.0 ppm were the protons of –CH-OH. Therefore the results of H-NMR prove the attachment of hydroxyl groups with the reaction time (Dai et. al. 2009).
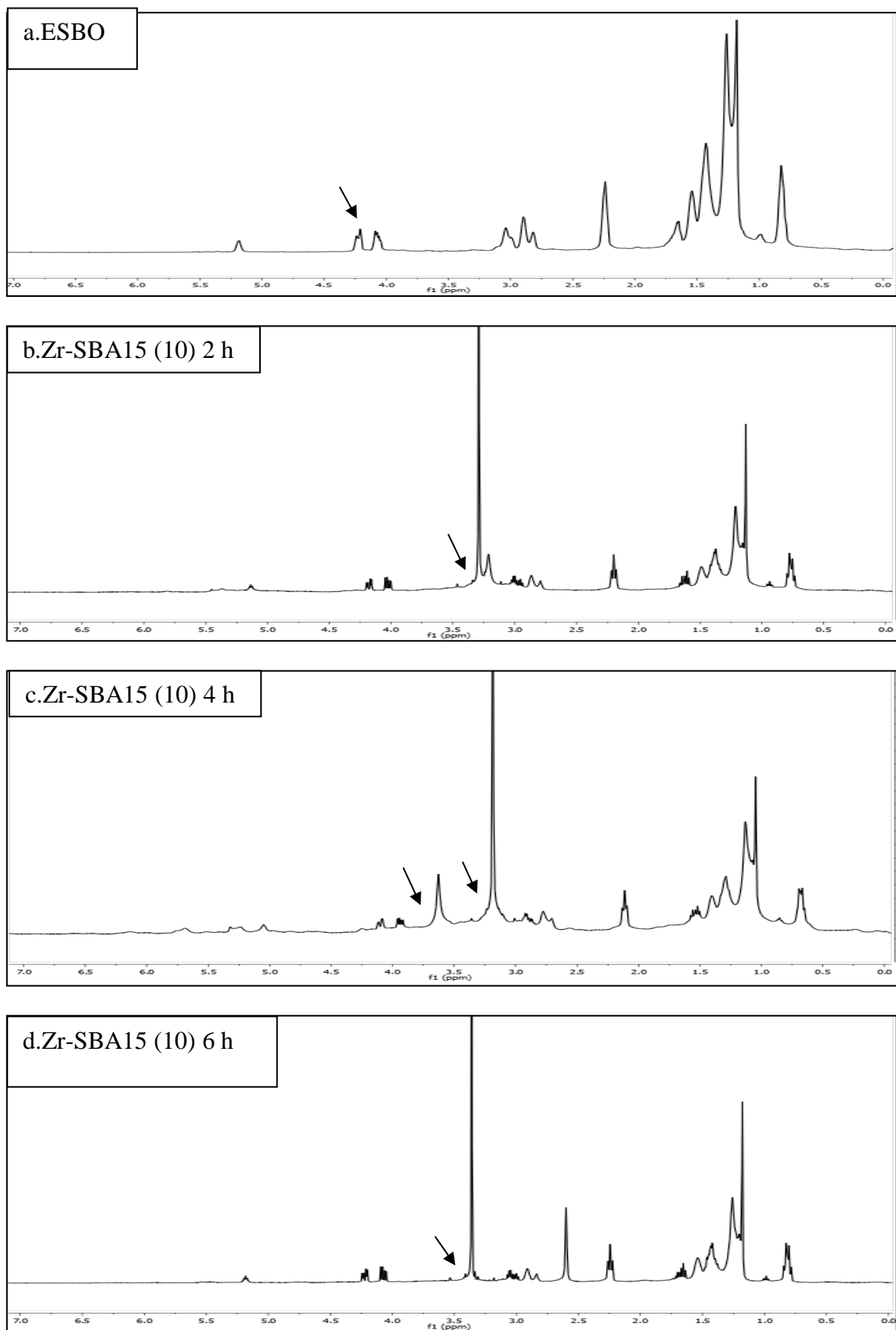
Figure 5. 32. H-NMR analysis of products formed over Zr-SBA15 (10).

The oxirane contents of the products formed over Zr-SBA15 (10) are given in Figure 5. 33. Oxirane content decreased with reaction time and oxirane conversion of 64.44 % was achieved by using Eqn 4.1.
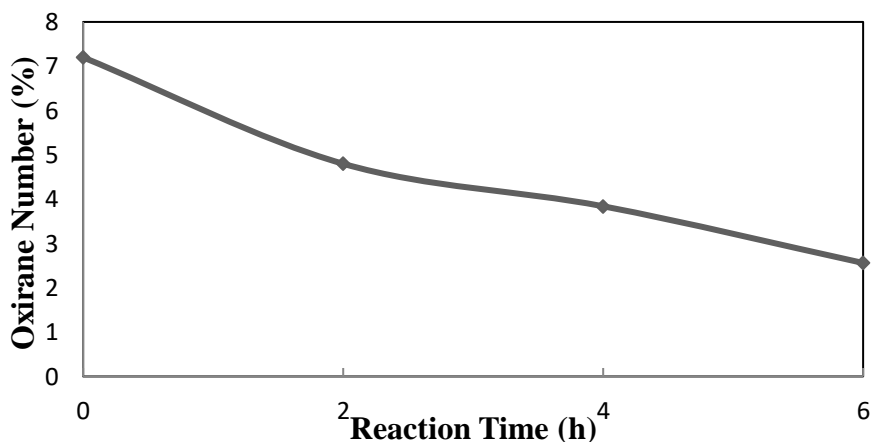

Figure 5. 33. The change in oxirane concentration with time over Zr-SBA15 (10).

While acidity of Zr based catalysts increased with Zr amount which is given in Table 5.1., oxirane number decreased. This was not expected, this could be due to Zr-SBA15 (08) had higher strong acid sites amounts.

The FT-IR analysis of products formed over SO_4/Zr-SBA15 (08) is given in Figure 5. 34. The bands of C=O, C-O stretching vibrations of aliphatic ester groups and secondary hydroxyl group were observed at 1743, 1240 and 1080 cm^{-1}, respectively. Besides, while the epoxy groups decreased during the reaction duration, the products were formed and they give a characteristic peak around 3400 cm^{-1} (Fang et al., 2015).
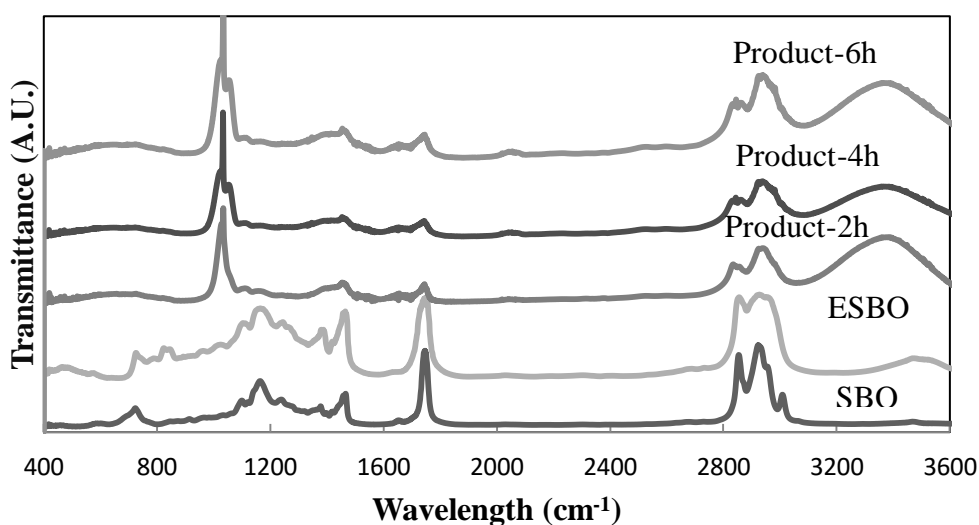

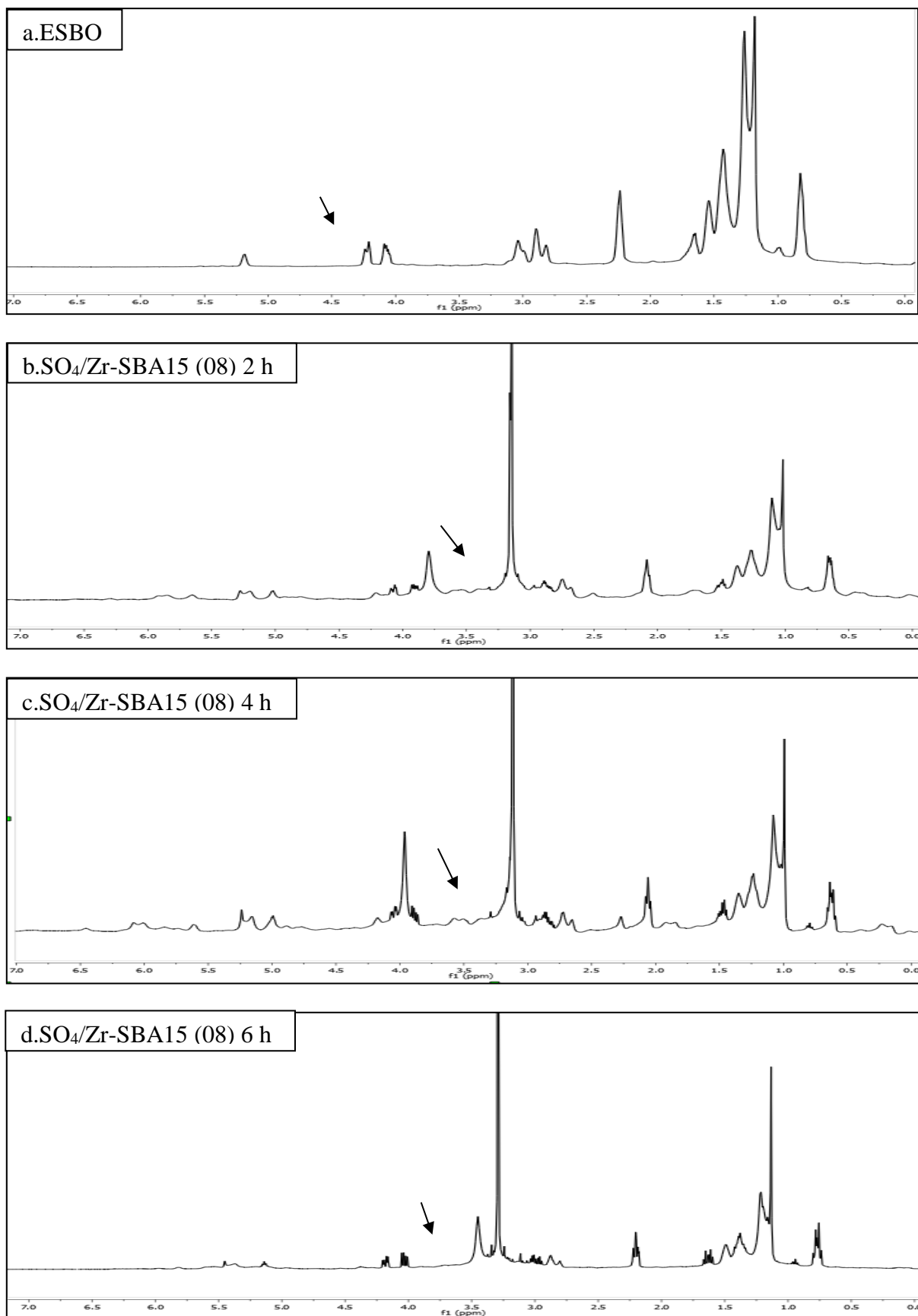Figure 5. 34. The FT-IR analysis of products formed over SO_4/Zr-SBA15 (08).

Figure 5. 35. H-NMR analysis of products formed over SO4/Zr-SBA15 (08).

The H-NMR analysis of products formed over SO_4/Zr-SBA15 (08) are given in Figure 5. 35. The soy-based polyol structure was obtained from the H-NMR spectra in Fig. 5.35. b-d. The epoxy protons were observed between 2.8 and 3. ppm (Fig. 5.35. a.). The new peaks were observed between 3.2 and 4.0 ppm were the protons of –CH-OH. Therefore the results of H-NMR prove the attachment of hydroxyl groups with the reaction time (Dai et. al. 2009).

The oxirane contents of the products formed over SO_4/Zr-SBA15 (08) are given in Figure 5. 36. Oxirane content decreased with reaction time and oxirane conversion of t 62.22 % was achieved by using Eqn 4.1.
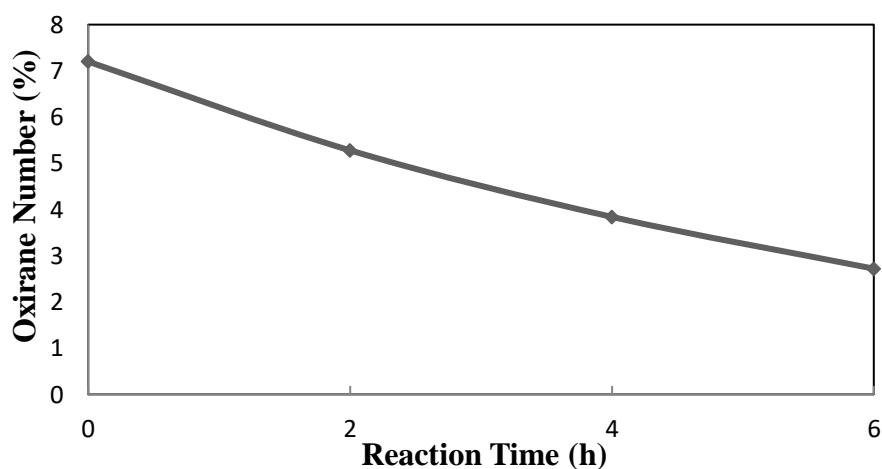

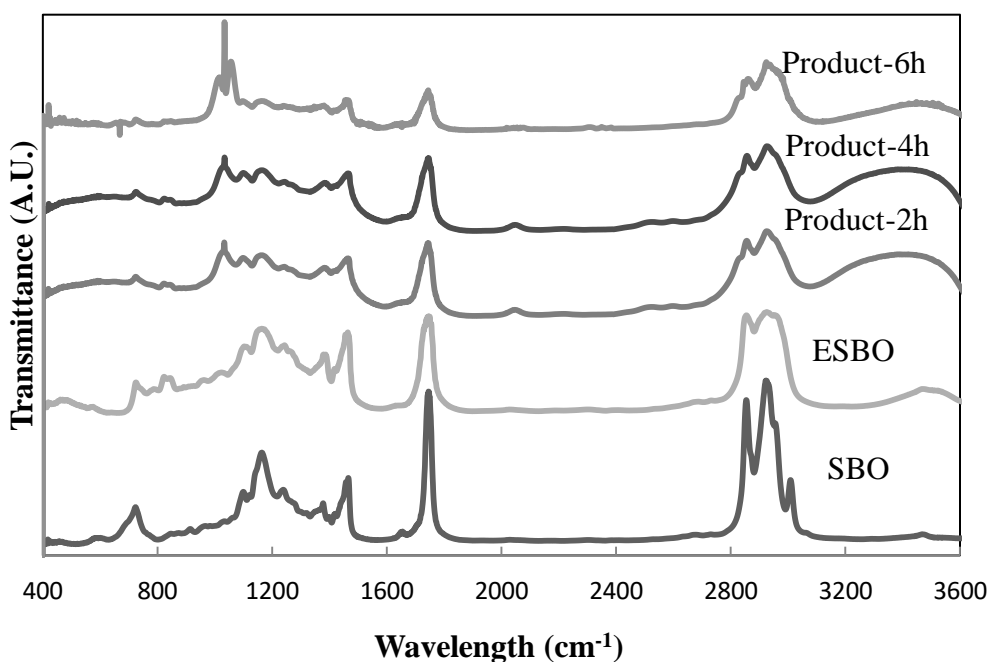Figure 5. 36. The change in oxirane concentration with time over SO_4/Zr-SBA15 (08).

Figure 5. 37. The FT-IR analysis of products formed over SO_4/Zr-SBA15 (10).

The FT-IR analysis of products formed over SO_4/Zr-SBA15 (10) are given in Figure 5. 37. The bands of C=O, C-O stretching vibrations of aliphatic ester groups and secondary hydroxyl group were observed at 1173, 1240 and 1080 cm^{-1}, respectively. Besides, while the epoxy groups decreased during the reaction duration, the products were formed and they give a characteristic peak around 3400 cm^{-1} (Ji et al., 2015).

The oxirane contents of the products formed over SO_4/Zr-SBA15 (10) are given in Figure 5. 38. Oxirane content decreased with reaction time and oxirane conversion of 55.56 % was achieved achieved by using Eqn 4.1.
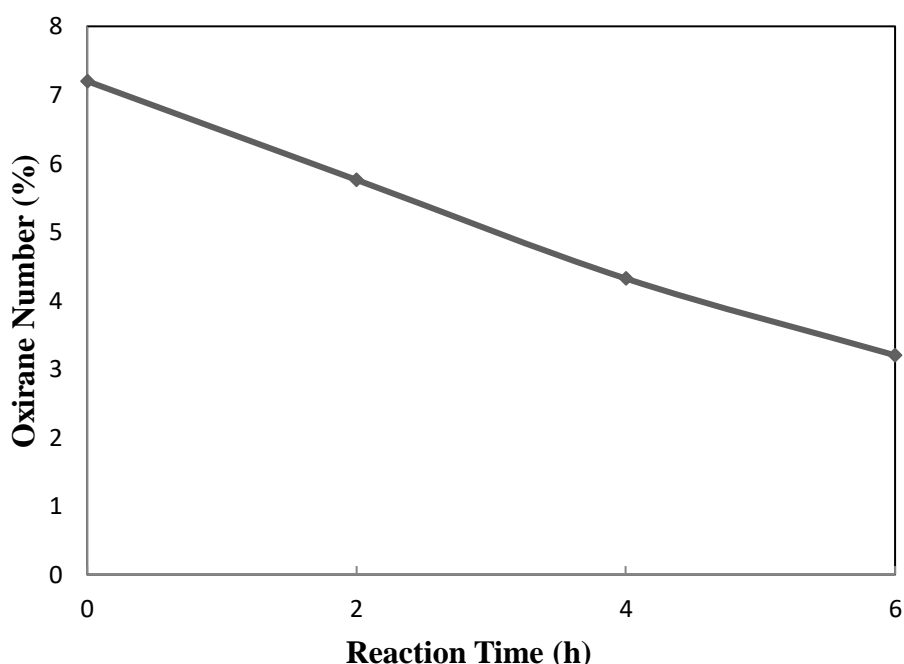

Figure 5. 38. The change in oxirane concentration with time over SO_4/Zr-SBA15 (10).

Acidity of the sulfated Zr based catalysts increased with the Zr amount as oxirane number decreased. This was not expected. Probably, Bronsted and Lewis acid sites affect he reaction differently. Further investigation is required to understand this situation.

The soy based polyol structure was obtained from the H-NMR spectra in Figure 5. 39. b-d. The epoxy protons were observed between 2.8 and 3.0 ppm (Fig. 5.39. a.). The new peaks were observed between 3.2 and 4.0 ppm were the protons of –CH-OH. Therefore the results of H-NMR prove the attachment of hydroxyl groups with the reaction time (Dai et. al. 2009).
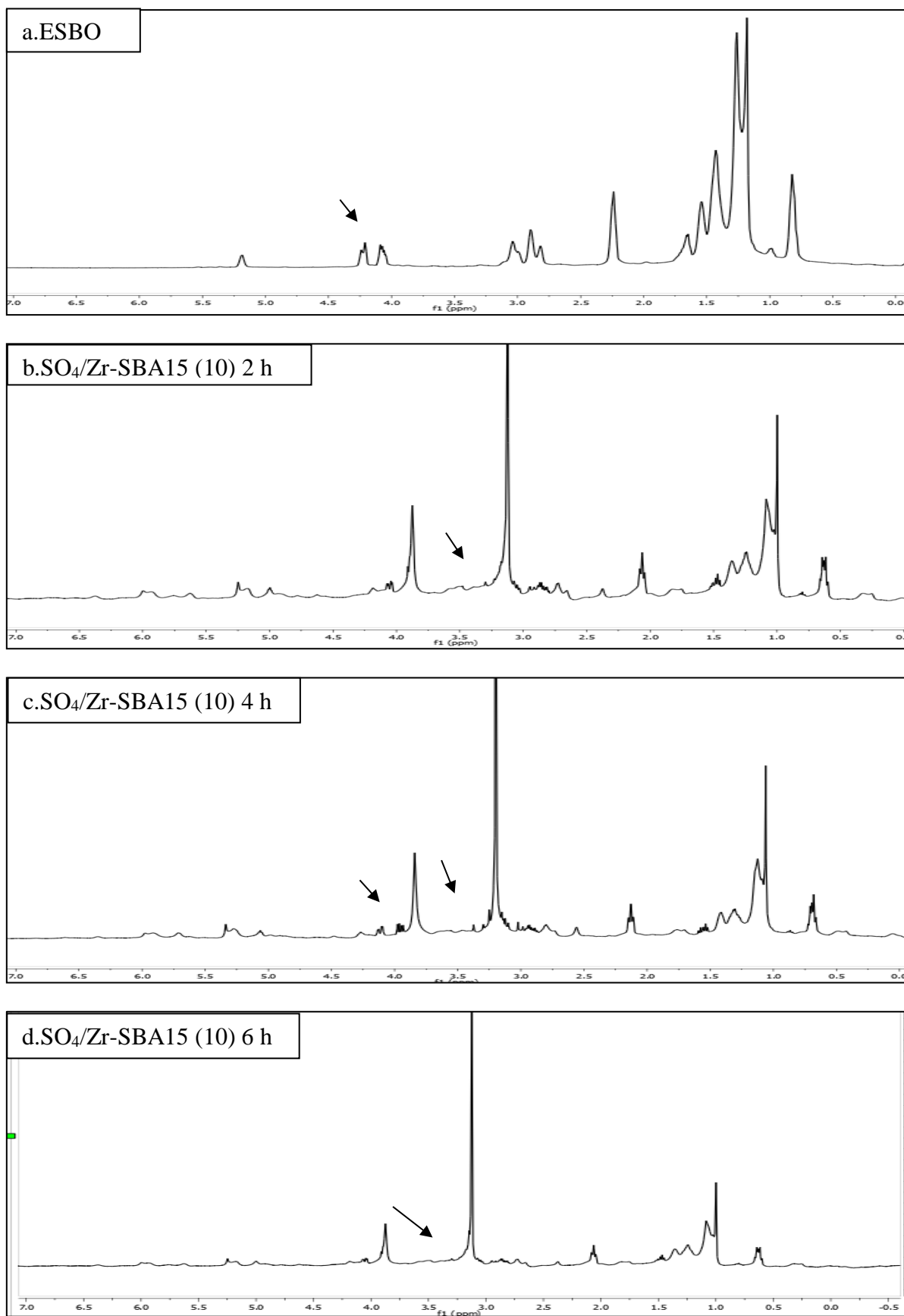
Figure 5. 39. H-NMR analysis of products formed over SO₄/Zr-SBA15 (10).

Heterogeneous catalysis reaction tests were also performed in the presence of Ti-SBA15 (10) and Ti-SBA15 (20) catalysts. The FT-IR analysis of products formed over Ti-SBA15 (10) is given in Figure 5. 40. The C=O, C-O stretching vibrations of aliphatic ester groups and secondary hydroxyl group bands gave peaks at 174, 1240 and 1080 cm^{-1}, respectively. Whereas the epoxy groups decreased during the reaction duration, the formed products increased. They give a characteristic peak around 3400 cm^{-1} (Ji et al., 2015).

Figure 5. 40. FT-IR analysis of products formed over Ti-SBA15 (10).

The oxirane contents of the products formed over Ti-SBA15 (10) are given in Figure 5. 41. Oxirane content decreased with reaction time and oxirane conversion of 57.78 % was achieved by using Eqn 4.1.

Figure 5. 41. The change in oxirane concentration with time over Ti-SBA15 (10).

71

Figure 5. 42. H-NMR analysis of products formed over Ti-SBA15 (10).

The H-NMR analysis of products formed over Ti-SBA15 (10) are given in Figure 5. 42. The soy based polyol structure was obtained from the H-NMR spectra in Fig. 5.42. b-d**.** The epoxy protons were observed between 2.8 and 3.0 ppm (Fig. 5.42. a.)**.** The new peaks were observed between 3.2 and 4 ppm referred to methylinic proton (H-C-OH) in the H-NMR spectra of products and the proton is associated with the OH groups (Roy 2009). Therefore, the results of H-NMR prove the attachment of hydroxyl groups.

The FT-IR analysis of products formed over Ti-SBA15 (20) are given in Figure 5. 43. The C=O, C-O stretching vibrations of aliphatic ester groups and secondary hydroxyl group bands gave peaks at 1743, 1240 and 1080 cm^{-1}, respectively. Whereas the epoxy groups decreased during the reaction duration, the formed products increased. They give a characteristic peak around 3400 cm^{-1} (Ji et al., 2015).
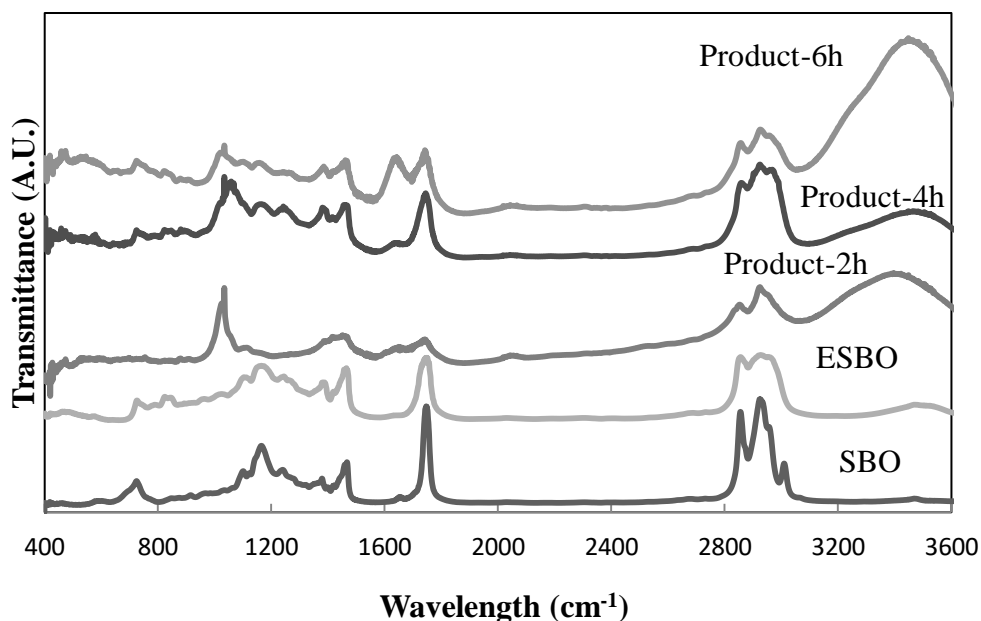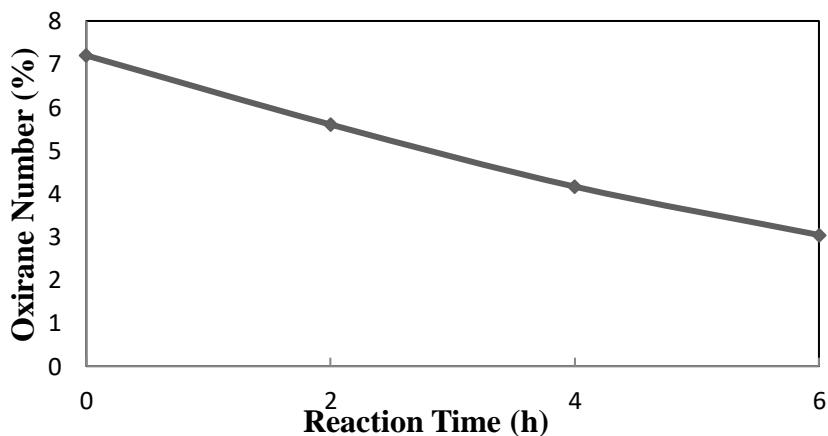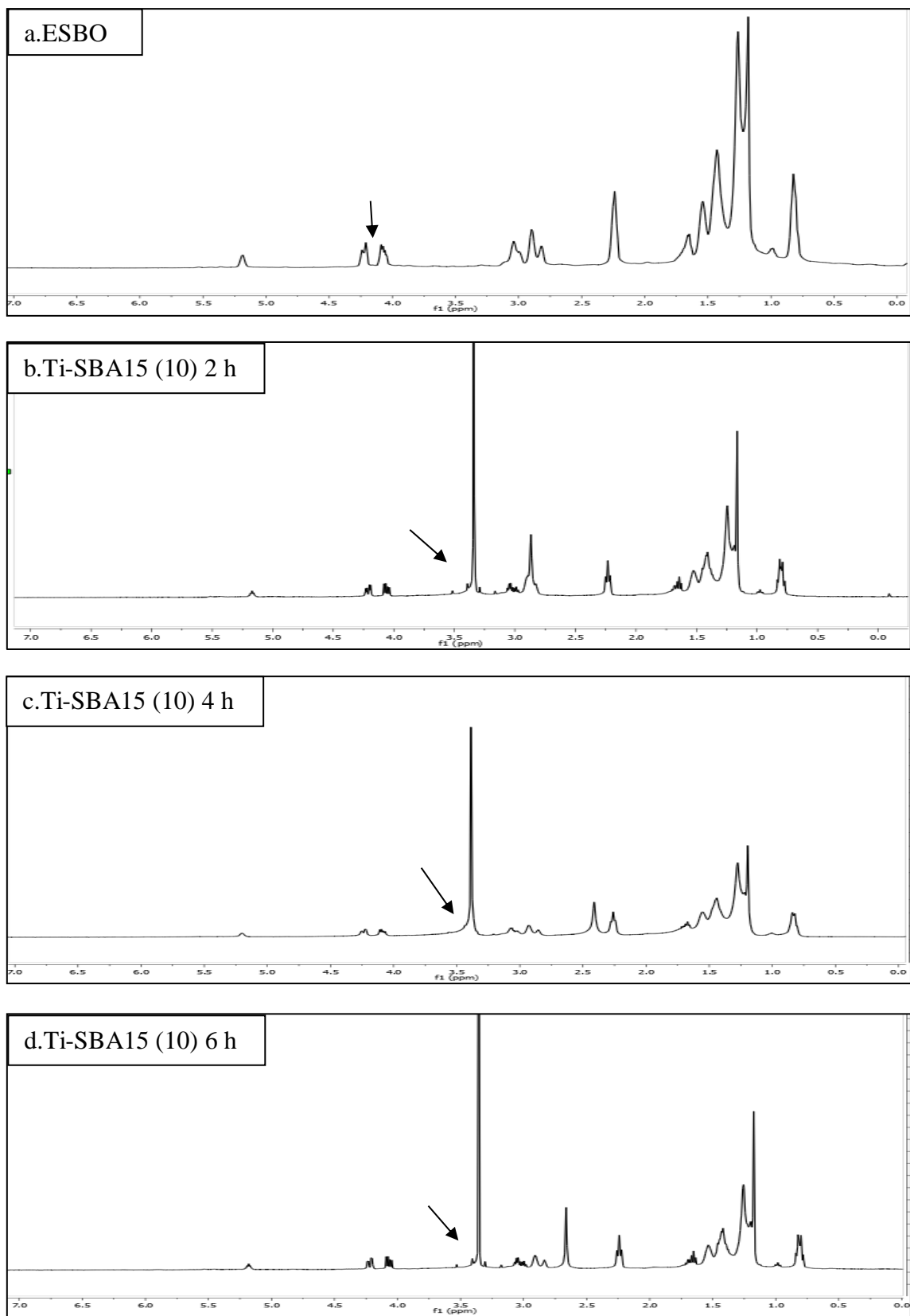

Figure 5. 43. FT-IR analysis of products formed over Ti-SBA15 (20).

The H-NMR analysis of products formed over Ti-SBA15 (20) are given in Figure 5. 44. The soy based polyol structure was obtained from the H-NMR spectra in Fig. 5.44. b-d**.** The epoxy protons were observed between 2.8 and 3.0 ppm (Fig. 5.44. a.)**.** The new peaks were observed between 3.2 and 4 ppm referred to methylinic proton (H-C-OH) in the H-NMR spectra of products and the proton is associated with the OH groups (Roy 2009). Therefore, the results of H-NMR prove the attachment of hydroxyl groups.
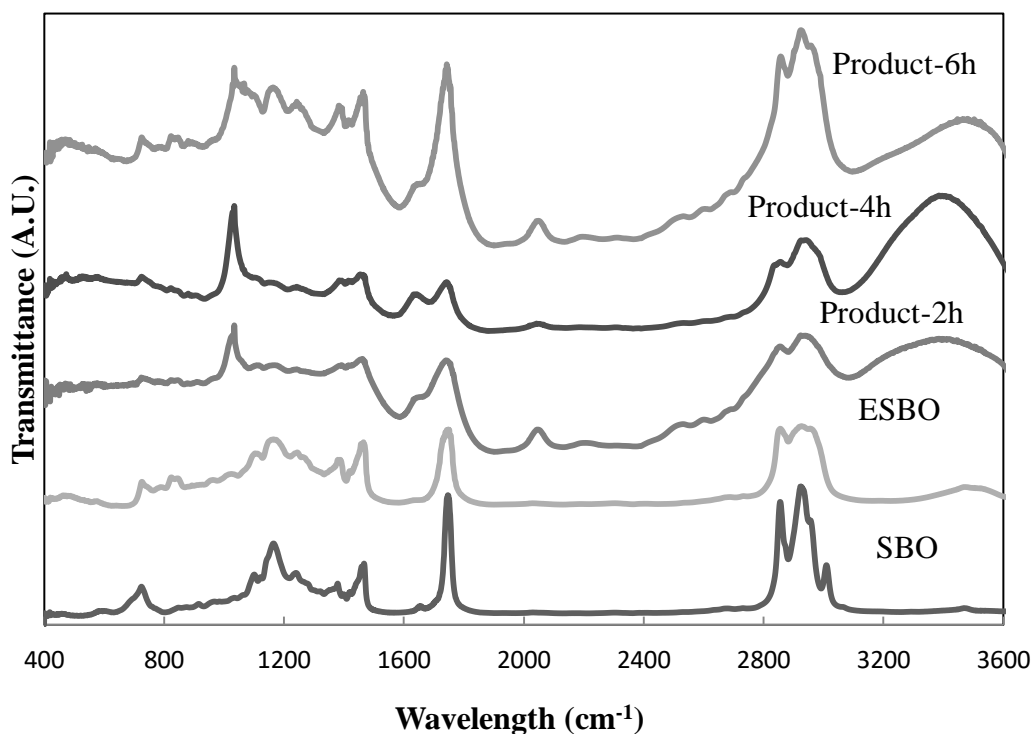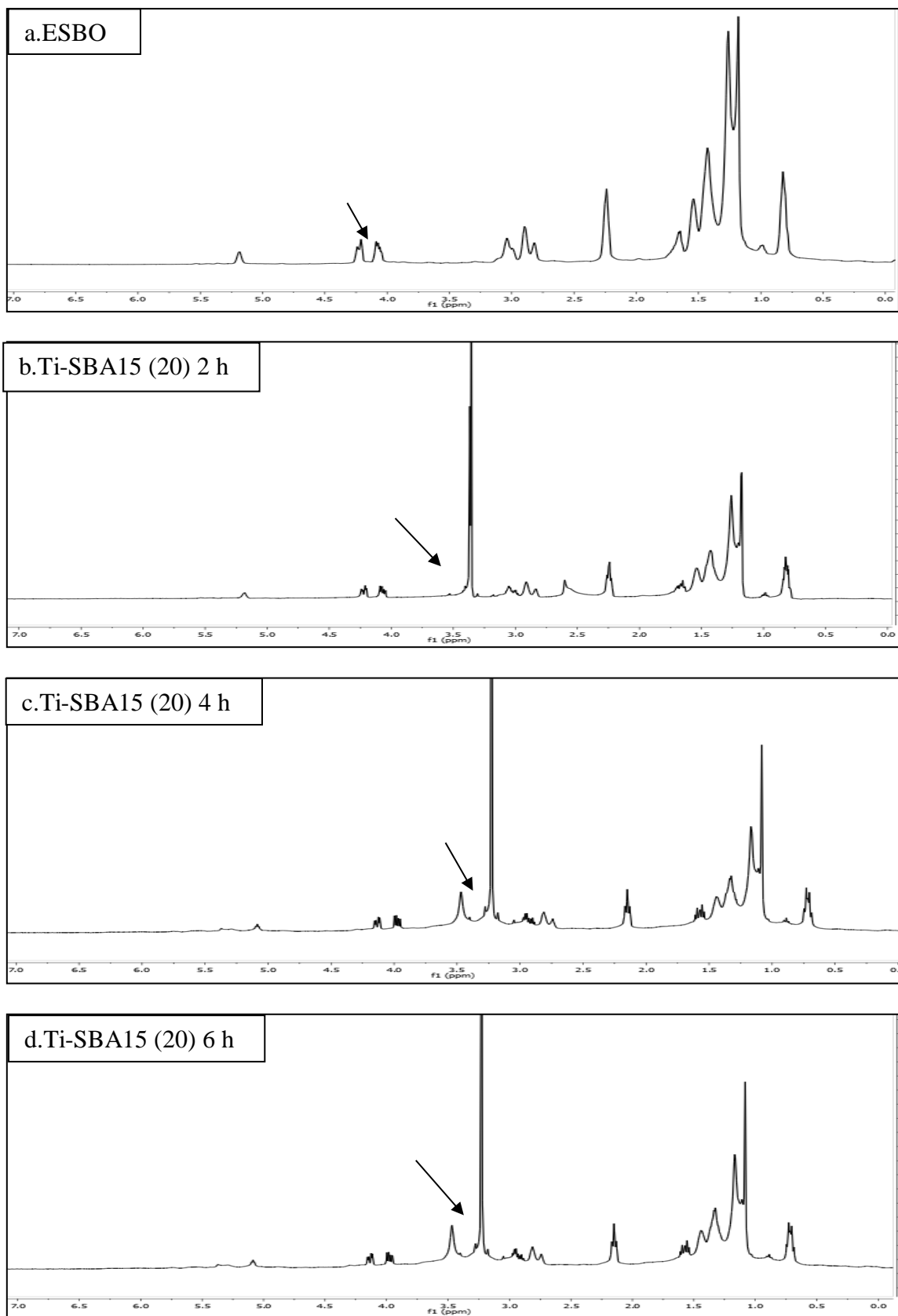
Figure 5. 44. H-NMR analysis of products formed over Ti-SBA15 (20).

The oxirane contents of the products formed over Ti-SBA15 (20) are given in Figure 5. 45. Oxirane content decreased with reaction time and oxirane conversion of 51.11 % was achieved by using Eqn 4.1.
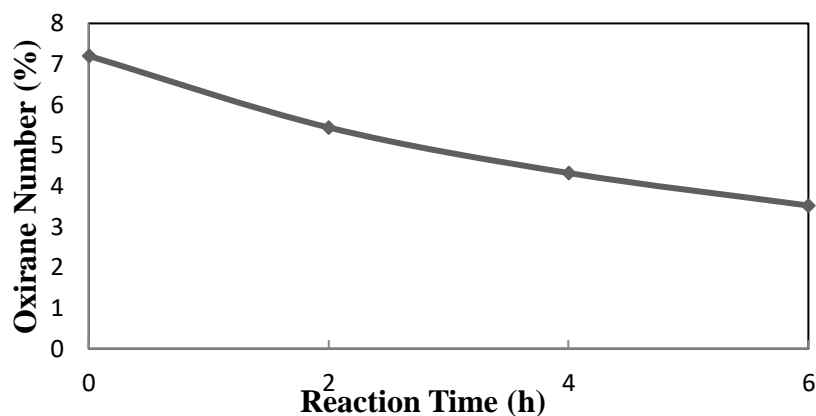

Figure 5. 45. The change in oxirane concentration with time over Ti-SBA15 (20).

Acidity of Ti based catalysts were close to each other. Therefore, similar oxirane conversions were obtained. Acidity of these catalysts were lower than Zr based catalysts. Thus, lower conversions were obtained.

The FT-IR analysis of products formed over SO_4/Ti-SBA15 (10) are given in Figure 5. 46. The bands of C=O, C-O stretching vibrations of aliphatic ester groups and secondary hydroxyl group bands gave peaks at 1743, 1240 cm^{-1} and 1080 cm^{-1}, respectively. Whereas the epoxy groups decreased during the reaction duration, the formed products increased. They give a characteristic peak around 3400 cm^{-1} (Ji et al., 2015).
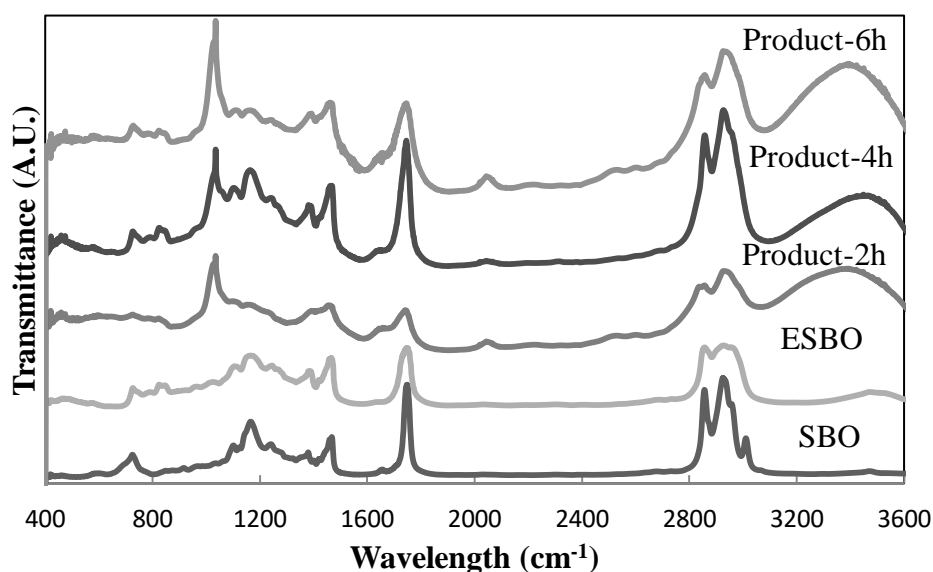

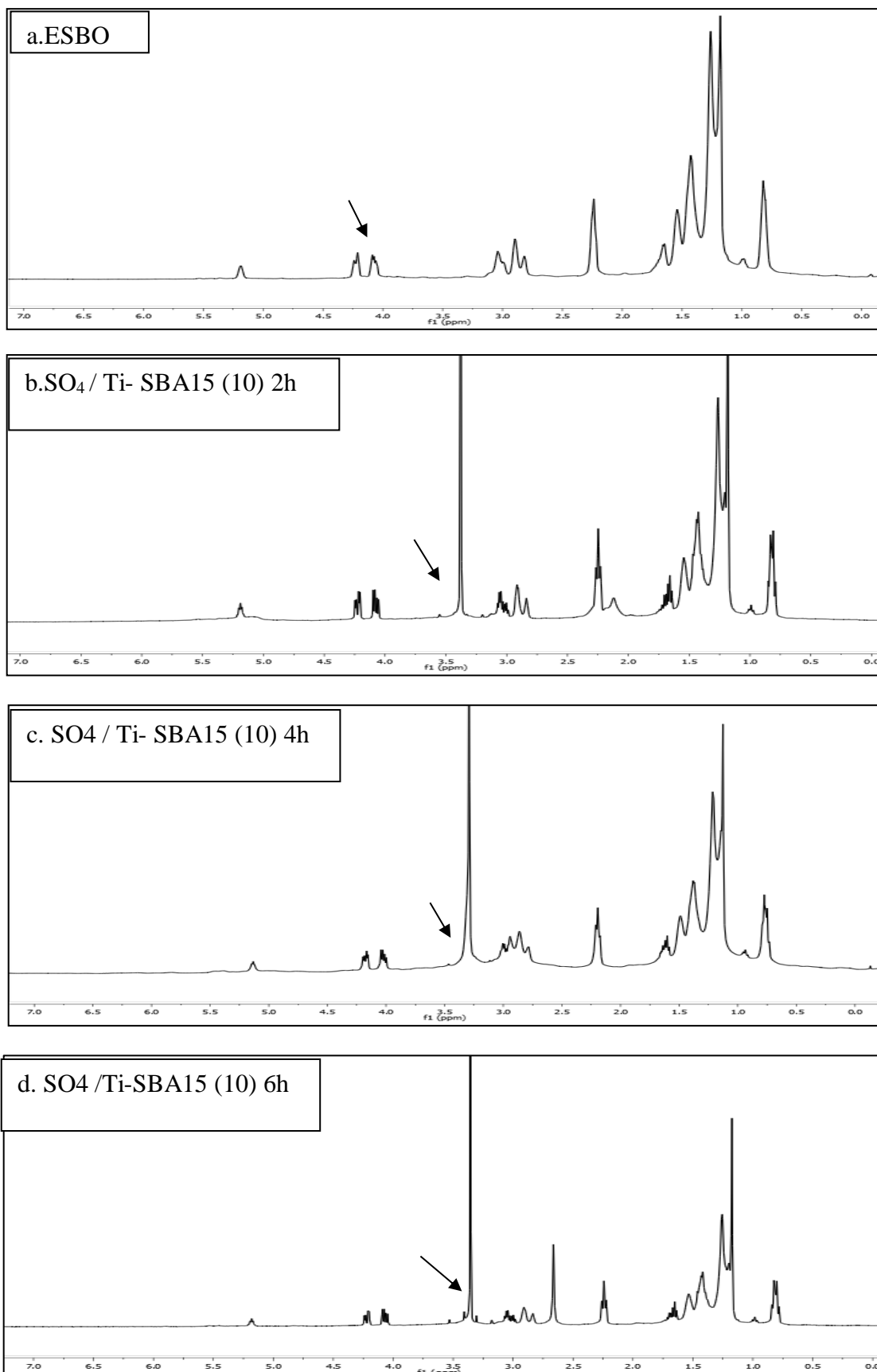Figure 5. 46. FT-IR analysis of products formed over SO_4/Ti-SBA15 (10).

Figure 5. 47. H-NMR analysis of products formed over SO₄/Ti-SBA15 (10).

The H-NMR analysis of products formed over SO_4/Ti-SBA15 (10) are given in Figure 5. 47. The soy based polyol structure was obtained from the H-NMR spectra in Fig. 5.47. b-d. The epoxy protons were observed between 2.8 and 3.0 ppm region (Fig. 5.47. a.). The new peaks were observed between 3.2 and 4 ppm referred to methylinic proton (H-C-OH) in the H-NMR spectra of products and the proton is associated with the OH groups (Roy 2009). Therefore, the results of H-NMR prove the attachment of hydroxyl groups.

The oxirane content of the products formed over SO_4/Ti-SBA15 (10) is given in Figure 5. 48. Oxirane content decreased with reaction time and oxirane conversion of 55.56 % was achieved by using Eqn 4.1.
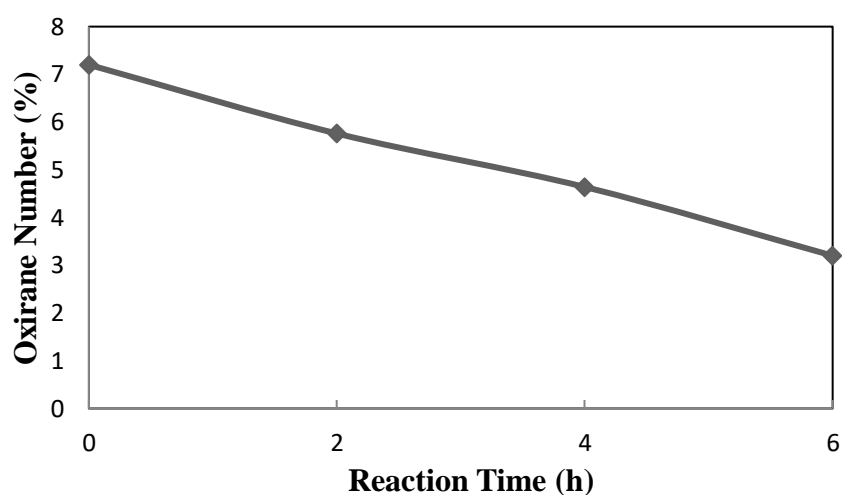

Figure 5. 48. The change in oxirane concentration with time over SO_4/Ti-SBA15 (10).
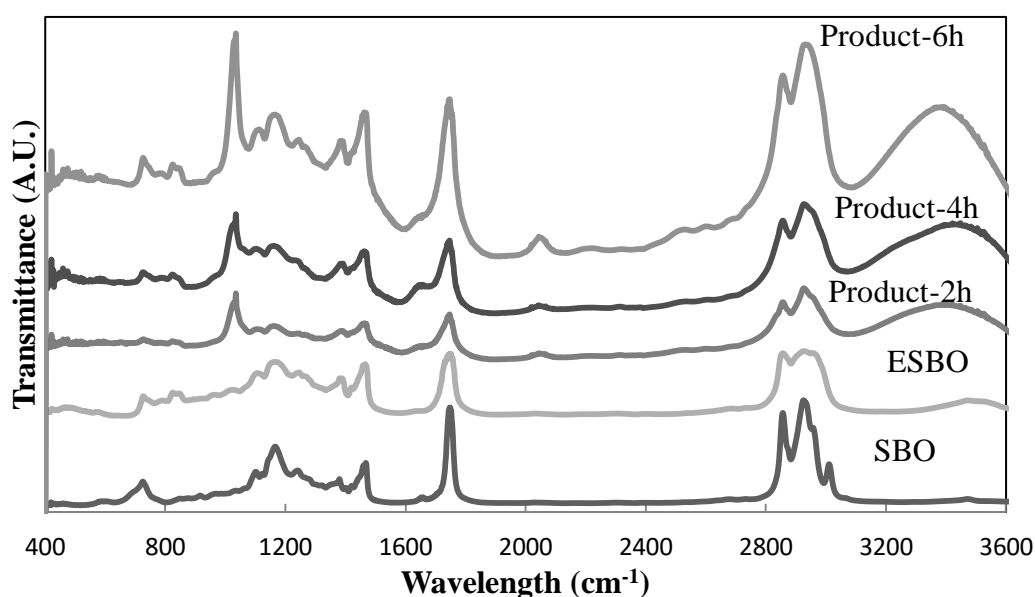

Figure 5. 49. FT-IR analysis of products which were formed using SO_4/Ti-SBA15 (20).

77

The FT-IR analysis of products formed over SO₄Ti-SBA15 (20) are given in Figure 5. 49. The bands of C=O, C-O stretching vibrations of aliphatic ester groups and secondary hydroxyl group bands gave peaks at 1743, 1240 cm^{-1} and 1080 cm^{-1}, respectively. Whereas the epoxy groups decreased during the reaction duration, the formed products increased. They give a characteristic peak around 3400 cm^{-1} (Ji et al., 2015).

The oxirane content of the products formed over SO₄/Ti-SBA15 (20) is given in Figure 5. 50. Oxirane content decreased with reaction time and oxirane conversion of 48.89 % was achieved by Eqn 4.1.
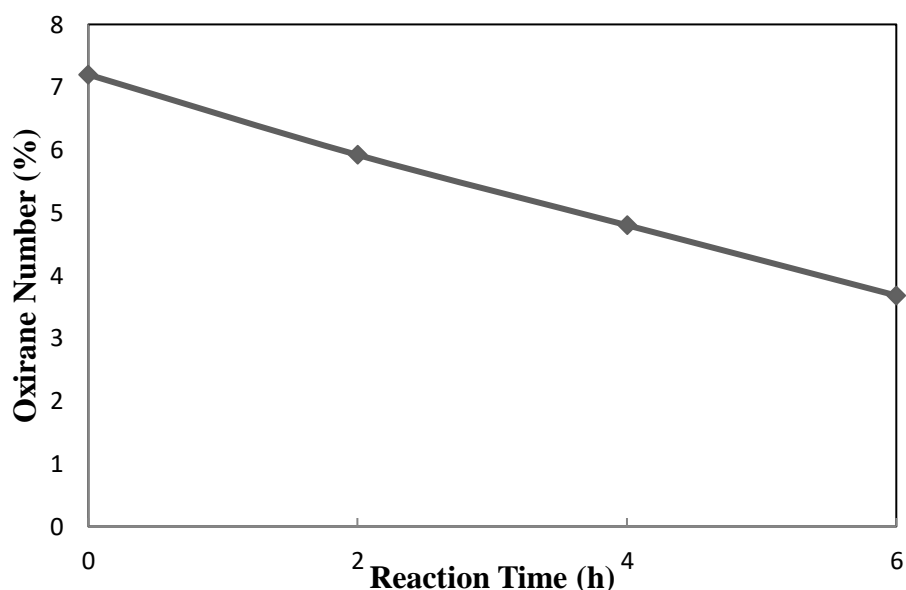
Figure 5. 50. The change in oxirane concentration with time over SO₄/Ti-SBA15 (20).

Whereas acidity of the sulfated Ti based catalysts increased with Ti amount, the activity of the catalysts decreased in oxirane conversion. This was attribute to its large amount of weak acid sites.

The H-NMR analysis of products formed over SO₄/Ti-SBA15 (20) are given in Figure 5. 51. The soy based polyol structure was obtained from the H-NMR spectra in Fig. 5.51. b-d**.** The epoxy protons were observed between 2.8 and 3.0 ppm (Fig. 5.51. a.). The new peaks were observed between 3.2 and 4 ppm referred to methylinic proton (H-C-OH) in the H-NMR spectra of products and the proton is associated with the OH groups (Roy 2009). Therefore, the results of H-NMR prove the attachment of hydroxyl groups.
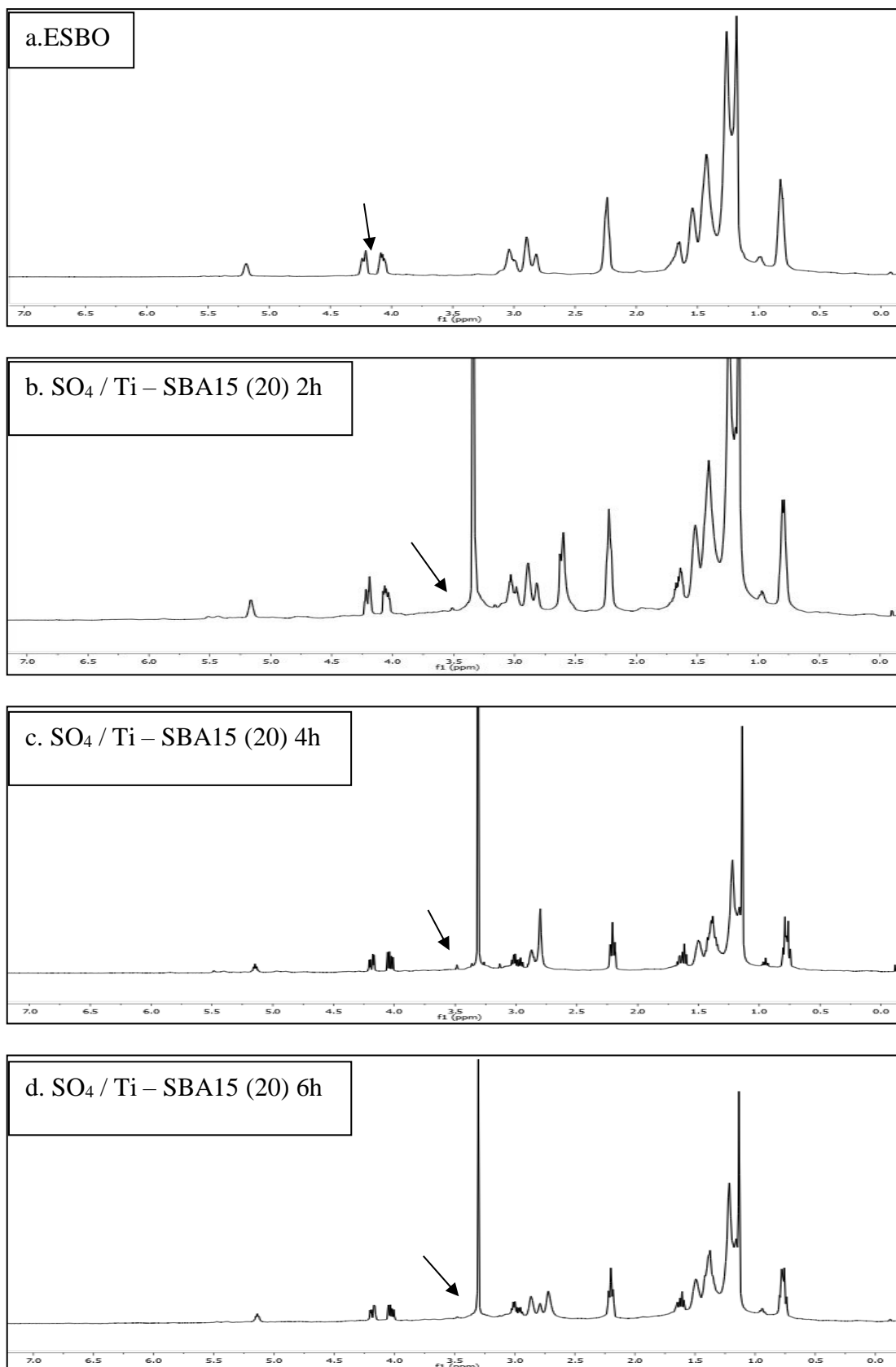
Figure 5. 51. H-NMR analysis of products formed over SO₄/Ti-SBA15 (20).

CHAPTER 6

CONCLUSION

Mesoporous Zr-SBA15 and Ti-SBA15 catalysts were prepared. Zr was and low Ti content was incorporated into SBA-15 succesfully while anatase phase of Ti was observed with high Ti loading. Surface area and pore diameter decreased with high loading. Increasing metal content and sulfation enhanced the acidity of the catalysts. While some catalysts had strong acid site, some catalysts had weak and medium acid sites.

Zr-SBA15 based catalysts provided higher oxirane conversion than Ti-SBA15 based catalysts. Sulfation did not improve catalyst activity of the catalysts. Activity of the catalysts decreased with acidity increase. The higher epoxy conversion (84 %) was obtained with Zr-SBA-15 (08) whidh had low Zr content and low acidity. For alcoholysis reaction, it was found that strong acid sites were much more important weak acid sites.

REFERENCES

Ahn, B,K ; Hongwang W ; Shona, R ; Shrestha, T,B ; Troyer, D,L ; Bossmann, S,H ; Sun, X,S ; Ring Opening of Epoxidized Methyl Oleate Using a Novel Acid-Functionalized Iron Nanoparticle Catalyst †. Green Chem., 14, 2012, 136–42.

Alagi, P ; Ghorpade, R ; Jang, J,H ; Patil, C ; Jirimalib, H ; Giteb, V ; Hong, S,C Functional Soybean Oil-Based Polyols as Sustainable Feedstocks for Polyurethane Coatings. Ind. Crops Prod., 113, 2018, 249–58.

Anya, A,U; Isa, M,T; Musa, S, H; Adegbe, E.A; Shittu,U.M ; A Review of Processes Used In Polyol Synthesis from Vegetable Oils. Sch. Acad. J. Biosci., 2(2), 2014, 141-143.

Barluenga, J. ; Vazquez-Villa, H. ; Ballesteros, A. ; Gonzalez, J.,M. ; Copper(II) Tetrafluoroborate Catalyzed Ring-Opening Reaction of Epoxides with Alcohols at Room Temperature.

Campanella, A ; Bonnaillie, L,M ; Wool, R,P ; Polyurethane Foams from Soyoil-Based Polyols. J. Appl. Polym. Sci., 112, 2009, 2567–2578.

Członka, S ; Bertino, M,F ; Kośny, J ; Strąkowska, A ; Masłowski, M; Strzelec, K ; Linseed Oil as a Natural Modifier of Rigid Polyurethane Foams. Ind. Crops Prod., 115, 2018, 40-51.

Dai, H. ; Yang, L. ; Lin, B. ; Wang, C. ; Shi, G. ; Synthesis and Characterization of the Different Soy-Based Polyols by Ring Opening of Epoxidized Soybean Oil with Methanol, 1,2-Ethanediol and 1,2-Propanediol. J. Am. Oil Chem. Soc., 86:3, 2009, 261-267.

Das, S. ; Asefa, T. ; Epoxide Ring-Opening Reactions with Mesoporous Silica-Supported Fe(III) Catalysts. Catal., 1, 2011, 502–510.

Desroches, M. ; Escouvois, M. ; Auvergne, R. ; Caillol, S. ; Boutevin, B. ; From Vegetable Oils to Polyurethanes: Synthetic Routes to Polyols and Main Industrial Products. Polym Rev., 52:1, 2012, 38-79.

Dhakshinamoorthy, A. ; Alvaro, M. ; Concepcion, P. ; Fornes, V. ; Garcia, H. ; Graphene Oxide as an Acid Catalyst for the Room Temperature Ring Opening of

Epoxides. Chem. Commun., 48, 2012, 5443–5445.

Dong, J ; Fang, Z ; He, W ; Luo, Z ; Jiang, X ; Wang, T ; Guo, K ; Polyurethane Rigid Foams Formed from Different Soy-Based Polyols by the Ring Opening of Epoxidised Soybean Oil with Methanol , Phenol , and Cyclohexanol. Ind. Crops Prod., 74, 2015, 76–82.

Dworakowska, S ; Bogdal, D ; Prociak, A ; Microwave-Assisted Synthesis of Polyols from Rapeseed Oil and Properties of Flexible Polyurethane Foams. Polymers., 4, 2012, 1462-1477.

Fan, H ; Tekeei, A ; Suppes, G,J ; Hsieh, F; Physical Properties of Soy-Phosphate Polyol-Based Rigid Polyurethane Foams. Int. J. Polym. Sci. 4, 2012, 1687-9422.

Fang, Z ; Yang, Z ; Ji, D ; Zhu, N ; Li, X ; Wan, L ; Zhang, K ; Kuo, K ; Synthesis and Application of a Novel Bio-Based Polyol for Preparation of Polyurethane Foams †. RSC Adv., 6, 2016, 3874–3878.

Guo, Y ; Hardesty, J,H ; Mannari, V,M ; Massingill Jr, J,L ; Hydrolysis of Epoxidized Soybean Oil in the Presence of Phosphoric Acid. J. Am. Oil Chem. Soc., 84, 2007, 929-935.

Kahandal, S.,S. ; Kale, S., R. ; Disale S.,T. ; Jayaram R.,V. ; Sulphated yttria–zirconia as a regioselective catalyst system for the alcoholysis of epoxides. Catal. Sci. Technol., 2012, 2, 1493–1499.

Lathi, P.,S. ; Mattiasson, B. ; Green Approach for the Preparation of Biodegradable Lubricant Base Stock from Epoxidized Vegetable Oil. Applied Catalysis B: Environmental, 69, 2007, 207–212.

Li, X. ; Fang, Z. ; Li, X. ; Tang, S. ; Zhang, K. ; Guo, K. ; Synthesis and Application of a Novel Bio-based Polyol for Preparation of Polyurethane Foams. New J. Chem., 38, 2014, 3874—3878.

Li, Y. ; Sun, X.,S. ; Polyols from Epoxidized Soybean Oil and Alpha Hydroxyl Acids and Their Adhesion Properties from UV Polymerization. International Journal of Adhesion & Adhesives, 63, 2015, 1–8.

Liu, Z ; Biswas, A ; General Fluoroantimonic Acid Hexahydrate (HSbF$_6$·6H$_2$O) Catalysis : The Ring-Opening Polymerization of Epoxidized Soybean Oil., Appl. Catal., A., 453, 2013, 370-375.

Lozada, Z. ; Suppes G.,J. ; Tu Y., Hsieh, F. ; Soy-Based Polyols from Oxirane Ring Opening by Alcoholysis Reaction. Journal of Applied Polymer Science, 113, 2009, 2552–2560.

Lubguban, A,A ; Synthesis and Testing of Soy-Based Polyols: Phosphate and Glycerolysis Oligomers. University of Missouri-Columbia, PhD. Thesis, 2009.

Mutlu, V.,N. ; Ylmaz, S. ; Esterification of Cetyl Alcohol with Palmitic Acid over WO_3/Zr-SBA-15 and Zr-SBA-15 Catalysts. Applied Catalysis A: General, 522, 2016, 194–200.

Petrović, Z.,S. ; Cvetković, I. ; Vegetable Oil-Based Hyperbranched Polyols in Flexible Foams. Contemp. Mater., III-1, ,2012, 63-71.

Petrović, Z.,S. ; Polyurethanes from Vegetable Oils. Polym Rev., 48:1, 2008, 109-155.

Piccolo, D ; Epoxidation of Soybean Oil by Conventional and Non-Conventional Methods. University of Padua, MsC. Thesis., 2016, 129.

Ping, B.,T.,Y. ; Hanzah, N.,A. ; Soi, H.,S. ; Determination of Hydroxyl Value of Palm-Based Polyols by Partial Least Squares Algorithm using NIR Spectroscopy. J. Oil Palm Res., 23, 2011, 1172-1177.

Purwanto, E. ; The Synthesis of Polyol from Rice Bran Oil (RBO) through Epoxidation and Hydroxylation Reactions. University of Adelaide, MsC. Thesis, 2010, 138.

Rakicka, M. ; Biegalska, A. ; Rymowicz, W. ; Dobrowolski, A. ; Mirończuk, A.,M. ; Polyol Production from Waste Materials by Genetically Modified Yarrowia Lipolytica. Bioresource Technol., 243, 2017, 393-399.

Rios, L.,A. ; Weckes, P.,P. ; Schuster, H., Hoelderich, W.,F ; Resin catalyzed alcoholysis of epoxidized fatty esters: Effect of the alcohol and the resin structures. Appl. Catal. A., l 284, 2005, 155–161.

Robinson, M.,W.,C. ; Buckle, R. ; Mabbett, I. ; Grant, G.,M. ; Graham, A.,E. ; Mesoporous aluminosilicate promoted alcoholysis of epoxides. Tetrahedron Letters, 48, 2007, 4723–4725.

Roy, G.,S. ; Novel Approaches for Synthesis of Polyols from Soy Oils. University of Toronto, MsC. Thesis, 2009, 61.

Sakarya, M. ; Sennur, D. ; Polyurethane Networks from Different Soy-Based Polyols by the Ring Opening of Epoxidized Soybean Oil with Poly(ethylene glycol)s. 2nd International Symposium on Innovative Technologies in Engineering and Science., 2014.

Sandler, S.,I. ; Chemical, Biochemical, and Engineering Thermodynamics. John Wiley & Sons Inc., 3rd edition, 1999, 914.

Saremi, K. ; Tabarsa, T. ; Shakeri, A. ; Babanalbandi, A. ; Epoxidation of Soybean Oil. Ann. Biol. Res., 3:9, 2012, 4254–58.

Sharma, R.,V. ; Soni, K.,K. ; Dalai, A.,K. ; Preparation, Characterization and Application of Sulfated Ti-SBA-15 Catalyst for Oxidation of Benzyl Alcohol to Benzaldehyde. Catalysis Communications, 29, 2012, 87–91.

Y, Q. Zhang, J.,l. ; Zhang, X. ; Feng, J. ; Li, W. ; Synthesis of SO_4^{2-}/Zr-SBA-15 Catalyst for the Transesterification of Waste Cooking Oil as a Bio-flotation Agent in Coal Flotation. Fuel, 143, 2015, 390–398.

Yebo, L. ; Xiaolan, L. ; Shengjun, H. ; Bio-based Polyols and Polyurethanes. Springer, Green Chemistry for Sustainability, 2015, 435.

Zhang, J. ; Tang, J.,J. ; Xia, J. ; College, Z. ; Polyols Prepared from Ring-Opening Epoxidized Soybean Oil by a Castor Oil-Based Fatty Diol. Int. J. Polym. Sci., 22, 2015, 1-8.